2015

Comparing diel cycles of dissolved inorganic carbon to diel cycles of Fe and Mn at a coal mine drainage site in Harrison Co., WV

Jill L. Riddell

Comparing diel cycles of dissolved inorganic carbon to diel cycles of Fe and Mn at a coal mine drainage site in Harrison Co., WV

Jill L. Riddell

Thesis submitted

to the Eberly College of Arts and Sciences

at West Virginia University

in partial fulfillment of the requirements for the degree of

Master of Science in

Geology

Dorothy J. Vesper, Ph.D., West Virginia University, Chair

Helen Lang, Ph.D., West Virginia University

Louis McDonald, Ph.D., West Virginia University

Harry M. Edenborn, Ph.D., National Energy and Technology Lab

Jonathan B. Martin, Ph.D., University of Florida

Department of Geology and Geography

Morgantown, West Virginia

2015

Keywords: [diel, geochemistry, metals, dissolved inorganic carbon, CO_2, coal mine drainage]

ABSTRACT

COMPARING DIEL CYCLES OF DISSOLVED INORGANIC CARBON TO DIEL CYCLES OF FE AND MN AT A COAL MINE DRAINAGE SITE IN HARRISON COUNTY, WV

Jill Leighanne Riddell

Diel (24 hour) cycles of dissolved inorganic carbon and dissolved metals have rarely been studied in concert in coal mine drainage systems containing high CO_2. Diel samples were collected from two locations at a site with elevated CO_2; the locations differed in their CO_2 concentrations and the amount of vegetation present. Field data and samples were collected from both locations during March, May, and July 2014. To determine if the parameters cycled in a diel fashion, the data were fit using a cosine model and the goodness of fit was determined using an f-test statistic. Overall, 15 of 20 selected parameters could be fit using the cosine model with an f-test statistic $p \leq 0.01$. Parameters found to have diel cycling patterns were pH, temperature, dissolved oxygen, CO_2, inorganic carbon, $\delta^{13}C_{DIC}$, Fe(II), Fe_{TOT}, Y, Zn, K, Al, Mn, As, and Ni. More parameters had a diel behavior according to the model fit in the downstream location (which is in a wetland) and as the seasons progressed. When the same model and analysis were applied to data from other sites and studies, similar phasing was observed. Metals concentrations were approximately 200% lower at this study site than in 2007 but stronger diel cycles were present in 2007. Likely mechanisms driving diel behavior at this site are a combination of solar-activated process such as pH; temperature-controlled sorption reactions; the photosynthesis-cellular respiration cycle; degassing of CO_2; and the residence time of the water. Future studies are needed to further separate and quantify these mechanisms on diel behavior as well as to investigate other possible mechanisms like hyporheic exchange and plant uptake.

ACKNOWLEDGMENTS

This work was performed as part of the National Energy and Technology Laboratory's Regional University Alliance (NETL-RUA), a collaborative initiative of the NETL, under RES contract DE-FE0001000 . Specifically, I would like to thank my advisor, Dr. Dorothy Vesper, for training me in field techniques and her patience and guidance during the duration of the project. I would also like to thank Drs. Louis McDonald, Helen Lang, Hank Edenborn, and Jon Martin for their input and guidance during this project as well as Dr. Marie Kurz for her statistical instructions. Finally, the completion of this field work would not have been possible without the help of several friends/field assistants: Habib Bravo-Ruiz, Lindsey Bowman, Beth Donovan, Catherine Patterson, Travis Wilson, Michael Vanhorn, and Chris Nicholson. A special thanks to Corey O'Malley for construction of the mobile chemistry lab as well his field assistant duties.

Table of Contents

List of abbreviations

AMD – acid mine drainage

BAC – benzoalkonium chloride

BDL – below detection limit

CBD – charge balance error

CM – carbonation meter

CMD – coal mine drainage

DIC – dissolved inorganic carbon

DO – dissolved oxygen

HDPE – high-density polyethylene

HFO – hydrous ferric oxide

IC – ion chromatography

ICP-MS – inductively coupled plasma-mass spectrometry

ICP –OES inductively coupled plasma optical emission spectroscopy

LRM – Lambert Run

MHW – mountain headwater

NETL – National Energy Technology Laboratory

NRCCE – National Research Center for Coal Energy

ODO – optical dissolved oxygen

RSD – relative standard deviation

RSSn – residual sum squares of null hypothesis (data)

RSSc – residual sum squares of cosine model fit

TMDL – total maximum daily load

YREE – yttrium and rare earth elements

List of Figures

List of Tables

List of Appendices:

1.0 Introduction and statement of purpose

The relationship between metals and dissolved inorganic carbon (DIC) concentrations in freshwater systems over diel periods is not well understood. Few studies (e.g., Poulson et al. 2010, Kurz et al. 2013) have reported concurrent metal and DIC or CO_2 concentration data. Furthermore, limited research addresses diel cycles in coal mine drainage (CMD) or in high CO_2 systems, evaluates the effect of seasonality, or compares between vegetative settings. This study compares the diel concentrations for DIC, CO_2, Fe, Mn, and other selected parameters at two locations in a CMD affected stream; one location has high CO_2 and little emergent vegetation, the other location has low CO_2 and abundant emergent vegetation. Data collection took place during three different seasons at both locations.

Primarily, this study seeks to understand how diel cycles of DIC and metals are affected by changing stream chemistry (i.e. degassing of CO_2 downstream, increased biological activity) and seasonal variation. Secondarily, it attempts to generally assess the effectiveness of a passive treatment in the form of a wetland in a CMD stream on total dissolved metal load and the importance of sampling at different times of day or in different seasons when assessing the results of such treatment.

1.1 Questions and objectives

To address the problem stated, the following questions were asked:

Question #1: Are diel cycles of DIC and metals consistent at locations with different CO_2 concentrations and vegetation?

Question #2: Do diel cycles of, and relationships between, DIC, and metals change with season?

Question 3: Does a cosine model curve fit all cycling parameters with the same statistical significance (α=0.01)?

2.0 Background

2.1 Diel background

Diel is defined as a period of 24 hours. This term is used in preference to diurnal which denotes a period of time during the day or 'daily'. Diel cycles of metals, trace elements, DIC, CO_2, and $\delta^{13}C$ have been recorded by various research groups but few groups have collected concurrent metal and CO_2 data. Metal and trace element diel cycles have been attributed to the following processes: hydrology, pH-temperature driven reactions, temperature dependent sorption, precipitation-dissolution reactions, and iron photoreduction (Nimick et al. 2003). The dominating processes controlling cycling depend on chemistry, which differs with geologic setting (karst, mountain headwater, mine drainage, etc.). Diel cycles of CO_2, DIC, and $\delta^{13}C$ have, in the majority of cases, been attributed to photosynthesis and cellular respiration (Sullivan et al. 1998, Finlay 2003, Gammons et al. 2005, Gammons et al. 2008, Parker et al. 2010, Poulson and Sullivan 2010, de Montety et al. 2011, Nimick et al. 2011). However, these parameters have also been shown to be dominated by calcite precipitation/dissolution and outgassing of CO_2 if the water flows through a carbonate-rich rock (Barnes 1965, Dandurand et al. 1982, Lorah and Herman 1988, Spiro and Pentecost 1991, Drysdale et al. 2003, Liu et al. 2006).

2.2 Diel cycles of CO_2 and DIC

Several mechanisms have been cited in literature to be the controlling mechanism of CO_2 and DIC diel cycling in different geologic settings. The majority of studies cited (in which diel behavior of DIC was the main research goal) attribute photosynthesis and cellular respiration as the control on diel behavior for these parameters as well as pH. Ultimately, the controlling driver is solar radiation because this is what activates photosynthesis and temperature. Other studies cite the kinetics of calcite dissolution and degassing of CO_2 as the controlling mechanism on CO_2, DIC, and pH diel behavior. These processes are discussed in detail below.

2.3 Photosynthesis and cellular respiration

Photosynthesis (Eq. 1) and cellular respiration (Eq. 2) typically control diel cycles of pH due to the consumption and release of CO_2 gas.

$$6CO_2 + 6H_2O + light \rightarrow C_6H_{12}O_6 + 6O_2 \quad \text{Eq. 1}$$

$$C_6H_{12}O_6 + 6O_2 \rightarrow 6CO_2 + 6H_2O$$ Eq. 2

Photosynthesis increases during the day due to solar radiation (Parker et al. 2010) and pH increases due to the uptake of dissolved CO_2 by organisms. At night, pH decreases due to cellular respiration releasing CO_2. This effect on diel cycles has been confirmed by field and laboratory experiments (Parker et al. 2010). Because photosynthesis consumes CO_2, concentrations typically decrease during the day and increase at night (Finlay 2003, Parker et al. 2010, Poulson and Sullivan 2010, de Montety et al. 2011, Nimick et al. 2011, Kurz et al. 2013). Dissolved oxygen (DO) concentrations that are below those at equilibrium with the atmosphere have exhibited inverse diel cycles relative to CO_2 provide further evidence of photosynthesis and cellular respiration controlling CO_2 and DIC, however the reporting study study took place in neutral to alkaline waters. (Poulson and Sullivan 2010). However, where O_2 was being controlled by rapid aeration of the water by the atmosphere, photosynthesis and cellular respiration had only small contributions to DO (Parker et al. 2010).

Stable isotopes of carbon, $\delta^{13}C$, and oxygen, $\delta^{18}O$, also show that photosynthesis and cellular respiration control DIC concentrations in waters with neutral to alkaline pH. Photosynthesis preferentially uses ^{12}C thus the water becomes more depleted in ^{12}C during the day (Finlay 2003, Parker et al. 2010, Poulson and Sullivan 2010, de Montety et al. 2011, Kurz et al. 2013). Conversely, cellular respiration uses lighter $\delta^{16}O$ enriching the water in the heavier isotope, $\delta^{18}O$, at night (Parker et al. 2010, Poulson and Sullivan 2010, Kurz et al. 2013). Diel behavior of DIC, $\delta^{13}C$, and related parameters observed in karst settings have been attributed to biological activity (Fig. 1).

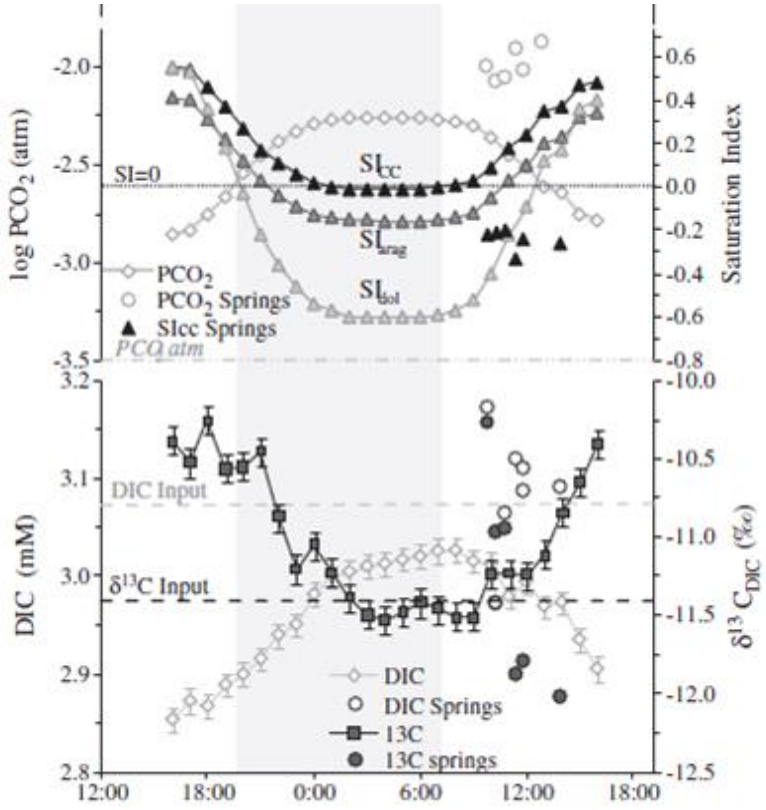

Figure 1. Examples of DIC cycling and related parameters from a karst river in Florida. Adapted from de Montety et al., 2011.

2.4 Kinetics of calcite precipitation and CO_2 exchange with the atmosphere

If water is dominated by a carbonate-rich source rock and/or tufa depositing site, then DIC and CO_2 cycling are likely dominated by calcite precipitation/dissolution and CO_2 gas exchange with the atmosphere. In areas with carbonate rocks, CO_2 degassing to the atmosphere causes super-saturation of calcite (Barnes 1965, Dandurand et al. 1982, Lorah and Herman 1988, Spiro and Pentecost 1991, Liu et al. 2006). DIC concentrations decreased during the day as CO_2 outgassing increased with temperature (Drysdale et al. 2003).

2.5 Mechanisms controlling metal cycling

Like CO_2 and DIC, various mechanisms have been cited in literature as the control on metal and trace element diel behavior. Sorption (controlled by pH and temperature) is the most frequently cited mechanisms with photoreduction being cited in very specific chemical settings. Like photosynthesis, these process are driven by solar radiation. They are described in detail below.

2.6 pH-Temperature

Water temperature and pH increase with air temperature. Cycles of pH are controlled by P_{CO2} (an increase in P_{CO2} decreases pH) (Barnes 1965, Dandurand et al. 1982, Lorah and Herman 1988, Spiro and Pentecost 1991, Drysdale et al. 2003, Finlay 2003, Nimick et al. 2003, Liu et al. 2006, Parker et al. 2010, Poulson and Sullivan 2010, de Montety et al. 2011, Nimick et al. 2011, Kurz et al. 2013). Diel changes in pH due to photosynthesis can facilitate the precipitation or dissolution of amorphous hydrous oxides, carbonates, or other minerals containing metals (Nimick et al. 2003). For example, when metal oxides, such as Fe and Mn, exhibit cyclic precipitation and dissolution in phase with changing pH, this could also result in cycles of other metals that adsorb/absorb to the oxides such as Zn, Mn, and Cd (Nimick et al. 2003).

Changes in pH and temperature impact sorption, photoreduction, and precipitation-dissolution reactions, therefore it can be difficult to separate the effects of pH from the effects of temperature on these mechanisms (Benjamin and Leckie 1981, Dzombak and Morel 1990, Nimick et al. 2003). Diel changes in pH and temperature were related to diel changes in concentration of Zn, Mn, and As in mine drainage influenced waters (Fig. 2).

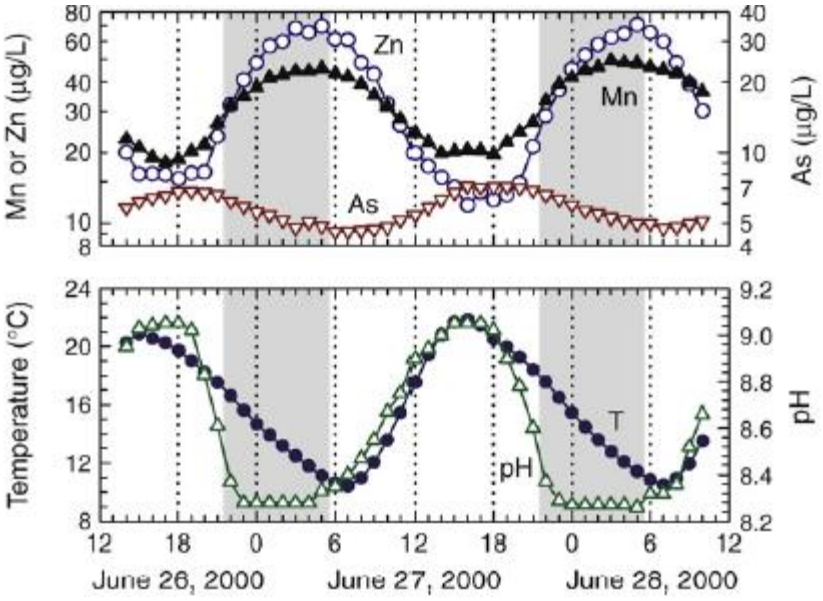

Figure 2. An example of Zn, Mn, and As cycling at Prickly Pear Creek, Mt. A creek that is influenced by mine drainage. Adapted from Nimick et al., 2010.

2.7 Sorption

In neutral to alkaline streams, cation adsorption increases and anion adsorption decreases when pH and temperature increase (Nimick et al. 2003). The percent change in dissolved metals and trace elements (Zn, Mn, Fe, Pb, Cu, As, etc.) concentrations was proportional to the magnitude of diel pH change and temperature in mine affected waters in the western United States (Nimick et al. 2003). Although, the effects of pH and temperature are less well understood for trace metals than for hydrous metal oxide surfaces (Nimick et al. 2003), adsorption of metal cations is favored by an increase in temperature. This has been observed for Zn and other metals (Benjamin and Leckie 1981, Dzombak and Morel 1990, Nimick et al. 2003, Nimick et al. 2011). This also explains why cation concentrations of Zn and Mn decreased as pH and temperature increased but As (in the arsenate form) decreased in one study (Nimick et al. 2005).

When pH increases, there is more sorption of cationic species and less sorption of anionic species thereby creating opposite cycles based on species charge. This is attributed to an increase in the negative surface charge on the solids or organic matter due to deprotonation of functional groups (Benjamin and Leckie 1981, Dzombak and Morel 1990).The potential for organic matter to be a source of CO_2 and sink for metals is very likely at the site chosen in this study.

2.8 Photoreduction of Fe(III)

The photoreduction of Fe(III) to Fe(II) occurs in the ultraviolet (UV) or near UV region of 200-450 nm at an optimal pH range of 2-4 pH units (Gammons et al. 2008) following this reaction:

$$Fe^{3+} + H_2O + e^- + \hbar\nu \rightarrow Fe^{2+} + H^+ + OH^- \quad \text{Eq. 3}$$

Fe(II) concentrations typically increase during the day due to photoreduction (Nimick et al. 2003, Gammons et al. 2005, Gammons et al. 2008). This process is also affected by the pH and temperature dependent precipitation of hydrous ferric oxides (HFOs). With increasing pH and temperature, HFOs precipitate more readily and thus, a reduction in Fe load has been observed in various settings with an initially acidic pH (~2-3) that became more neutral (~7-8) downstream

(Gammons et al. 2005, Gammons et al. 2008). In one study, as pH increased, Fe species did not cycle significantly (Gammons et al. 2005). Further, as pH increased, Fe(II) occurred in higher concentrations than dissolved Fe (III), indicating that HFO particles on the streambed were the reactant for photoreduction and not Fe (III) (Gammons et al. 2005). Any HFO dissolution, such as that occurring as a result of photoreduction, could theoretically result in an increase in dissolved metal concentrations (Cd, Mn, and Zn can all adsorb to HFOs) during the day time hours when solar radiation is at its peak (Nimick et al. 2003). Yet, this was not observed (Nimick et al. 2003), indicating that photoreduction does not always control the cycles of other metals.

2.9 Seasonal variation of diel cycling

Few authors have compared diel cycling of parameters in different seasons. Nimick etal. (2005) compiled the results of several diel cycles conducted at different times of year in mine waters in Montana and Idaho. Although seasonal variation was not an initial objective of these diel studies, the results indicated diel cycles of metals had the largest magnitude in August and the smallest magnitude in December. However, some degree of diel variation was present during each diel sampling season and maxima and minima of various metals occurred at the same time during each season. Kurz etal. (2013) compared diel behavior of pH, temperature, DO, inorganic carbon, and iron in a karst river and observed a general increase in amplitude of diel behavior of these parameters but consistent phasing from late fall to spring.

3.0 Field Site Description

3.1 Location

This study took place at a coal mine drainage site that drains into Lambert Run in Harrison County, north-central West Virginia (Fig. 3). The site is on the property of the J.F. Allen Muzzleloader Club. Lambert Run is a sub-watershed of the larger West Fork watershed (50200020602, USGS Hydrologic Unit Code 12) which contains parts of the West Virginia counties Marion, Taylor, Barbour, Lewis, Harrison, and Upshur (Smilley 2007). The region is located in the Appalachian Plateau, the westernmost physiographic province of the Appalachian Mountains, and is separated from the Valley and Ridge province to the east by the Allegheny Front. This site has known diel cycles of metals, high CO_2 (Smilley 2007) and is partially located in a natural wetland with abundant biological activity.

3.2 Geology

This area of north central West Virginia has a hilly to mountainous topography varying from approximately 335 to 550 m in elevation resulting in an approximate relief of ~250-300 m. The strata in the Lambert Run area are nearly horizontal. The Lambert Run sub-watershed is underlain by the upper Monongahela and upper Connemaugh Series, both of which are upper Pennsylvanian in age. The Connemaugh Series only crops out upstream in the Lambert Run sub-watershed, thus the study area is dominated by the Monongahela series (Fig. 4). The Monongahela series consists of alternating coal, shale, sandstone, and limestone units of varying thickness, the overall thickness is ~125 m. Outcrops of this series are at the surface due to uplift of the Arches Fork, Wolf Summit, and Chestnut ridge anticlines (Hennen 1912). The mine drainage likely comes from mining of the Pittsburgh coal (although historical documentation in the area is lacking) which forms the base of the Monongahela series and is approximately 2 m thick (Fig. 5).

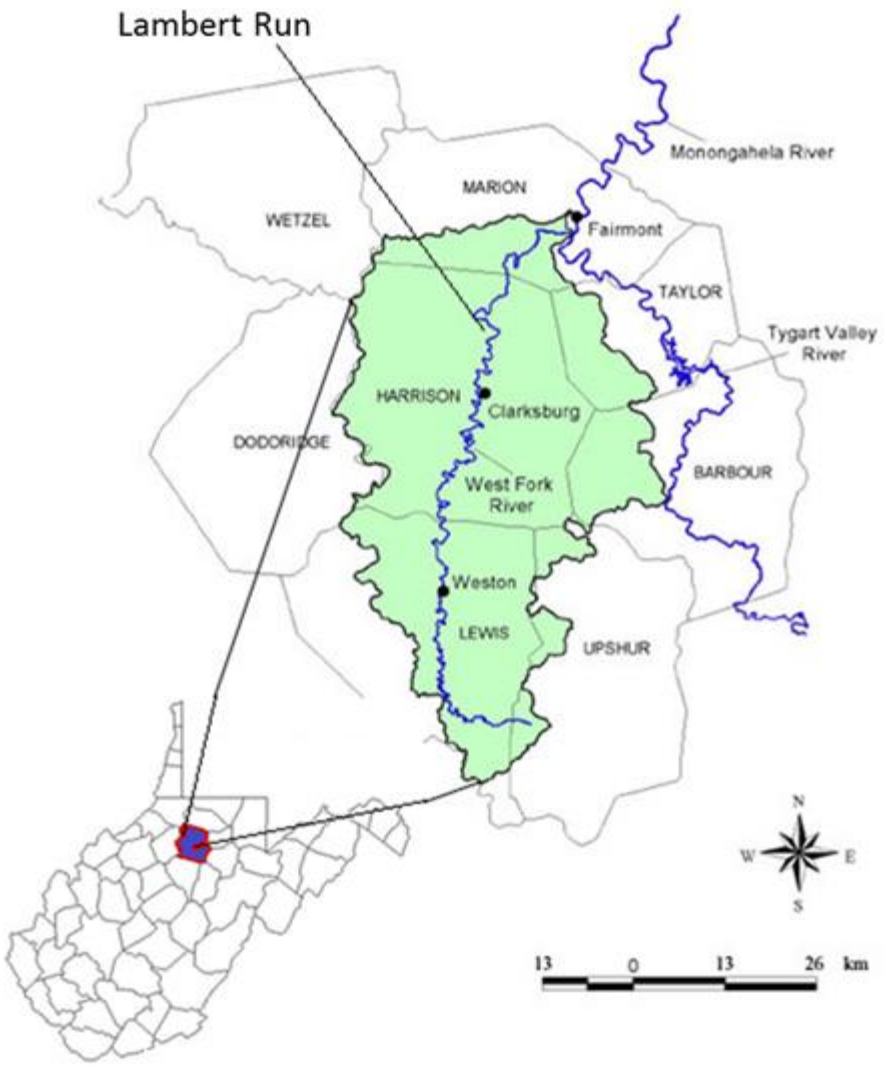

Figure 3. Map and schematic showing the location of Lamberts Run mine portal and major watershed. Adapted from Guardians of the West Fork (2004) and Smilley (2007).

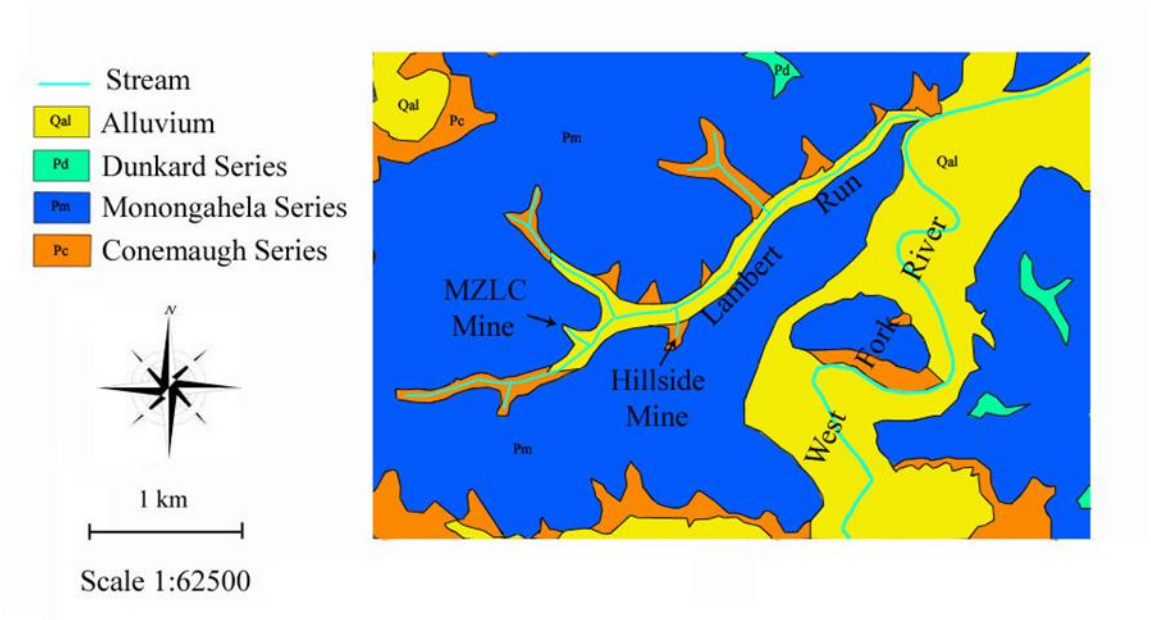

Figure 4. Geology of the Lambert Run area in Harrison Co., WV from Smilley, 2007.

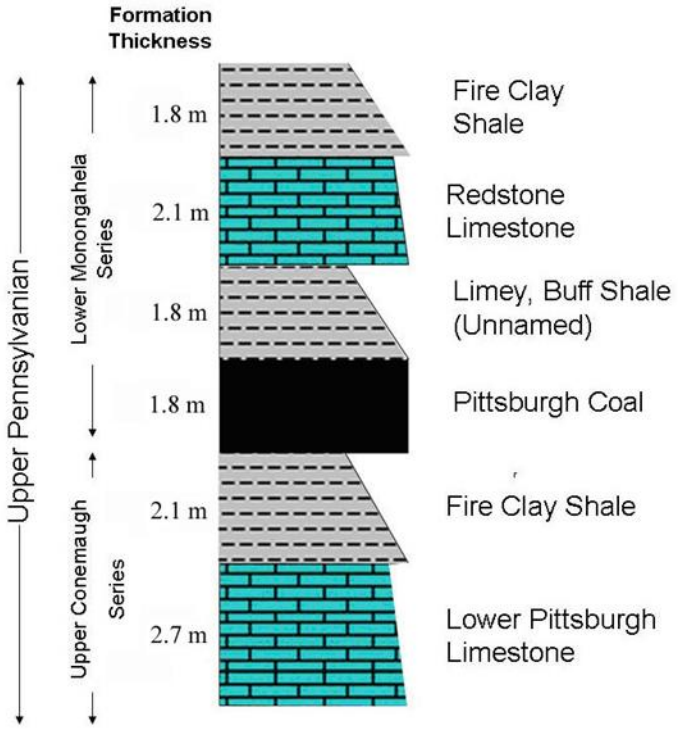

Figure 5. Figure 1. Stratigraphic section of the geology near Lamberts Run, from Smilley, 2007 and Renner, 1912.

3.3 History of mining, sampling locations, remediation and past studies

3.3.1 History of mining

Coal near the Lambert Run mine portal was mined for at least one hundred years (Hennen 1912)- from the late 19th century through the early 20th century. The lack of historical documentation makes it unclear how long the area was mined, which former mines contributed to CMD in the area, and which coal seam(s) were mined in each area. Because of the coal mining history in the area, the water chemistry from the drain portal is high in concentrations of dissolved metals and ions relative to natural waters.

3.3.2 Sampling location

Six sampling locations were designated from the drainage portal to the end of the natural wetland (Fig. 6); the locations were selected to vary in tree cover, vegetation, and CO_2 concentration. The sampling locations are named according to their location at Lambert Run (LRM) and distance in meters from the portal (LRM000). Table 1 gives a description of each sampling site. All of the sites were sampled during two longitudinal-sampling events; of those sites, two (LRM050 and LRM138) were chosen for this diel study.

3.3.3 Remediation and previous studies

Remediation of this site began in October 2006 when the National Research Center for Coal Energy (NRCCE) made an effort to reduce dissolved metals and meet the total maximum daily load limit (TMDL) at the portal into Lambert Run and ultimately the West Fork River (Smilley 2007). Passive treatment techniques were used to reduce the dissolved metal load. The natural wetland was altered using a series of baffles to increase length of travel time in the stream in order to promote hydrolysis or precipitation of metals (Fig. 7). Post remediation, there has been an increase in vegetation (Fig. 8) in the wetland.

In a previous study at the Lambert Run Mine, diel data was obtained from the output of the natural wetland, near LRM172 (Smilley 2007). Over a thirty-hour period, cycles of Fe, Mn, Y and rare earth elements (YREE) were observed. These elements had a mean percent variation of 154% (Smilley 2007). Fe and Mn diel cycles occurred with minimum concentrations at approximately 1500 hours and maximum concentrations at approximately 0500 hours, just before sunrise.

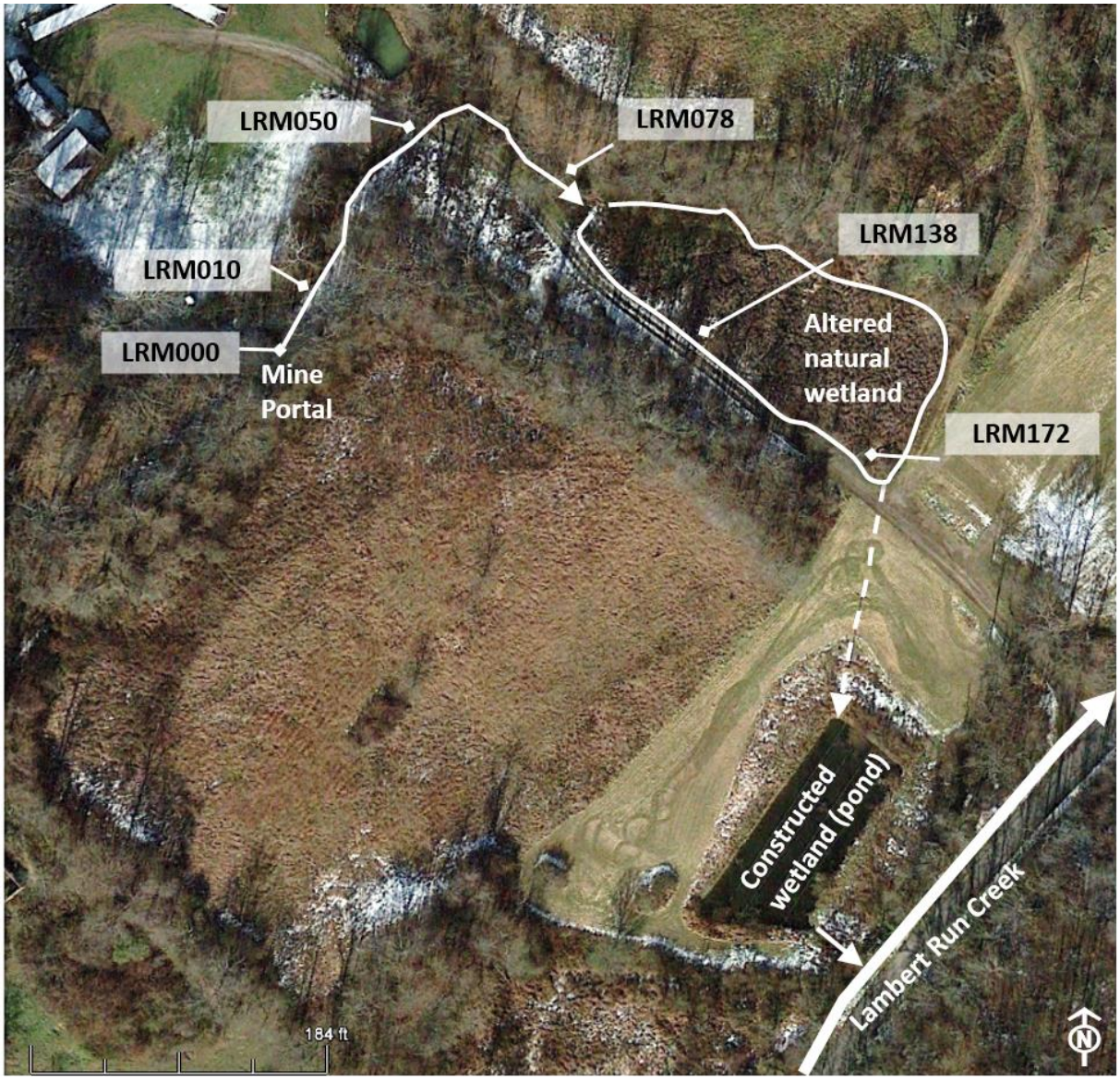

Figure 6. Plan view of Lamberts Run site indicating sampling locations and diel cycling locations. Note scale in the bottom left corner, image from Google Earth.

Table 1. Location description

Location Code	Distance from source (m)	Description	Diel or spatial
LRM000	0	At the portal, tree cover, and little emergent vegetation.	spatial
LRM010	10	~ Half way between the portal and dirt road, tree cover, and little emergent vegetation	spatial
LRM050	50	Just after flow goes under the road and reemerge, little tree cover and emergent vegetation.	diel, spatial
LRM078	78	Just before the altered wetland, and moderate tree cover.	spatial
LRM138	138	~ In the middle of the altered wetland, no tree cover, more emergent vegetation.	diel, spatial
LRM172	172	At the end of the altered wetland, no tree cover, and more emergent vegetation.	spatial

Note: LRM = Lambert Run

Figure 7. Photo of the natural wetland between LRM078 and LRM138 soon after baffles were installed. Photo by Mike Smilley, ca 2007.

Figure 8. Figure 1. Picture of the wetland taken on Nov. 7, 2013. Vegetation has totally overgrown the baffles. Researchers for scale. Photo by Donna O'Malley.

YREE element cycles occurred with minimum concentrations approximately 1900 hours and maximum concentrations at approximately 0500 hours, just before sunrise (Fig. 9). Also, pH changed over the cycling period, although the cycle was less well defined. Generally, pH reached minimum values during nighttime hours and maximums in the mid-morning, approximately 1000 hours. (Smilley 2007).

The likely mechanisms suggested for the observed diel cycles in the Smilley study are pH-temperature driven sorption reactions. Sorption of cations increased with increasing temperature and pH, however it was difficult to separate the effects of pH and temperature s (Smilley 2007). Furthermore, sorption chemistry was often difficult to quantify from precipitation, especially at sites that exhibit inconsistent pH cycles like those in this study (Smilley 2007). Despite these difficulties, however, temperature driven sorption was still considered the likely mechanism due to lack of evidence for other mechanisms.

Data from the same study observed that the initially high CO_2 concentrations at the portal decreased downstream (Fig. 10). This evidence supports degassing as distance from the portal increases and was used to choose sampling locations for the current diel cycle study.

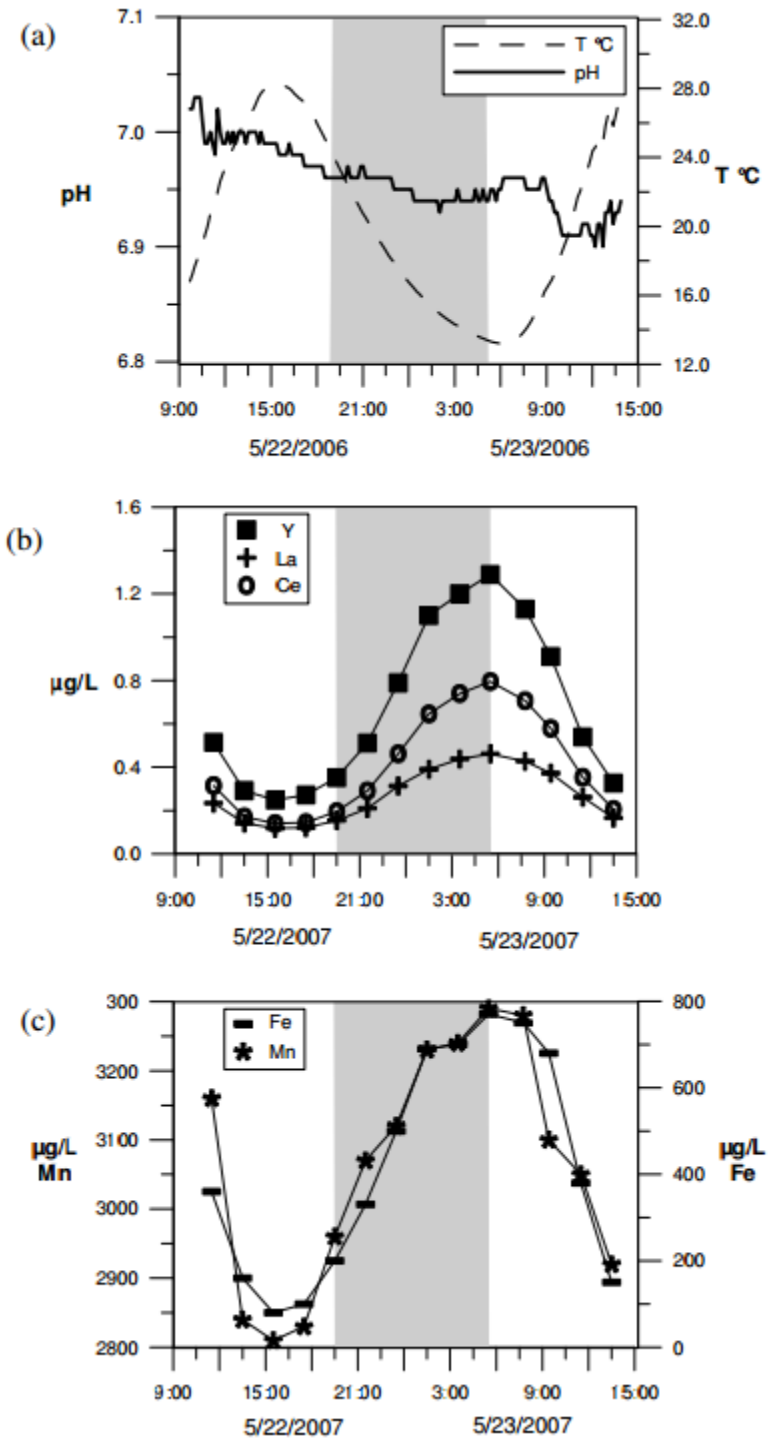

Figure 9. Diel cycling results from near LRM138. Smilley, 2007.

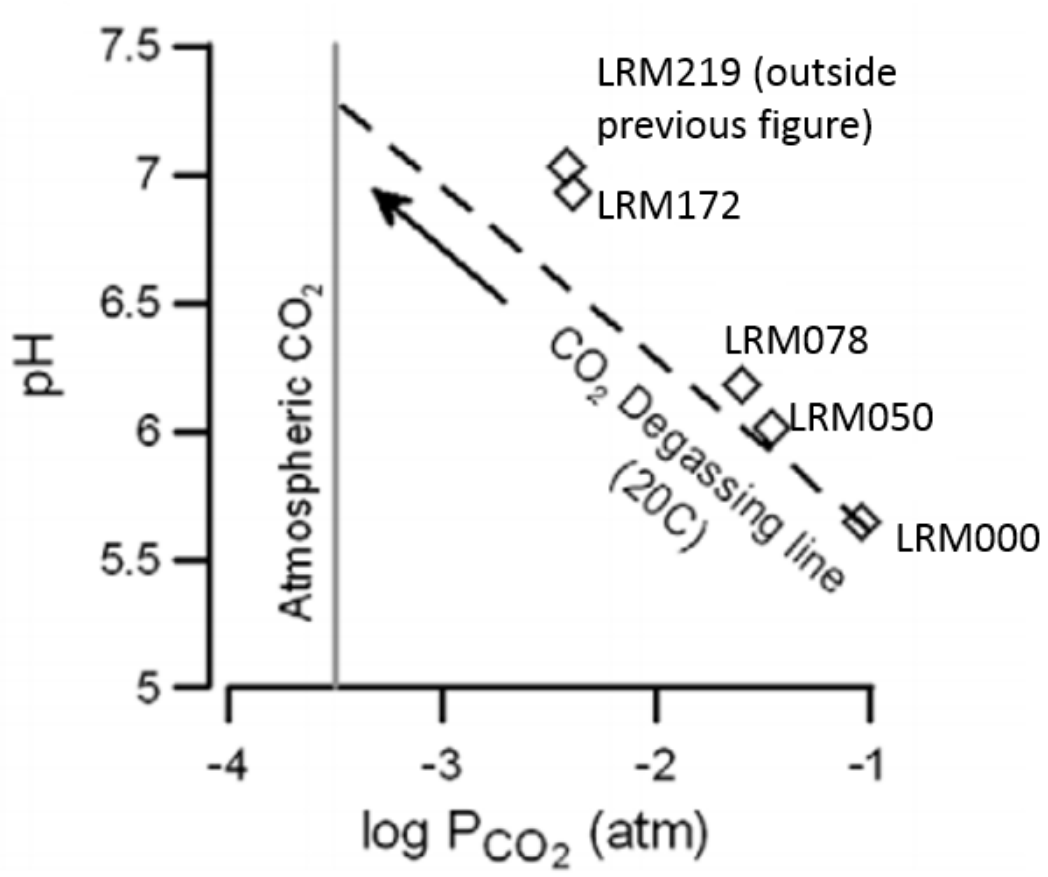

Figure 10. Figure 1. Degassing of CO2 along the sampling sites at LRM (Vesper and Smilley 2010), data collected April 2007.

4.0 Methods

4.1 Diel sampling sites

Diel sampling rounds occurred at LRM050 and LRM138, which were selected for the range of CO_2, different physical settings, different vegetative settings, and different pH ranges (Table 2). Three separate diel sampling periods took place:

- Diel A (DA): 3/14/2014-3/15/2014,
- Diel B (DB): 5/19/2014-5/20/2014, and
- Diel C (DC): 7/16/2014-7/17/2014.

Two rounds of longitudinal data were collected on 5/12/2014 and 7/03/2014 which included all six locations from the portal to the end of the natural wetland.

4.2 Temperature, pH, optical dissolved oxygen (ODO), and field data

A variety of standard field methods were used to measure temperature, pH, optical dissolved oxygen (ODO), field DIC and CO_2, iron (Fe(II) and total Fe), and discharge (Table 3).

4.2.1 Temperature, pH, and ODO

Temperature and pH were measured using a TROLL 9000 (LRM050) multi-parameter sensor data logger and a TROLL 9500 (LRM138) data logger (InSitu, Colorado, United States). These data loggers were calibrated for pH using pH 4 and 7 buffer solutions. The loggers recorded one measurement every 15 minutes. Handheld meters, an YSI 556 multi-parameter meter and YSI Professional Plus multi-parameter meter (YSI, Yellow Springs, Ohio), were used to collect additional data. To collect ODO an YSI Pro Series ODO handheld meter was set up at each site and logged ODO in mg/L every 15 min.

4.2.2 Field measurement of DIC and CO_2

Field DIC (DIC-CM) and CO_2 (CO_2-CM, where CM = carbonation meter) were measured directly using a CarboQC (Anton Parr, Gmbh, Austria) commercial beverage carbonation meter (Fig.11). Samples for CO_2 measurement were collected in 140-mL syringes, the syringes were filled and plunger attached under water. Then, the apparatus was gently tapped to drive any air bubbles to the syringe tip, the excess air was then expelled. Excess water was also expelled so

Table 2. Description of LRM050 and LRM138

	LRM050	LRM138
Description	50 m downstream of the portal. Site is just below a series of baffles for aeration. The water is distinctly orange in color.	In the middle of the natural wetland, 138 m from the portal. Flow is controlled by baffles.
Vegetation	There is little emergent vegetation here. Tree cover is moderate and surrounding brush is ~1.5 m tall in summer months.	Emergent vegetation is abundant. There are no trees at this site but surrounding vegetation is at least 1.5 m tall in summer months.
Substrate	Unconsolidated limestone rock	Soft sediment.

Table 3. Field data summary

Parameter	Instrument	Frequency
pH, temp., EC.	In Situ Troll 9000 multi-paramter	log every 15 min.
	In Situ Troll 9500 multi-parameter	log every 15 min.
	YSI 556	log every 15min
field DIC and CO_2	Anton Paar CarboQC Carbonation meter	every 2 hr (DA) every 1.5 hr (DB and DC)
Fe(II) and total Fe	DR2800 spectrometer	every 2 hr (DA) every 1.5 hr (DB and DC)
optical dissolved oxygen (ODO)	YSI Pro Series ODO Meter	log every 15 min.

Figure 11. Commercial carbonation beverage meter, CarboQC. Photo by Jill Riddell.

that the syringe contained 120-140 mL of sample. The syringe was then attached to the meter via a piece of tubing and the sample delivered to the instrument. Approximately 100 mL of sample was used to rinse the meter chamber. Then dissolved CO_2 in the sample was measured (in g/L) by filling the chamber on the meter with ~10 mL of sample. The meter expands the volume of the sample by 10% and then by 30% and uses the pressure and temperature equilibrium during both expansions to calculate the CO_2 concentration in g/L based on the difference in the relative solubilities of CO_2 and and other gases present (Vesper and Edenborn 2012). The meter reports dissolved CO_2 concentration in g/L and temperature in Celsius. Three or more samples were collected at each sampling time and reported as an average.

To measure DIC using the CarboQC meter, 10 mL of Orion Carbon Dioxide Buffer (citrate) is added to a 100 mL sample (collected in the same way as for CO_2) and is mixed by inverting the syringe end over end for approximately one minute, using a gloved fingertip to cover the syringe tip. Then, 110 mL of the mixed sample was delivered to the meter, the meter results and pH of the mixed solution were recorded. DIC was then calculated by manipulating the carbonate equilibrium equation (Eq. 4). The equilibrium constants (K_1 and K_2) are adjusted for temperature using the equations set by Plummer and Busenberg (1982) and the gammas are fixed values (Vesper et al. 2015). Multiplying by 1.1 is a correction factor for volume dilution by the buffer. See Appendix I for more details on this method.

$$DIC = \left[\frac{aCO_2}{\gamma_{CO_2}} + \left(\frac{K_1}{a_H \gamma_{HCO_3^-}}\right) aCO_2 + \left(\frac{K_1 K_2}{a_H^2 \gamma_{CO_3^{2-}}}\right)\right] x\ 1.1 \qquad \text{Eq. 4}$$

The addition of the buffer brings the pH of the sample down to a value where all DIC should be present in the form of CO_2 gas. The buffer also stabilizes the ionic strength of the solution so that the same activity coefficient of each carbonate species can be used for each sample. Three or more samples were collected at each sampling time and reported as an average.

4.2.3 Fe(II) and total Fe

Fe(II) concentrations were measured according to the ferrozine method (Stookey 1970) which involves adding ferrozine ($C_{20}H_{13}N_4NaO_6S_2$) solution to a sample to complex the ferrous ions. The complex forms a purple color in proportion to the concentration of Fe(II). The

concentration was determined by measuring absorbance at a wavelength of 562 nm using a Hach DR2800 spectrophotometer (Hach Co., Colorado, United States). Ferrozine solution was made using 0.25 g of ferrozine, 2.75 g HEPES buffer, and 5 mL of 1 N NaOH in a 250-mL volumetric flask and brought to volume with deionized water. Freshly made solution was used for each sampling event.

In the field, ferrozine was added to 4-mL cuvettes by pipetThe cuvettes were carried to the sampling location and sample water was added to the cuvettes by pipet and then capped. Each cuvette was inverted 5-10 times to mix the solution, wiped clean with a fresh Kimwipe, and inserted into the spectrophotometer for absorbance reading. During the first of three diel sampling rounds, a fixed ratio of 2 mL ferrozine and 2 mL of sample water was used at LRM050 and 1 mL ferrozine and 3 mL sample at LRM 138. During the second and third diel sampling rounds, a ratio of 1 mL ferrozine and 3 mL of sample was used at both sites. Sampling ratios are different between sampling rounds because enough iron must be present to react with the compounds and it was theorized that Fe amounts varied during seasons. The ratios were determined in the two hours before each sampling round began. At least six samples were taken at each sampling time. A calibration curve of Fe(II) concentrations was created using standard solutions of Fe(II) and the same ferrozine solution and sample ratio(s) used in the field. A separate curve was created for each diel collection round and used to determine Fe(II) concentrations in mg/L of each sample collected in the field.

Total Fe was measured using a similar method. Ferrozine and 0.5 N hydroxylamine HCl were both added to the cuvettes before the sample. Hydroxylamine HCl reduces all Fe to the Fe(II) species (Lovley and Phillips, 1987). During the first diel sampling round, a ratio of 2 mL ferrozine, 1 mL hydroxylamine HCl, and 2 mL sample was used at LRM050 and a ratio of 1 mL ferrozine, 1 mL hydroxylamine HCl, and 3 mL sample at LRM138. For the second and third diel sampling rounds, a ratio of 0.5 mL of ferrozine, 0.5 mL hydroxylamine HCl, and 3 mL of sample was used at both sites. Again, ratios differed due to the same reason described above. At least six samples were taken per sampling time. Absorbance of field samples was analyzed in the same way as the Fe(II) samples. A calibration curve was created using samples of standard solution and subjected to the same method. Again, a separate curve was created for each diel round and used to determine concentrations of total Fe of field samples.

4.3 Sample collection and laboratory analyses

Samples were submitted for laboratory analysis of cations (filtered), anions (filtered), and $\delta^{13}C_{DIC}$ as described in the following sections (Table 4).

4.3.1 Cations and anions

Samples for analysis of anions and cations were collected at each sampling time. Samples for cation and anion analysis were collected by filling and assembling a syringe under water, attaching a 0.45 um Whatman filter, and delivering the sample to an HDPE (high-density polyethylene) bottle until the bottle was full. Then HNO_3 was delivered to the cation samples via 1-mL, disposable pipets for preservation leaving as minimal headspace as possible.

The samples were analyzed at the Department of Energy, National Energy Technology Laboratory (NETL) in Pittsburgh, PA. Samples were analyzed for cations by Inductively Coupled Plasma Optical Emission Spectroscopy (ICP-OES), EPA method 6010 B; for anions by Ion Chromatography (IC), EPA method 300.1; and for trace elements by Inductively Coupled Plasma- Mass Spectrometry (ICP-MS), EPA method 6020 A. For quality control, two duplicate samples were collected during each diel round.

From all field and laboratory data outlined above, acidity was calculated for two sampling rounds of spatial analysis (Eq. 5).

$$Acidity\frac{meq}{L} = 10^{-pH} + 3[Fe^{3+}] + 2[Fe^{2+}] + 2[Mn^{2+}] + 3[Al^{3+}] \quad \text{Eq. 5}$$

Here, brackets represent concentration of metals.

4.3.2 $\delta^{13}C_{DIC}$

Isotope samples for $\delta^{13}C_{DIC}$ were collected in 40-mL amber glass vials with butyl or silica septa and preserved with 3 drops benzalkonium chloride (BAC) solution. Samples were collected by adding the BAC to the sample bottle first and then filling the bottle, quickly, with a beaker of sample and attaching the cap immediately. The samples were analyzed on a Thermo Finnigan DeltaPlus XL isotope ratio mass spectrometer with a GasBench II universal on-line gas preparation device (Thermo Fisher Scientific, Waltham, MA, USA) at the Light Stable Isotope Mass Spectrometry Laboratory at the University of Florida. Carbon isotopic ratios of DIC were measured by injecting water into vials that contained 0.5 mL of phosphoric acid and then filled with helium. The acidification of the sample releases all DIC into the headspace and the mixture

Table 4. Summary of laboratory analysis methods

Parameter	Bottle, number, size, and material	Preservative or digestive	Laboratory and method
Cations, filtered	1 x 125 mL HDPE	1 mL trace-element grade HNO_3	NETL ICP-OES (EPA Method 6010 B)
Cations, unfiltered-digested	1 x 250 mL HDPE	2 mL trace-element grade HNO_3	NETL ICP-OES (EPA Method 6010 B)
Anions	1 x 60 mL HDPE	No	NETL Ion Chromatography (EPA Method 300.1)
$\delta 13C_{DIC}$	1 x 30 mL glass vial	3-4 drops BAC	Thermo-Finnigan gas bench and mass spec. University of Florida

Filters were 0.45-um Whatman filters and used for anion and cations, filtered.

of CO_2 and He is sampled by the GasBench II. CO_2 and any N_2 are separated by gas chromatography prior to being measured on the mass spectrometer. Samples were collected in duplicate at each sampling time.

4.4 Geochemical software analysis

The solution spread function in PhreeqC (Parkhurst and Appelo, 2013 USGS) was used to calculate the charge balance error (CBE) of the data from all three diel rounds, to assess data quality. If the data for a sample had a CBE < 10%, they were considered acceptable.

4.5 Modeling and statistical analysis

Following the method of Kurz etal. (2013), a cosine model was fit to a graph of each parameter concentration or value over time since diel patterns can be expected to follow a similar pattern as a cosine curve (Appendix I). The results from the model fit and the raw data were then statistically analyzed using an F-test with the raw data as the null hypothesis. Parameters whose cosine model fit had a p-value of less than 0.01 were considered for further analysis and discussion. The cosine model fit predicts a mean for the data as well as a phase which correlates to the time of peak concentration for that parameter. For all parameters subjected to the cosine model fit, the model predicted a mean within 5% of the actual mean of the data. The results from the model fit and statistical analysis are graphed on polar plot where p-value is graphed on the radial axis (decreasing going away from the center) and phasing as a function of time (24-hours) on the angular axis. This allows for easy interpretation of the model fit relative to separate parameters. Parameters that plot near each other on the polar plot are considered to have similar phasing, meaning they reach maxima and minima values at approximately the same time. Parameters that plot opposite each other on the polar plot are considered to have opposite phasing.

5.0 Results

5.1 Data overview

Three rounds of diel data and two rounds of spatial data were collected (Table 5). For the spatial rounds (5/12/2014 and 7/3/2014), pH, temperature, and ODO were recorded as grab samples.

For each of the three diel sampling rounds 20 parameters were included for detailed analysis of diel concentration patterns and are discussed in this section and tabulated in Appendix II. The parameters were chosen were in groups based on: relationship to coal mine drainage chemistry (e.g. Fe, Mn, SO_4), relationship to CO_2 and limestone bedrock (Ca, Mg, CO_2-CM, and DIC-CM), trace elements (e.g. Ni, Zn, As), and meter data (pH, temperature, and ODO). After modeling and statistical analysis, any parameter with a cosine model fit p-value $\leq$ 0.01 was considered to have a significant diel pattern.

Appendix II shows concentrations/values of all 20 parameters chosen for analysis at each sampling time as well as results from the cosine model analysis. Appendix III shows summary graphs of all data from each sampling round and location; all data specific to each sampling round and location are highlighted in the following sections and are summarized in tables and graphs throughout the text.

As the seasons progressed, the amount of vegetation and tree cover increased at both LRM050 and LRM138. Figures 12 and 13 show the progression of increased vegetation at both sites.

5.2 Data quality

Data quality for the laboratory analysis methods was assessed by calculating the charge balance error (CBE). Samples with a CBE of -10% to +10% were considered to be acceptable quality. Duplicate samples were also collected and analyzed for cations and anions according to the described methods for both spatial and diel sampling rounds. Percent difference between duplicate samples was variable but if the individual samples had an acceptable CBE, the data were still considered to be acceptable quality. Of the ions considered for further analysis and discussion, 70% of sample duplicates agreed within 10%. No entire sample rounds were

Table 5. Summary of collected parameters

	spatial		diel cyling					
	LRM000, 010, 050, 078, 138, 172		LRM050	LRM 138	LRM 050	LRM138	LRM050	LRM138
			A		B		C	
	5/12/14	7/3/14	3/14/2014-3/15/2014		5/19/2014-5/20/2014		7/16/2014-7/17/2014	
Field monitor								
pH	✓	✓	✓	✓	✓	✓	✓	✓
Temp	✓	✓	✓	✓	✓	✓	✓	✓
Light intensity	✓	✓	✓	✓	✓	✓	✓	✓
ODO	✓	✓	✓	✓	✓	✓	✓	✓
Field analysis								
CO_2	✓	✓	✓	✓	✓	✓	✓	✓
DIC	✓	✓	✓	✓	✓	✓	✓	✓
Fe (II)	✓	✓	✓	✓	✓	✓	✓	✓
Fe tot	✓	✓	✓	✓	✓	✓	✓	✓
Discharge	-	-	✓	✓	✓	✓	✓	✓
Lab analysis								
DIC	✓	✓	✓	✓	✓	✓	✓	✓
Filtered cations	✓	✓	✓	✓	✓	✓	✓	✓
Anions	✓	✓	✓	✓	✓	✓	✓	✓
$\delta^{13}C_{DIC}$	✓	✓	✓	✓	✓	✓	✓	✓

Figure 12. Comparison photo of vegetation at LRM050 in March (DA), left, and July (DC), right.

Figure 13. Figure 1. Comparison photo of vegetation at LRM138 in March (DA), left, and July (DC), right.

excluded but individual samples were excluded if the results of analysis were suspect (Appendix III). About 30 individual sample points were left out of analysis from a total of ~1400 individual sample points.

5.3 Longitudinal results

Longitudinal sampling rounds were conducted before the May and July diel rounds to determine range of concentration of parameters (between the sampling locations and between seasons. LRM000, LRM010, and LRM050 are all located in a limestone channel while LRM078, LRM138, and LRM172 are all located in the wetland. The results from both the 5/12/2014 and 7/03/2014 longitudinal sampling rounds show a general increase in pH and general decrease in CO_2-CM, DIC-CM, and acidity (Fig. 14) from the portal (LRM000) to the end of the natural wetland (LRM172). Calcium and magnesium showed a general decrease on 5/12/2014 but a slight increase on 7/03/2014. The percent change in concentration of parameters from LRM000 to LRM172 ranges from 98% (Al) to 5% (Ca+Mg) on 5/12/2014 and 99% (Fe(II)) to 17% (Ca+Mg) on 7/03/2014 (Tables 6 and 7). The pH and Ca+Mg concentration decreased from 5/12 to 7/03 while acidity, CO_2-CM, and DIC average values all increased (Table 6 and 7).

5.4 DA results: 3/14/2014-3/15/2014 (March)

The first of the three diel cycle sampling rounds was conducted in late winter/early spring at both LRM050 and LRM138. Sampling began at 1400 3/14/2014 just before peak sun and ended on 3/15/2014 at 1900; the sun set at approximately 1920 on 3/14 and rose at approximately 0735 on 3/15. On 3/14/2014 the maximum and minimum air temperatures were approximately 15.6 C and 4.4 C (Weather Underground). Trace amounts of precipitation fell between ~0000 hours and 0400 hours on 3/15/2014.

At LRM050, six parameters (pH, temperature, CO_2-CM, ODO, Al, and K) had statistically significant diel patterns at LRM050 ($p \leq 0.01$) based on their fit of a cosine model (Table 8, in bold). The cosine model for the Y data had a p-value 0.0125. The five parameters in Table 8 not in bold show statistically significant diel patterns in later sampling rounds. A summary graph of the seven parameters, as well as DIC, is shown in Fig. 15. This figure shows the changes in concentration of each parameter with its cosine model fit.

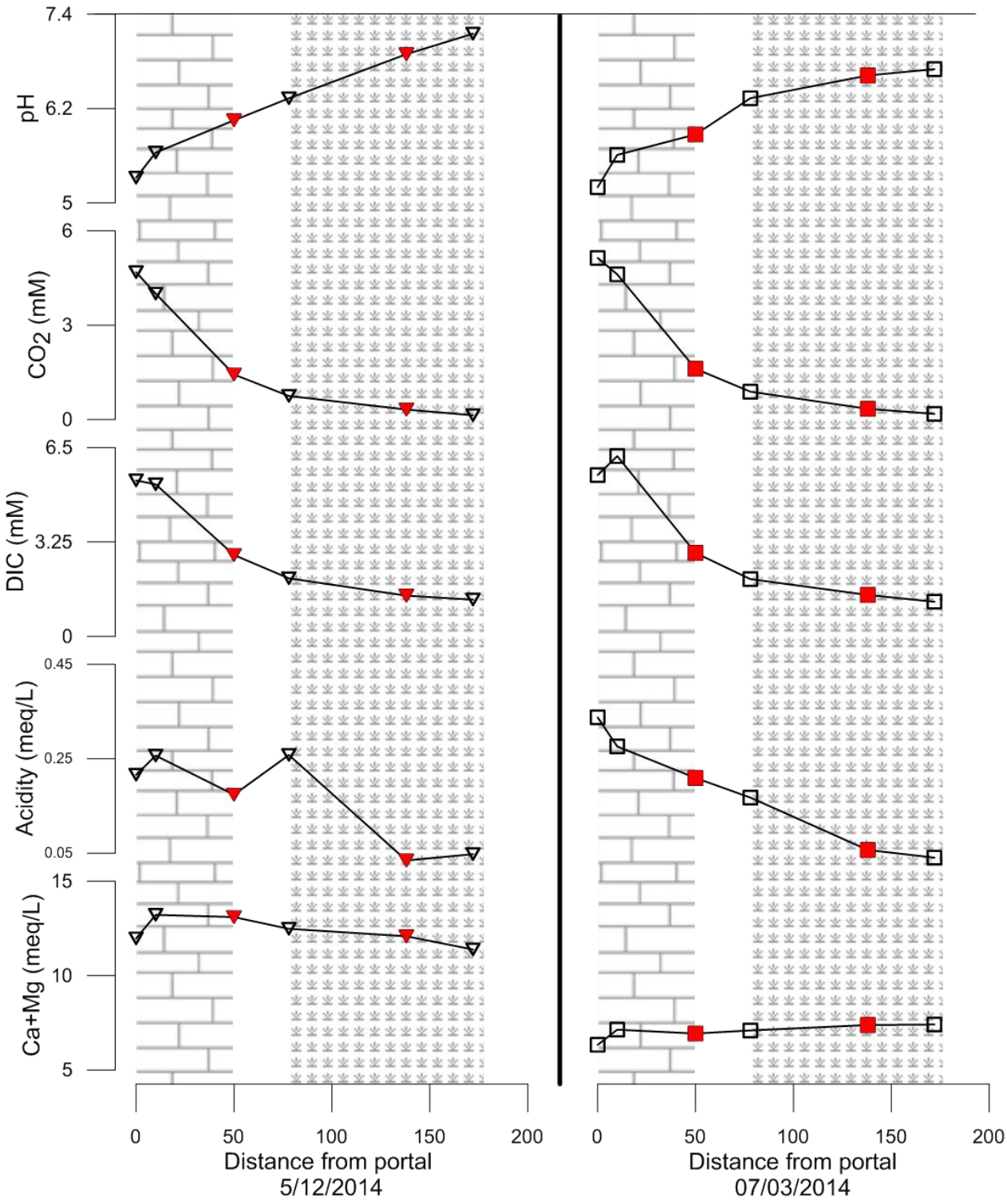

Figure 14. Results from spatial sampling rounds. Decrease in pH and increase in other parameters are shown as distance from the portal increase. Substrate type is also shown- bricks pattern is limestone and leaf pattern is wetland. Solid red symbols indicated LRM050 and LRM138.

Table 6. Spatial results 5/12/2014

parameter	Conc. @ LRM000	% change to LRM172	Increase or decrease downstream
pH	5.32	34.4	increase
CO_2-CM (mM)**	4.68	97.1	decrease
DIC-CM (mM)**	5.34	76.4	decrease
Acidity (meq/L)	2.21E-4	84.3	decrease
Fe(III) mM	BDL*	BDL*	N/A
Fe(II) mM	5.0E-5	96.8	decrease
Mn mM	5.82E-5	74.3	decrease
Al mM	1.88E-5	97.5	decrease
Ca+Mg meq/L	1.20E-2	4.89	decrease

*BDL= below detection limit; see Appendix I for detection limit data.

**CM = carbonation meter

Table 7. Spatial results 7/03/2014

parameter	Conc. @ LRM000	% change to LRM172	Increase or decrease downstream
pH	5.20	28.8	increase
CO_2-CM (mM)	5.14	96.5	decrease
DIC-CM (mM)	5.55	78.5	decrease
Acidity (meq/L)	3.44E-4	88.1	decrease
Fe(III) mM	2.78E-6	101	decrease
Fe(II) mM	8.33E-5	99.1	decrease
Mn mM	5.61E-5	66.3	decrease
Al mM	1.69E-5	97.3	decrease
Ca+Mg meq/L	6.33E-3	16.97	increase

Table 8. LRM050 DA-March: Diel variability of cycling parameters

Parameter	Max	Min	Time of max value	% RSD	p-value
pH	**6.32**	**6.23**	**3/15 1744**	**3.00E-1**	**<0.01**
Temperature (C)	**12.53**	**12.00**	**3/15 1514**	**1.44**	**<0.01**
ODO(mg/L)	**9.50**	**9.21**	**3/14 1412**	**7.90E-1**	**<0.01**
CO_2-CM (g/L)	**4.80E-2**	**4.20E-2**	**3/15 300**	**3.79**	**<0.01**
DIC-CM (mM)	2.45	2.09	3/15 1500	3.92	1.91E-1
$\delta^{13}C_{DIC}$ (permil)	8.75E-1	1.57E-1	3/15 1100	32.1	9.25E-2
Fe(II) (mg/L)	8.34E-1	6.98E-1	3/15 1500	4.64	1.36E-2
Fe_{TOT} (mg/L)	8.43E-1	7.36E-1	3/15 1700	3.50	7.27E-2
Al (ug/L)	**145**	**86.9**	**3/14 2100**	**17.4**	**<0.01**
Y (ug/L)	2.64	2.36	3/15 1700	3.18	1.25E-2
Zn (ug/L)	17.1	63.0	3/15 0900	56.2	8.18E-2
K (mg/L)	**3.92**	**3.50**	**3/14 1700**	**3.47**	**<0.01**

*ODO = optical dissolved oxygen. Parameters in bold indicate statistically significant diel behavior based on the cosine model.

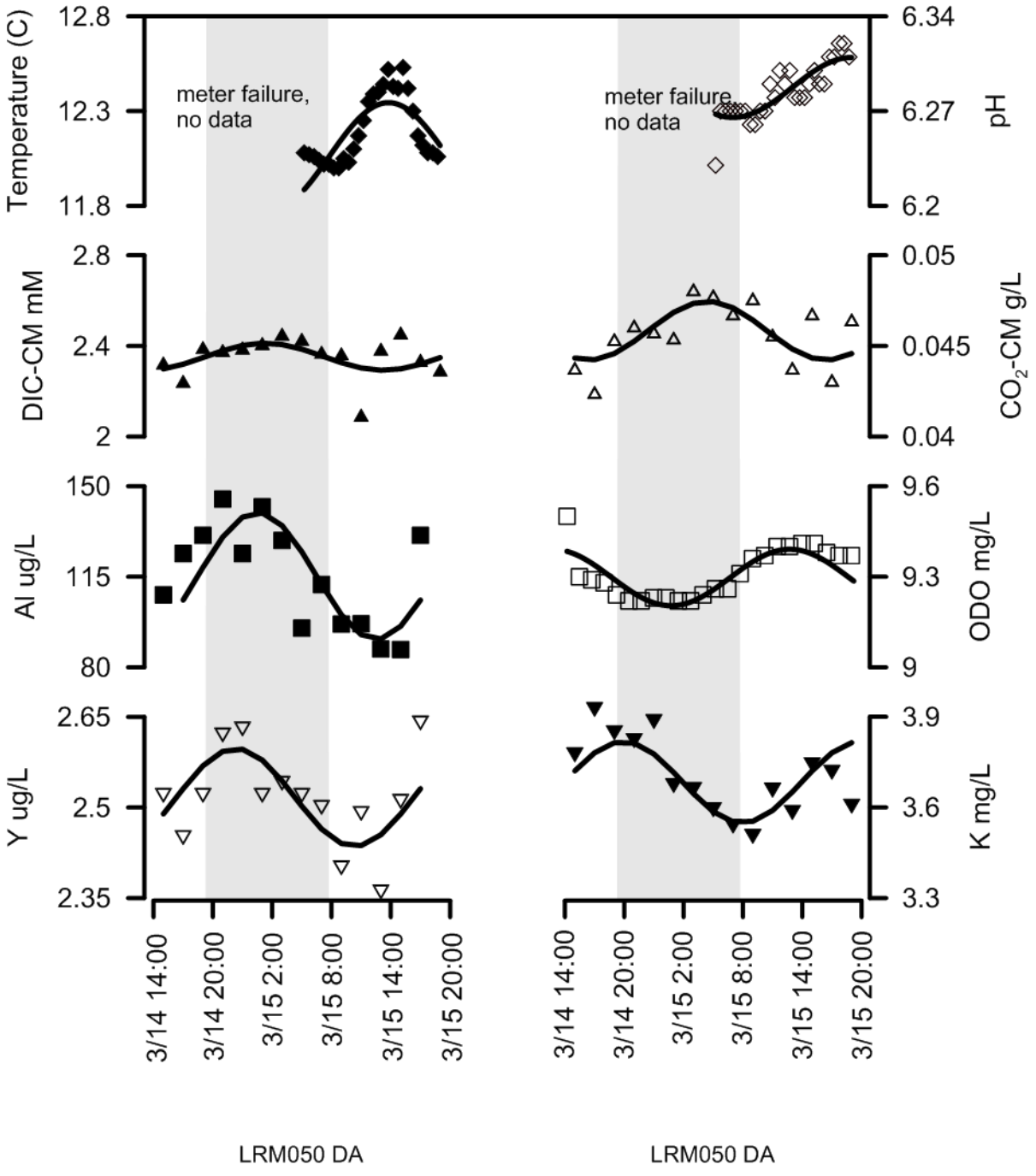

Figure 15. LRM050 DA-March: Cyclical behavior of parameters having a statistically significant cosine model fit at α=0.01 and Y and DIC. Symbols are used for the data, lines are the cosine model fit. Shaded areas represent hours of darkness.

Temperature and ODO all cycled in approximately the same phase (generally increasing in concentration or value during the same time interval); these parameters increased during the daytime hours and decreased during the nighttime hours (Fig. 15). Peak values occurred in mid to late afternoon. K, Al, and Y all generally increased during the day and decreased at night; peak concentrations occurred in late evening around sunsetCO_2 and pH cycled almost directly out of phase with each other- peak pH values occurred in midafternoon and CO_2 in late night (0300). CO_2 and pH did not cycle in phase with any other parameter (Fig. 16). These parameters (including Y) had an average relative standard deviation (RSD) 4.34% with a range of 0.300% (pH) to 17.4% (Al).

At LRM138, seven different parameters had statistically significant diel patterns (Table 9, in bold) and the five parameters not in bold had statistically significant diel patterns in later sampling rounds. A summary graph of the seven parameters plus $\delta^{13}C^{DIC}$ (significant at $p \leq 0.05$, with $p=0.025$), is shown in Fig. 17. This figure shows the changes in concentration of each parameter with its cosine model fit.

Temperature, pH, ODO all generally reached maximum concentration in approximately the middle of the daytime hours. Ni, DIC, and CO_2 cycled out of phase with temperature, pH, and ODO, these generally reached maximum concentration in the middle of the nighttime hours. Arsenic did not cycle in phase with any of the other elements; peak concentration of As occurred at 1200 on 3/15 (Fig. 18). These parameters had an average RSD 9.31% with a range of 1.12% (pH) to 18.1% (As).

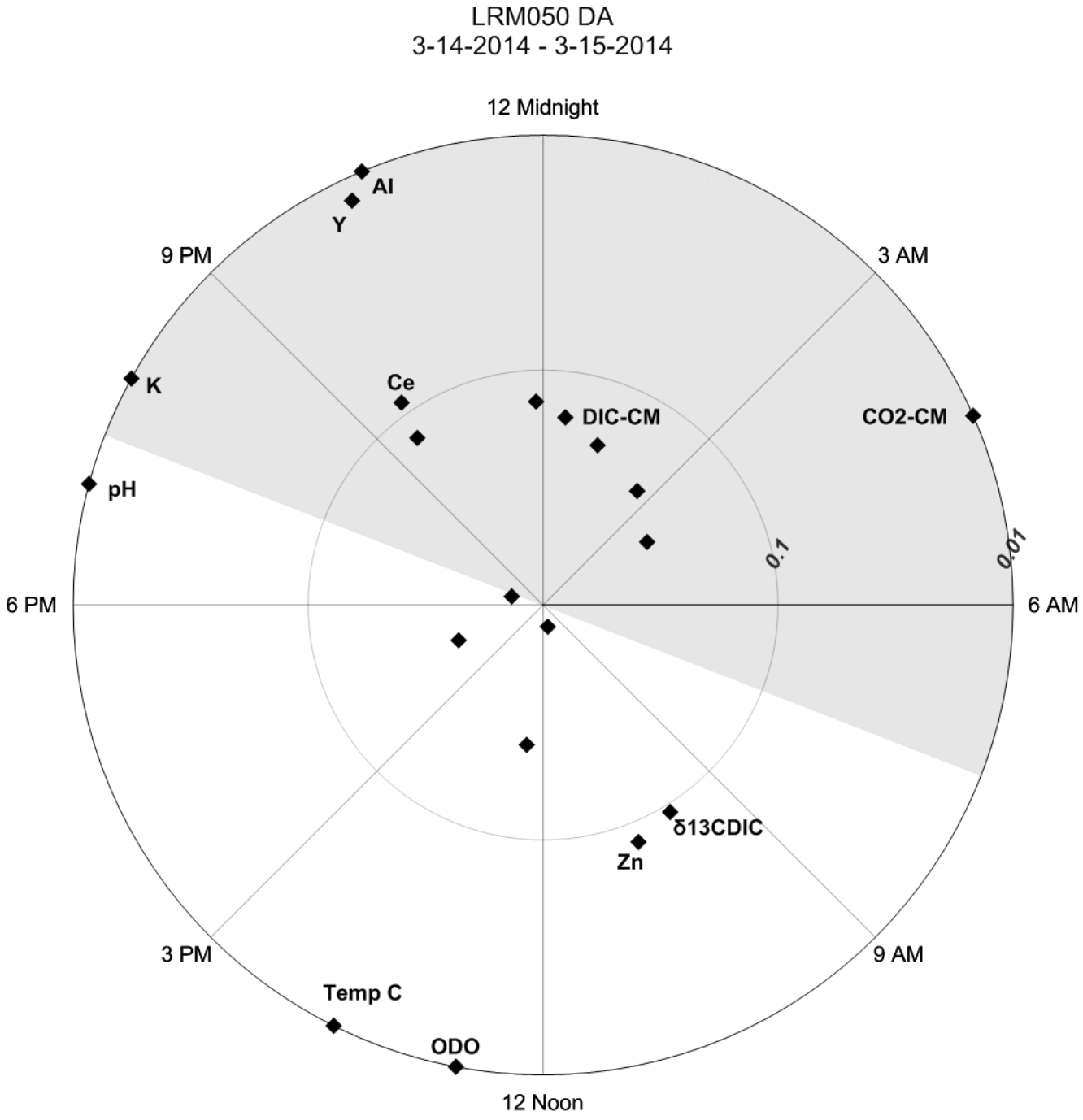

Figure 16. Polar plot for LMR050 DA-March. Parameters that had significant cosine model fit are those with p<= 0.01. The time of predicted maximum concentration or value is graphed on the angular axis and p-value on the radial axis. For example, the predicted maximum concentration time based on the cosine model fit for Al occurs around 10:30pm and the p-value of the modelfit relative to the date was at least 0.01. Other interesting points are also labeled.

Table 9. LRM138 DA-March: Diel variability of cycling parameters

Parameter	Max	Min	Time of max value	% RSD	p-value
pH	**6.93**	**6.70**	**3/14 1411**	**1.12**	**<0.01**
Temperature (C)	**12.5**	**16.9**	**3/15 1315**	**10.3**	**<0.01**
ODO(mg/L)	**11.5**	**8.66**	**3/15 1235**	**10.8**	**<0.01**
CO_2-CM (g/L)	**1.20E-2**	**7.37E-3**	**3/15 0400**	**13.3**	**<0.01**
DIC (mM)	**1.77**	**1.36**	**3/15 0200**	**6.64**	**<0.01**
$\delta^{13}C_{DIC}$ (permil)	-3.64E-1	-1.54	3/14 1400	38.9	2.52E-2
Fe(II) (mg/L)	BDL*	BDL			
Fe_{TOT} (mg/L)	BDL	BDL			
Mn (mg/L)	8.69E-1	6.91E-1	3/14 1600	5.83	0.317
Y (ug/L)	4.24E-1	1.76E-1	3/15 0800	25.4	0.660
Ni (ug/L)	**8.57**	**7.38**	**3/15 0000**	**4.90**	**<0.01**
As (ug/L)	**9.68E-2**	**5.29E-2**	**3/15 1200**	**18.1**	**<0.01**

Parameters in bold indicate statistically significant diel behavior based on the cosine model.

BDL = below detection limit. See Appendix II for detection limit values.

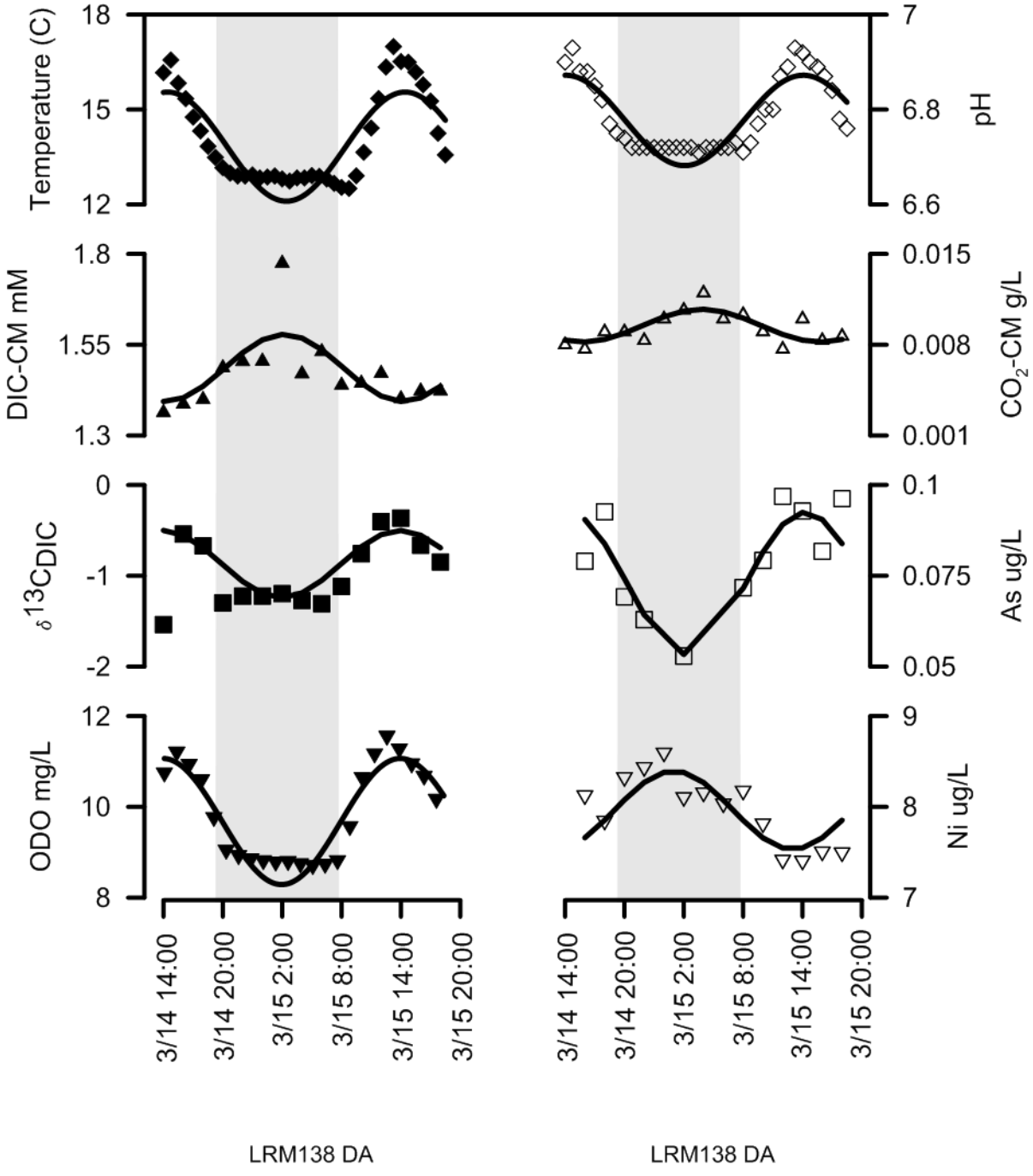

Figure 17. LRM138 DA-March: Cyclical behavior of parameters having statistically significant cosine model fit at α=0.01 and δ13CDIC. Symbols are used for the data, lines are the cosine model fit. Shaded areas represent hours of darkness.

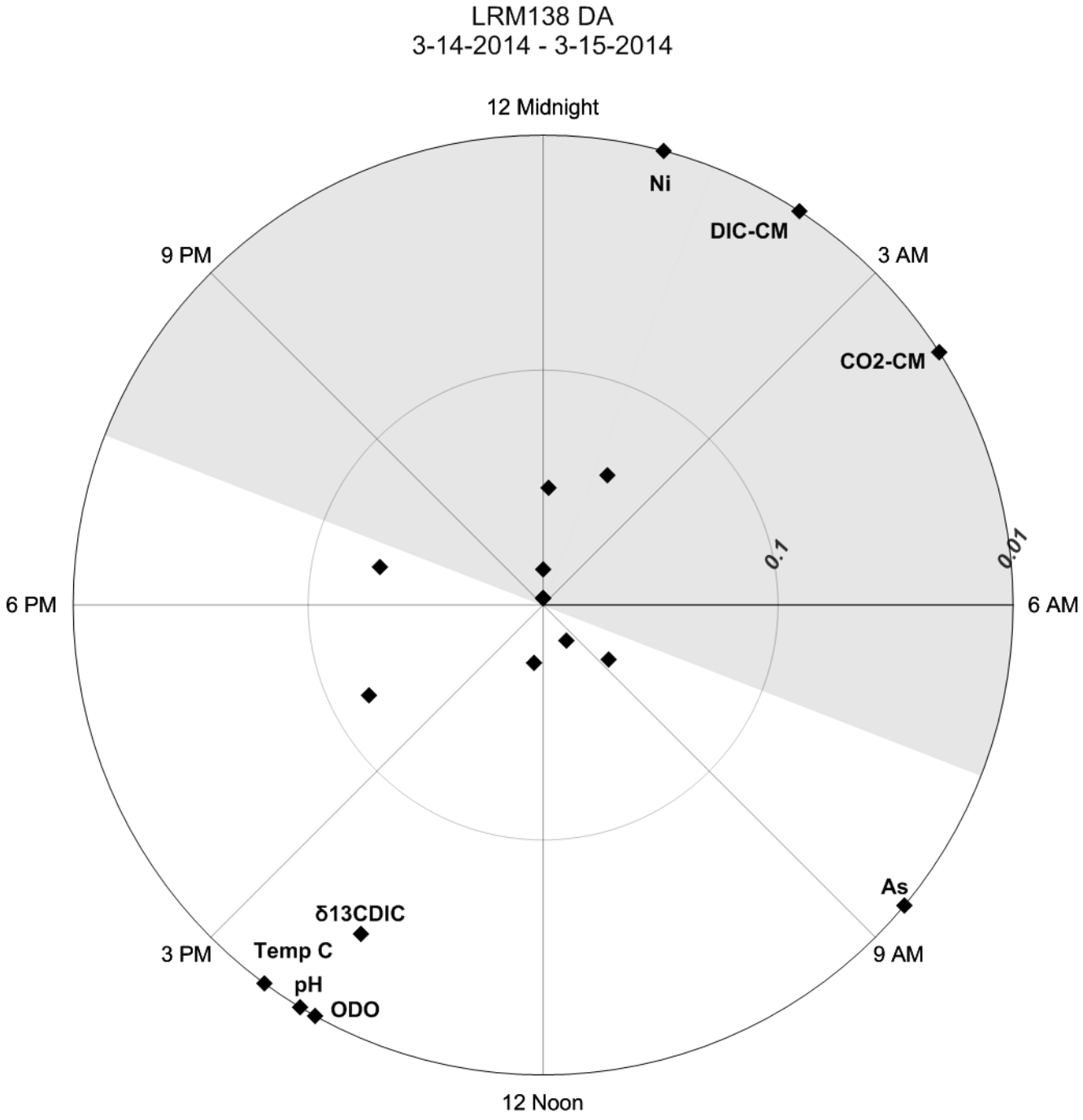

Figure 18. Polar plot for LMR138 DA-March. Parameters that had significant cosine model fit are those with p<= 0.01. The time of predicted maximum concentration or value is graphed on the angular axis. Other important points are also labeled.

5.5 DB results: 5/19/2014-5/20/2014 (May)

The second of the three diel cycle sampling rounds was conducted in the spring at both LRM050 and LRM138. Sampling began at 1400 5/19/2014 just before peak sun and ended on 5/20/2014 at 1915, the sun set at approximately 2045 on 5/19 and rose at approximately 0630 on 5/20. The maximum and minimum air temperatures were approximately 23.9 C and 6.67 C (Weather Underground).

5.5.1 LRM050 and LRM138 - May

At LRM050, only five parameters (pH, temperature, ODO, Al, and Zn; Table 10, in bold) had significant cosine model fit. A summary graph of the five parameters, as well as DIC and CO_2, is shown in Fig. 19. This figure shows the changes in concentration of each parameter with its cosine model fit.

These five parameters did not cycle in phase with each other (Fig. 20). Times of peak concentration and increasing values can be seen in Table 10 and Fig. 19. The parameters had an average RSD of 20.2% ranging from pH 0.60% (pH) to 70.2% (Zn). Though they did not show significant diel patterns, CO_2 and DIC did reach maximum value shortly after temperature and followed a similar pattern of concentration change (Fig. 19).

At LRM138, eight parameters had significant diel patterns (Table 11, in bold) but are different than those in Diel A. A summary graph of the eight parameters plus CO_2 and DIC is shown in Fig. 21. This figure shows the changes in concentration of each parameter with its cosine model fit.

Temperature, pH, ODO, and $\delta^{13}C_{DIC}$ all generally reached maximum concentration in approximately the middle of the daytime hours. Y, Fe_{TOT}, and Mn cycled out of phase with temperature, pH, ODO, and $\delta^{13}C_{DIC}$, they generally reached maximum concentration in the mid to late evening hours. Ni did not cycle in phase with any of the other elements; peak concentration of Ni occurred at 0500 on 5/20(Fig. 22). These parameters had an average RSD 11.3% with a range of 2.06% (pH) to 27.9% ($\delta^{13}C_{DIC}$).

Table 10. LRM050 DB-May: Diel variability of cycling parameters

Parameter	Max	Min	Time of max value	% RSD	p-value
pH	**6.24**	**6.07**	**5/19 1515**	**0.60**	**<0.01**
Temperature (C)	**13.1**	**12.3**	**5/20 1400**	**2.02**	**<0.01**
ODO(mg/L)	**7.99**	**7.63**	**5/19 1406**	**1.10**	**<0.01**
CO_2-CM (g/L)	9.43E-2	5.57E-2	5/20 1915	13.1	1.62E-1
DIC-CM (mM)	3.21	2.49	5/20 1915	6.56	7.92E-2
$\delta^{13}C_{DIC}$ (permil)	-5.57	-6.75	5/19 1415	9.80	1.99E-1
Fe(II) (mg/L)	2.09	1.89	5/20 1915	2.13	7.71E-1
Fe_{TOT} (mg/L)	2.09	1.33	5/20 1615	8.19	5.32E-1
Al (ug/L)	**269**	**78.1**	**5/20 1915**	**27.3**	**<0.01**
Y (ug/L)	3.07	2.72	5/20 174	3.12	1.51E-1
Zn (ug/L)	**163**	**21.5**	**5/20 1015**	**70.2**	**<0.01**
K (mg/L)	4.70	4.05	5/20 0415	4.15	1.35E-1

Parameters in bold indicate statistically significant diel behavior based on the cosine model.

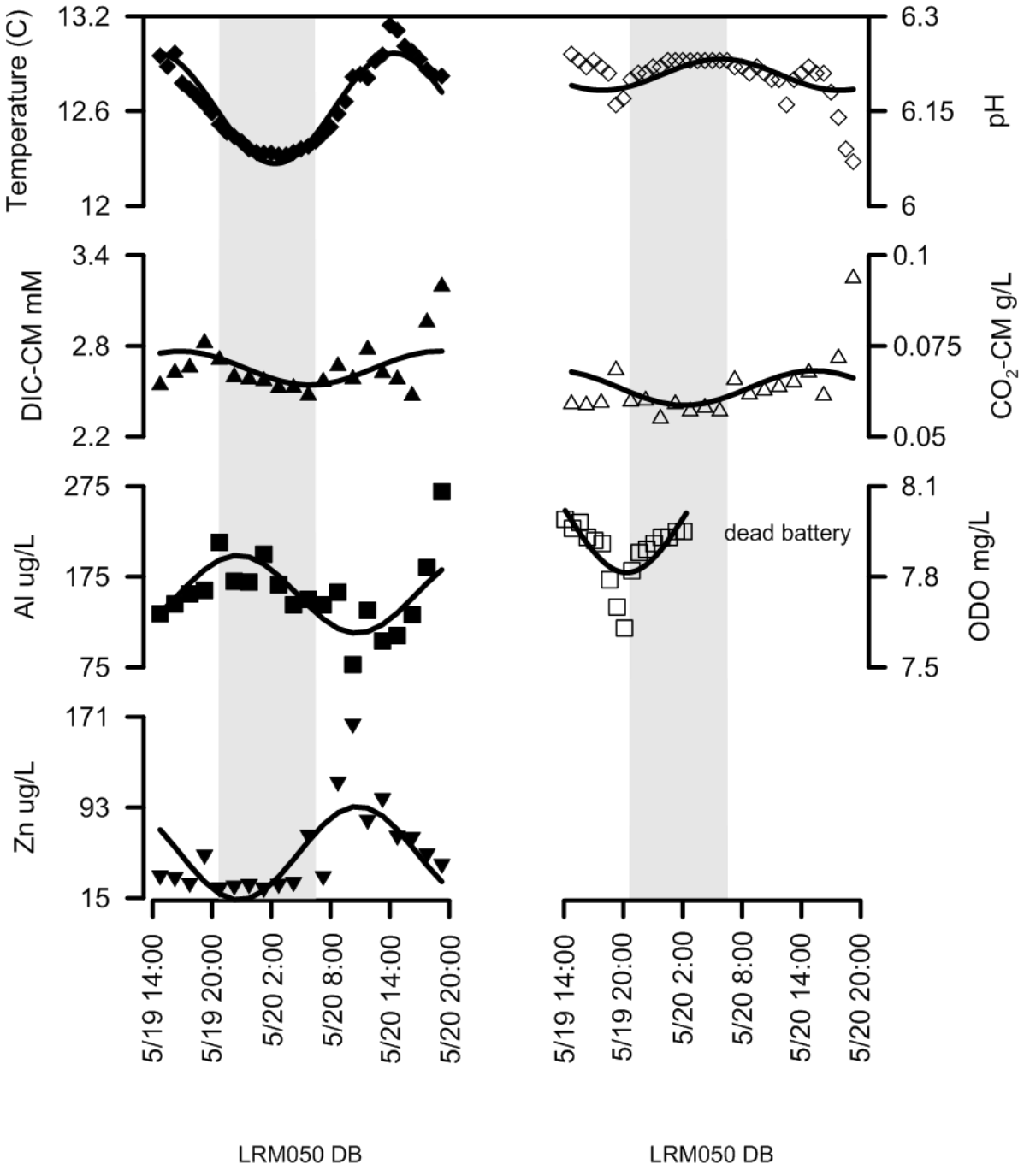

Figure 19. LRM050 DB-May: Cyclical behavior of parameters having a statistically significant cosine model fit at α=0.01 and CO2 and DIC. Symbols are used for the data, lines are the cosine model fit. Shaded areas represent hours of darkness.

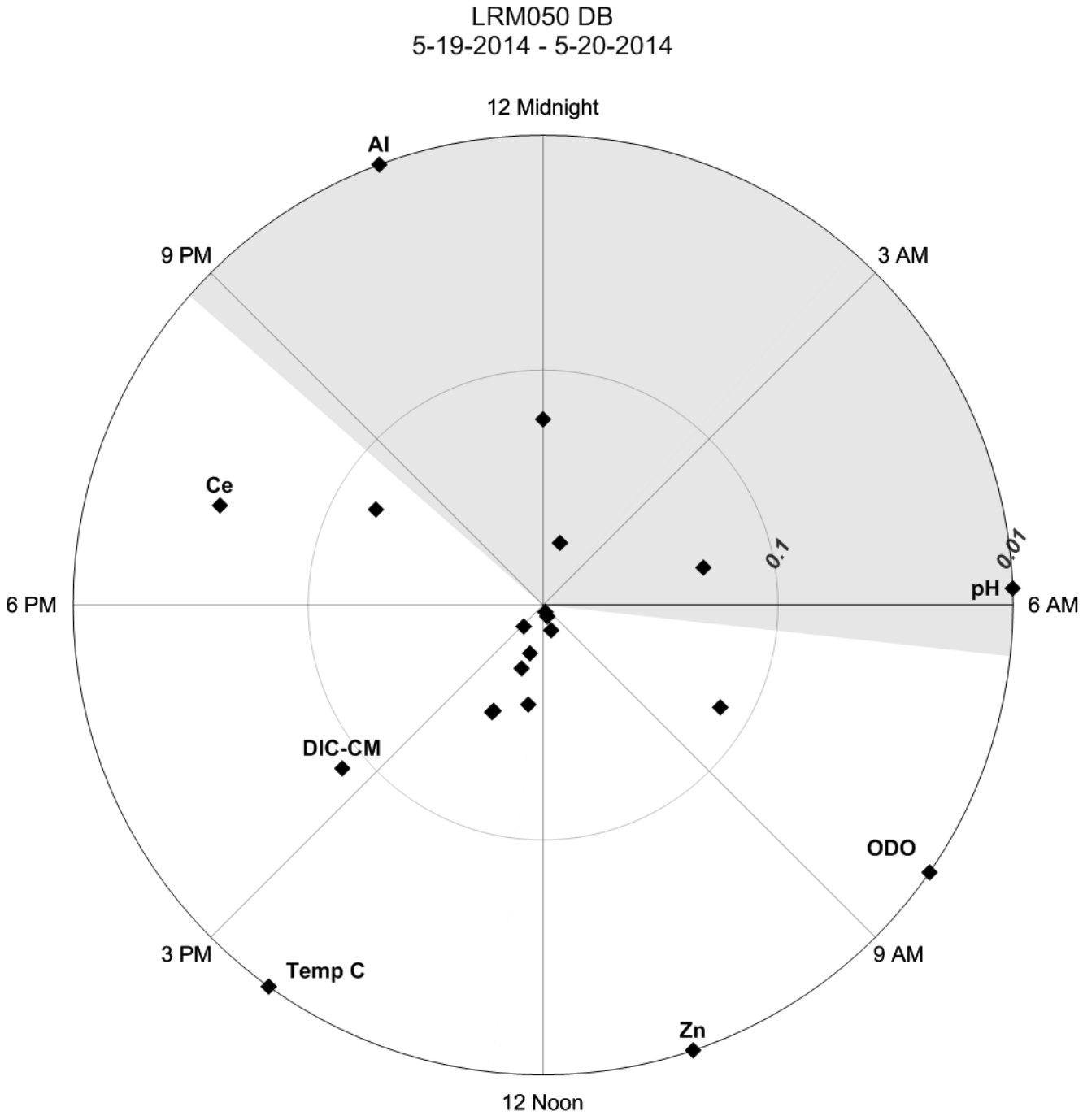

Figure 20. Polar plot for LMR050 DB-May. Parameters that had significant cosine model fit are those with p<= 0.01. The time of predicted maximum concentration or value is graphed on the angular axis. Other important points are also labeled.

Table 11. LRM138 DB-May: Diel variability of cycling parameters

Parameter	Max	Min	Time of max value	% RSD	p-value
pH	**6.82**	**6.37**	**5/19 1415**	**2.06**	**<0.01**
Temperature (C)	**20.4**	**13.1**	**5/19 1415**	**15.1**	**<0.01**
ODO(mg/L)	**10.34**	**8.98**	**5/20 1304**	**3.77**	**<0.01**
CO_2-CM (g/L)	1.33E-2	8.00E-3	5/20 1830	10.1	6.28E-1
DIC-CM (mM)	1.66	1.34	5/20 1100	4.57	8.49E-1
$\delta^{13}C_{DIC}$ (permil)	**-1.06**	**-3.39**	**5/20 1230**	**27.9**	**<0.01**
Fe(II) (mg/L)	1.75E-1	1.32E-1	5/20 1230	7.46	2.30E-1
Fe_{TOT} (mg/L)	**1.67E-1**	**6.42E-2**	**5/19 2130**	**23.9**	**<0.01**
Mn (mg/L)	**1.19**	**9.39E-1**	**5/19 2300**	**6.66**	**<0.01**
Y (ug/L)	**2.58E-1**	**1.88E-1**	**5/20 1830**	**9.19**	**<0.01**
As (ug/L)	2.37E-1	1.60E-1	5/20 1230	9.67	8.05E-2
Ni (ug/L)	**14.4**	**12.7**	**5/20 0500**	**2.16**	**<0.01**

Parameters in bold indicate statistically significant diel behavior based on the cosine model.

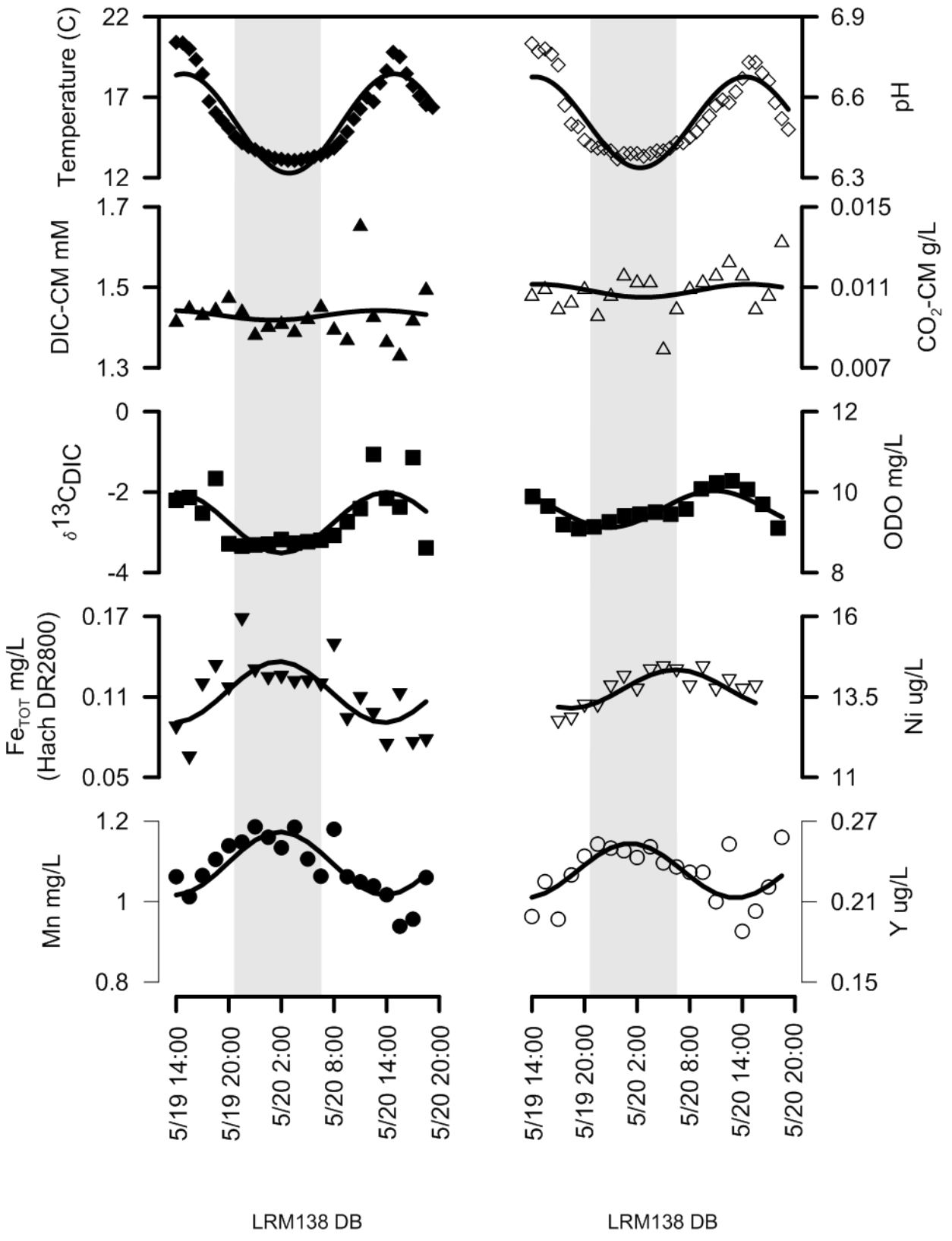

Figure 21. LMR138 DB-May. Cyclical behavior of parameters having a statistically significant cosine model fit at α=0.01 and CO2 and DIC. Symbols are used for the data, lines are the cosine model fit. Shaded areas represent hours of darkness.

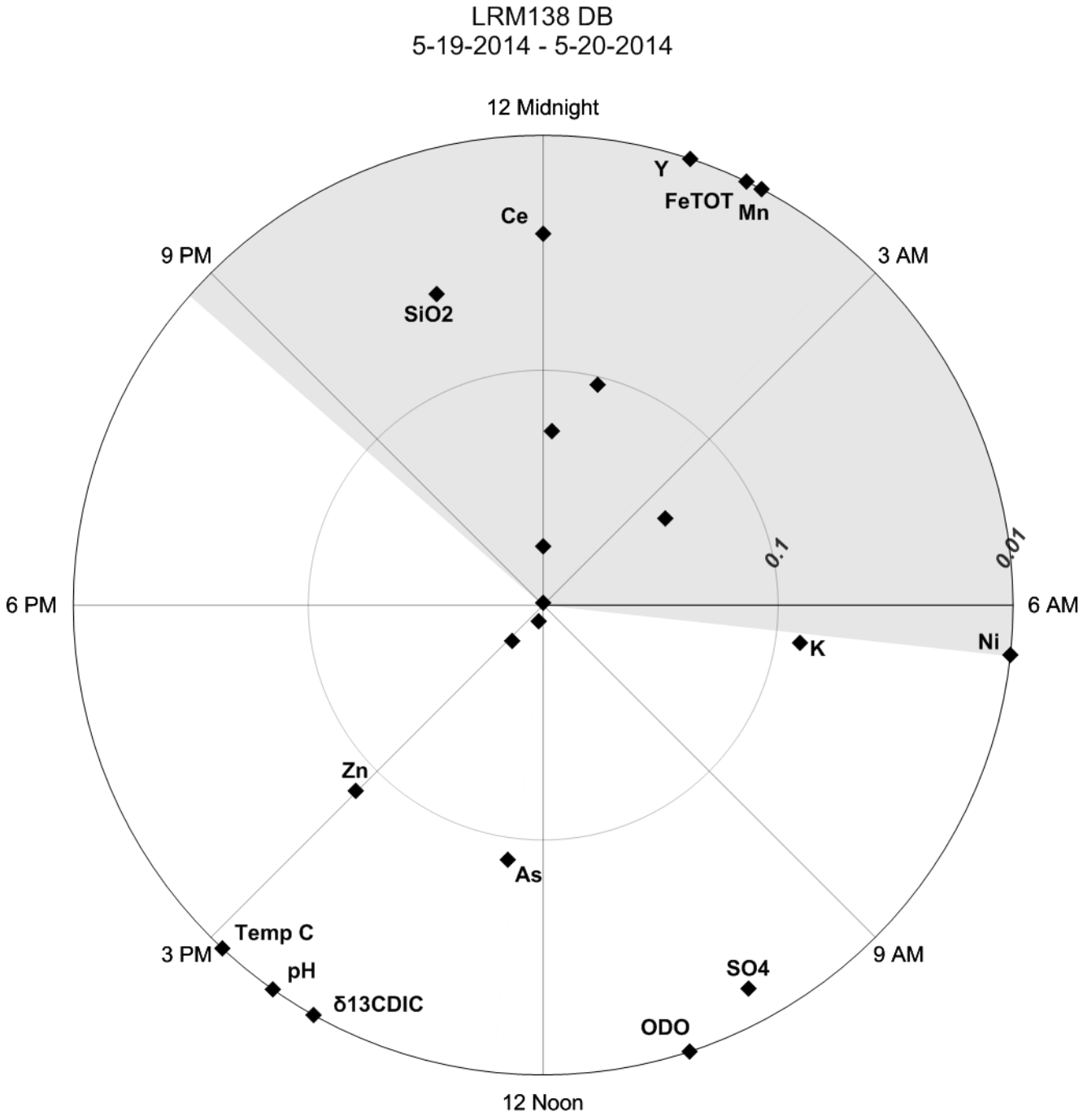

Figure 22. Polar plot LMR138 DB-May. Parameters that had significant diel behavior are those with p<= 0.01. The time of predicted maximum concentration or value is graphed on the angular axis. Other important points are also labeled.

5.6 Diel C results: 7/16/2014-7/17/2014 (July)

The third and final diel sampling round was conducted in the summer at LRM050 and LRM138. To match the previous data sets, sampling began at 1400 on 7/16/2014 and ended at 1845 on 7/17/2014. The sun set at approximately 2025 on 7/16/2014 and rose at approximately 0540 on 7/17/2014. Maximum and minimum air temperature during the sampling round were 23.9 C and 12.8 C with maximum temperatures being ~ 10 C lower than average for that date (Weather Underground). Light, intermittent precipitation fell between 0500 and 0700 on 7/17/2014.

5.6.1 LRM050 and LRM138 - July

At LRM050, six parameters (pH, temperature, ODO, Al, Fe(II), and $Fe_{TOT;}$ Table 12, in bold) had significant diel patterns based on their fit of a cosine model. A summary graph of the five parameters, as well as DIC and CO_2, is shown in Fig.23. This figure shows the changes in concentration of each parameter with its cosine model fit.

Of the six parameters, pH and ODO cycled in phase with each other, reaching maximum values in the early afternoon on both days. Fe(II) and Fe_{TOT} also cycled in phase with each other, reaching maximum concentrations around sunrise and shortly after on 7/17. Temperature and Al did not cycle in phase with each other or with the other parameters (Fig. 24). Times of peak concentration and increasing values can be seen in Table 12 and Fig. 23. The six parameters had an average RSD of 5.09% ranging from 0.81% (pH) to 21.5% (Al). Though they did not show significant diel patterns, CO_2 and DIC did reach maximum value at 2045 on 7/16 and showed a similar pattern of concentration change (Fig. 23).

At LRM138, nine parameters show significant diel patterns but are different than those in March and May (Table 13, in bold) A summary graph of the nine parameters plus CO_2 is shown in Fig. 25. This figure shows the changes in concentration of each parameter with its cosine model fit.

Temperature, pH, ODO, $\delta^{13}C_{DIC}$, and Fe_{TOT} all generally reached maximum concentration in approximately the middle of the daytime hours. However, while Fe_{TOT} reached maximum concentration at 1230 on 7/17, this was a high concentration on an otherwise

Table 12. LRM050 DC-July: Diel variability of cycling parameters

Parameter	Max	Min	Time of max value	% RSD	p-value
pH	**6.15**	**5.97**	**7/16 1500**	**8.07E-1**	**<0.01**
Temperature (C)	**13.4**	**12.9**	**7/17 1330**	**1.04**	**<0.01**
ODO(mg/L)	**8.89**	**7.66**	**7/17 1100**	**3.59**	**<0.01**
CO_2-CM (g/L)	9.77E-2	6.53E-2	7/16 2045	11.8	1.66E-1
DIC-CM (mM)	3.35	2.58	7/16 2045	7.65	8.63E-2
$\delta^{13}C_{DIC}$ (permil)	-6.51	-7.79	7/16 1445	4.43	6.59E-1
Fe(II) (mg/L)	**3.50**	**3.30**	**7/17 0545**	**1.67**	**<0.01**
Fe_{TOT} (mg/L)	**3.65**	**3.43**	**7/17 0715**	**1.94**	**<0.01**
Al (mg/L)	**207**	**86.6**	**7/16 1445**	**21.5**	**<0.01**
Y (ug/L)	4.76	3.07	7/16 1445	11.3	9.83E-1
Zn (ug/L)	20.3	18.5	5/20 1015	2.30	1.84E-1
K (mg/L)	5.66	5.42	7/16 2045	1.30	6.45E-1

Parameters in bold indicate statistically significant diel behavior based on the cosine model.

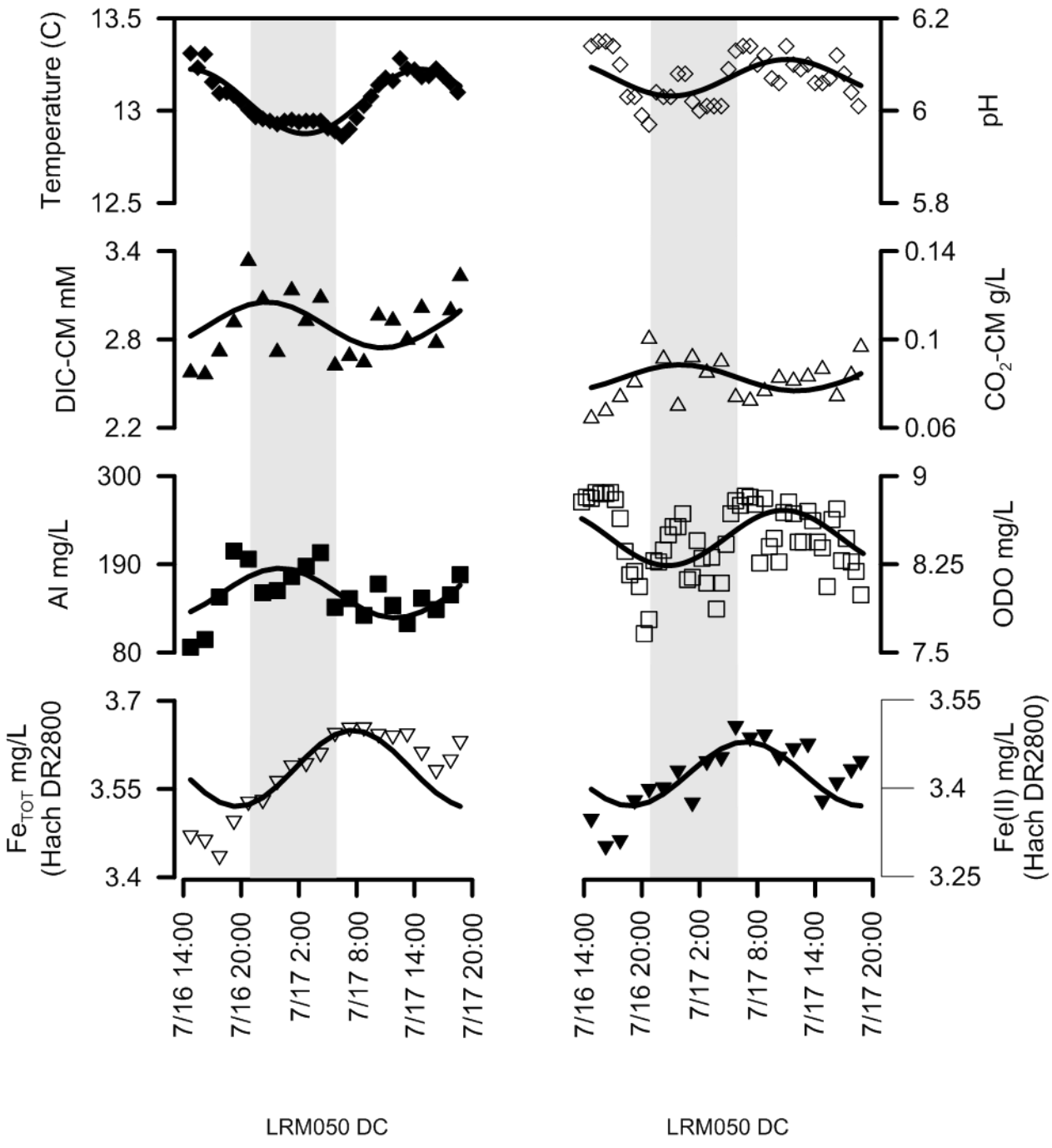

Figure 23. LMR050 DC-July. Cyclical behavior of parameters having a statistically significant cosine model fit at α=0.01 and CO2 and DIC. Symbols are used for the data, lines are the cosine model fit. Shaded areas represent hours of darkness.

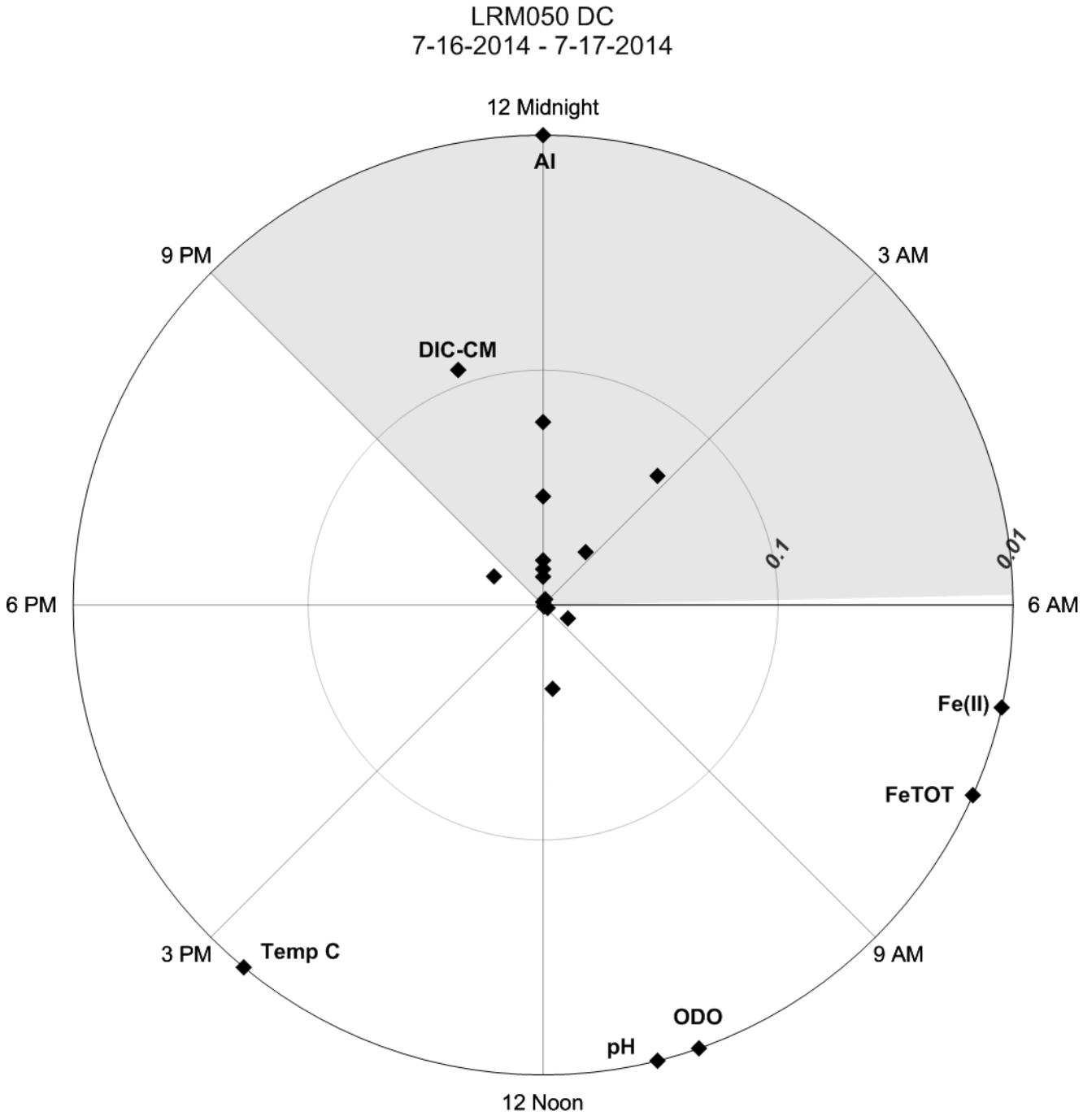

Figure 24. Polar plot LMR050 DC-July. Parameters that had significant diel behavior are those with p<= 0.01. The time of predicted maximum concentration or value is graphed on the angular axis. Other important points are also labeled.

Table 13. LRM138 DC-May: Diel variability of cycling parameters

Parameter	Max	Min	Time of max value	% RSD	p-value
pH	**6.84**	**6.32**	**7/16 1400**	**2.34**	**<0.01**
Temperature (C)	**23.1**	**15.2**	**7/16 1500**	**13.6**	**<0.01**
ODO(mg/L)	**9.11**	**7.62**	**7/17 1330**	**6.08**	**<0.01**
CO_2-CM (g/L)	1.20E-2	8.00E-3	7/17 0500	8.78	8.48E-2
DIC-CM (mM)	**1.24**	**1.11**	**7/17 0200**	**3.31**	**<0.01**
$\delta^{13}C_{DIC}$ (permil)	**-3.42**	**-5.75**	**7/16 1400**	**16.8**	**<0.01**
Fe(II) (mg/L)	**1.60E-1**	**2.02E-2**	**7/16 2130**	**37.1**	**<0.01**
Fe_{TOT} (mg/L)	**2.02E-1**	**1.05E-1**	**7/17 1230**	**22.9**	**<0.01**
Mn (mg/L)	**9.39E-1**	**6.77E-1**	**7/17 0630**	**11.2**	**<0.01**
Y (ug/L)	1.22	2.35E-1	7/17 0800	46.1	1.88E-1
As (ug/L)*	BDL				
Ni (ug/L)	**12.2**	**8.04**	**7/17 0930**	**13.3**	**<0.01**

Parameters in bold indicate statistically significant diel behavior based on the cosine model. As is below detection limit, detection limit on ICP-MS is 0.1 ug/L.

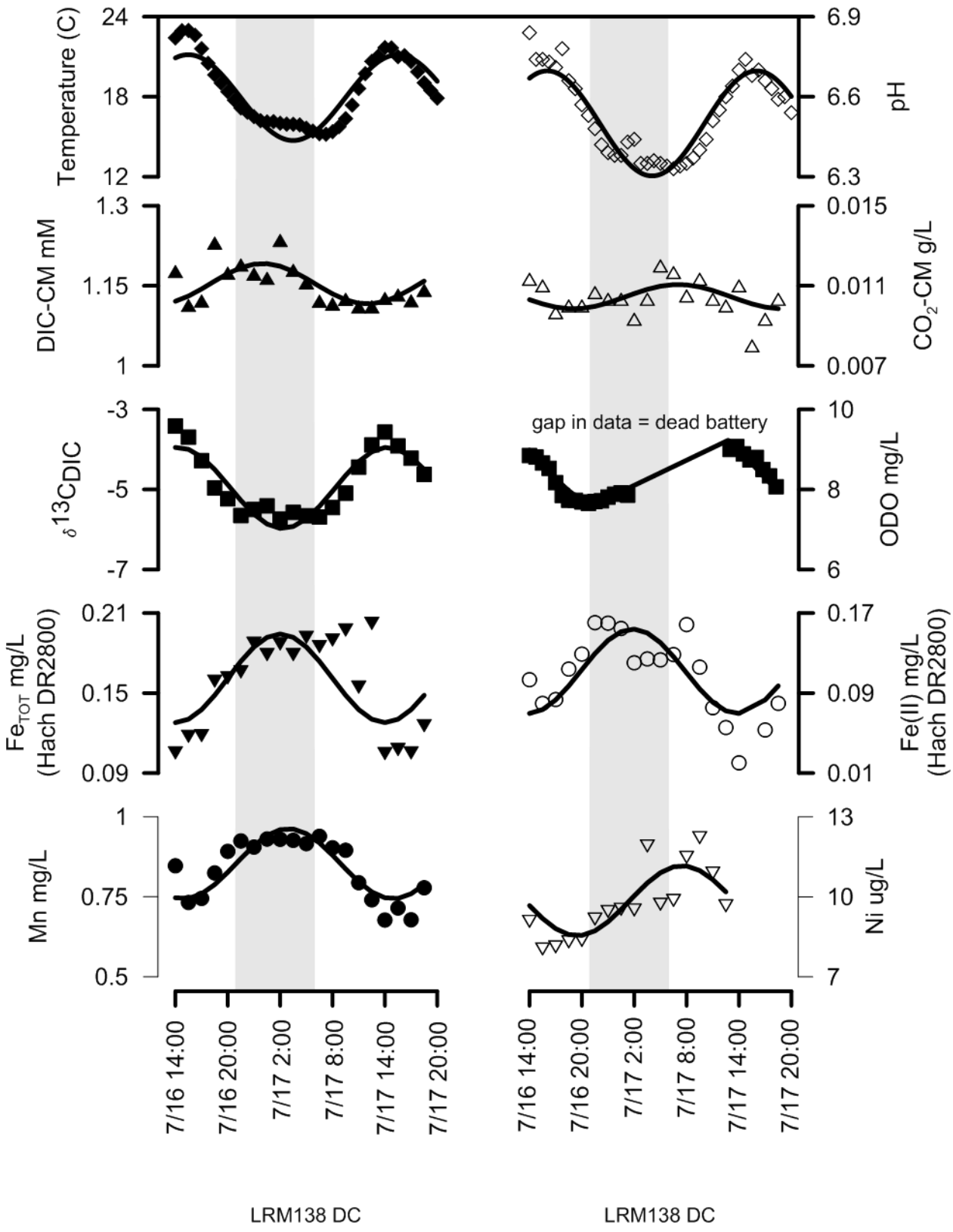

Figure 25. LRM138 DC-July: Cyclical behavior of parameters having a statistically significant cosine model fit at α=0.01 and CO2 and DIC. Symbols are used for the data, lines are the cosine model fit. Shaded areas represent hours of darkness.

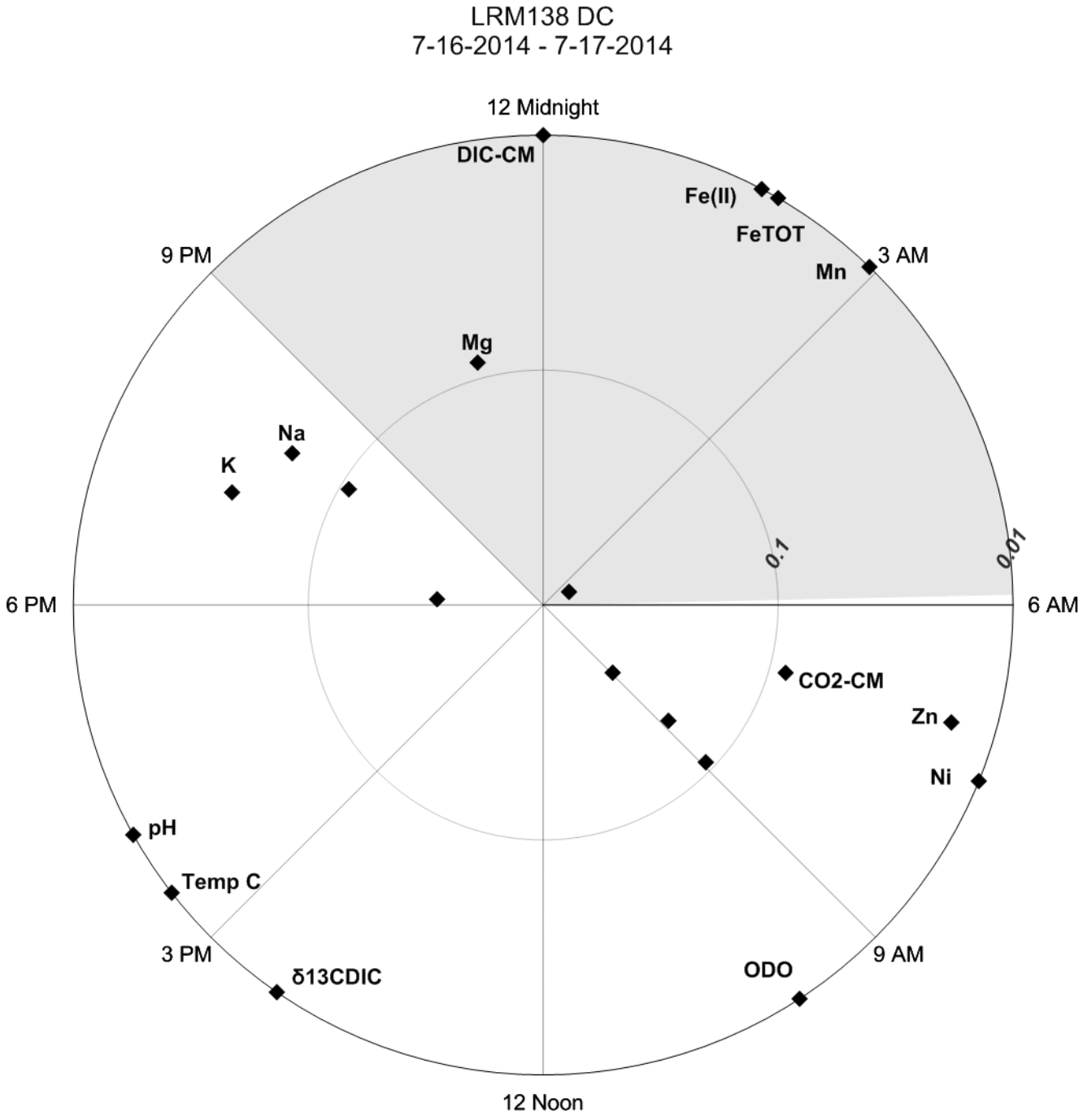

Figure 26. Polar plot LMR138 DC-July. Parameters that had significant diel behavior are those with p<= 0.01. The time of predicted maximum concentration or value is graphed on the angular axis. Other important points are also labeled.

decreasing trend during that time of day. Mn, Ni, DIC, and Fe(II) cycled out of phase with temperature, pH, ODO, and $\delta^{13}C_{DIC}$ (Fig. 26). Mn and Ni generally reached maximum concentration in the early to mid-morning hours, while DIC and Fe(II) reached maximum concentrations at 0200 on 7/17 and 2130 on 7/16, respectively. The nine parameters here had an average RSD 14.07% with a range of 2.34% (pH) to 37.1% (Fe(II)).

5.7 Seasonal comparison of diel patterns

5.7.1 LRM050

As the seasons progressed, ODO and pH generally decreased while temperature, CO_2, DIC, Fe(II), $Fe_{TOT,}$ Y, and K all increased (Figs. 27 and 28). Other parameters did not show a general trend across the seasons. Further, while all parameters had some change in concentration, only Fe(II), $Fe_{TOT,}$ and $\delta^{13}C_{DIC}$ increased more than an order of magnitude. However, only Fe(II) and Fe_{TOT} had a consistent decrease in p-value of the f-test of the model fit with an increase in magnitude.

Temperature, pH, ODO, and Al had significant cosine model diel patterns (α=0.01) during all diel sampling rounds (March, April, and May). CO_2, K, and Y had significant diel patterns during March only; Zn had significant cosine model diel patterns during May only; and Fe(II) and Fe_{TOT} had diel patterns during July only. DIC never had significant cosine model diel patterns (Table 14). Of the parameters that had significant cosine model diel patterns during all three diel sampling rounds, ODO and temperature had the greatest changes in p-value throughout the seasons. ODO had the smallest p-value (~most significant behavior) during March. Temperature had the smallest p-value during May; this could be attributed to air temperature showing the most fluctuation during the May sampling round (17.2 C versus 11.2C (May) and 11.1 C (July)) and thus influencing changes in water temperature. No parameter had any correlation between the cosine model amplitude and p-value, indicating that increases or decreases in amplitude did not influence the significance of diel patterns.

5.7.2 LRM138

As the seasons progressed, ODO, DIC, $\delta^{13}C_{DIC}$, and pH all decreased in concentrations while temperature, CO_2, and Y all generally increased in concentration (Figs. 29 and 30). Other parameters did not show a general trend across the seasons. CO_2 had an increase by an order of

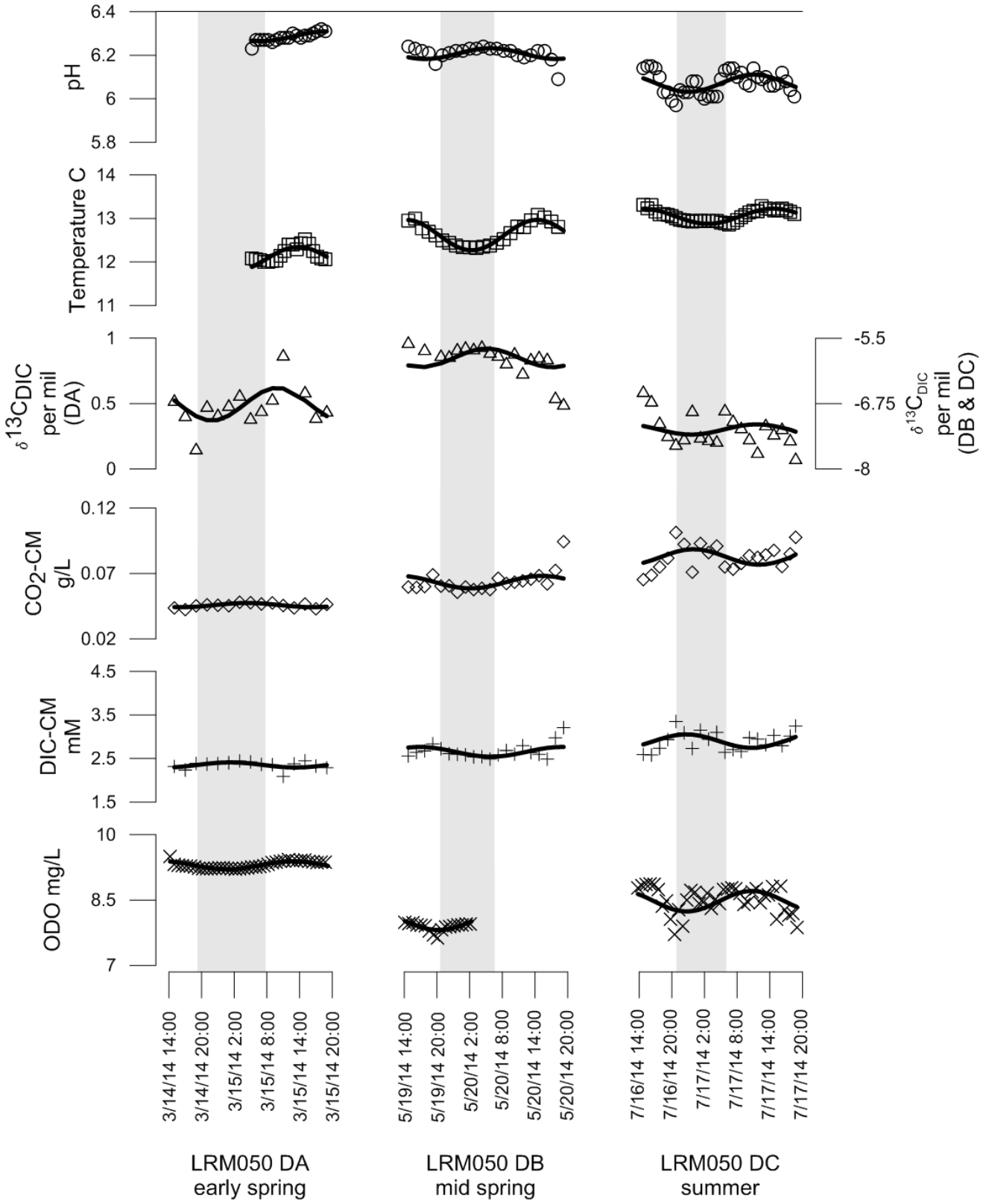

Figure 27. LRM050. Cyclical behavior of parameters that showed diel behavior during at least one diel sampling period. Note the different scales for some parameters, these are used to better show the magnitude change of the parameter.

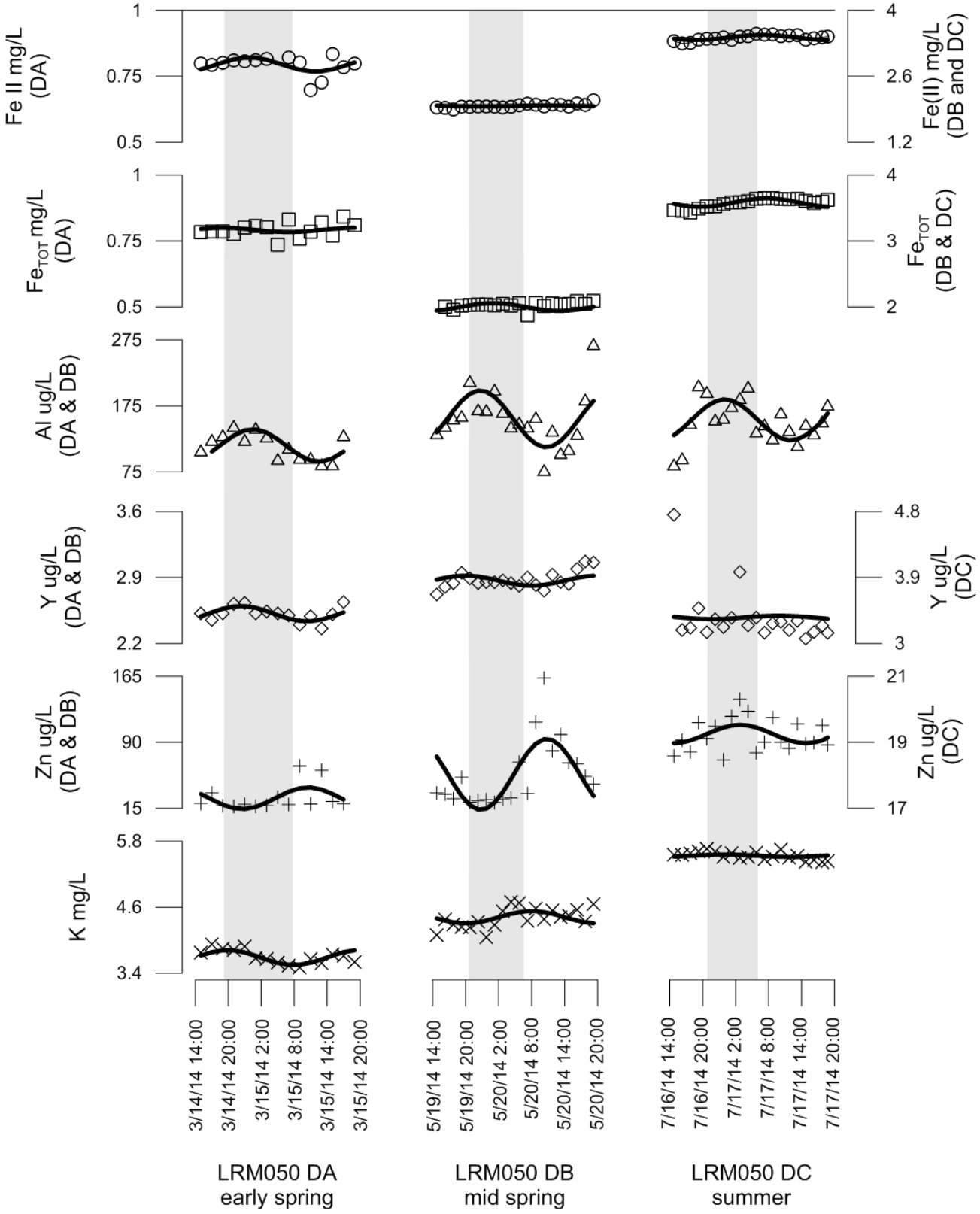

Figure 28. LRM050. Cyclical behavior of parameters that showed diel behavior during at least one diel sampling period. Note the different scales for some parameters, these are used to better show the magnitude change of the parameter.

Table 14. LRM050. Cosine model results of statistically significant parameters

Parameter	DA-March			DB-May			DC-July		
	Mean	**Amp.**	**p-value**	**Mean**	**Amp.**	**p-value**	**Mean**	**Amp.**	**p-value**
pH	6.29	2.21E-2	<**0.01**	6.21	2.46E-2	<**0.01**	6.07	3.96E-2	<**0.01**
Temperature (C)	12.1	0.284	<**0.01**	12.6	3.49E-1	<**0.01**	13.1	1.74E-1	<**0.01**
ODO(mg/L)	9.30	9.35E-2	<**0.01**	8.01	1.95E-1	<**0.01**	8.47	2.35E-1	<**0.01**
CO_2-CM (g/L)	4.58E-2	1.12E-3	<**0.01**	6.34E-2	4.80E-3	1.62E-1	8.26E-2	5.93E-3	1.66E-1
DIC-CM (mM)	2.35	5.98E-2	1.91E-2	2.65	1.13E-1	7.92E-2	2.90	1.56E-1	8.63E-2
$\delta^{13}C_{DIC}$ (permil)	4.95E-1	1.26E-1	9.25E-2	-5.88	1.78E-1	1.99E-1	-7.25	9.83E-2	6.59E-1
Fe(II) (mg/L)	7.95E-1	2.37E-2	1.36E-2	1.97	1.02E-2	7.71E-1	3.42	5.46E-2	<**0.01**
Fe_{TOT} (mg/L)	7.92E-1	7.95E-3	7.27E-1	2.00	5.95E-2	0.532	3.26	6.49E-2	<**0.01**
Al (ug/L)	115	24.6	<**0.01**	156	43.0	<**0.01**	154	30.9	<**0.01**
Y (ug/L)	2.52	8.11E-2	1.25E-2	2.87	5.33E-2	1.51E-1	3.36	2.35E-2	9.83E-1
Zn (ug/L)	26.5	12.3	8.18E-2	53.6	40.4	<**0.01**	19.3	2.77E-1	1.84E-1
K (mg/L)	3.68	1.35E-1	<**0.01**	4.42	1.11E-1	1.35E-2	5.53	2.24E-2	6.45E-1

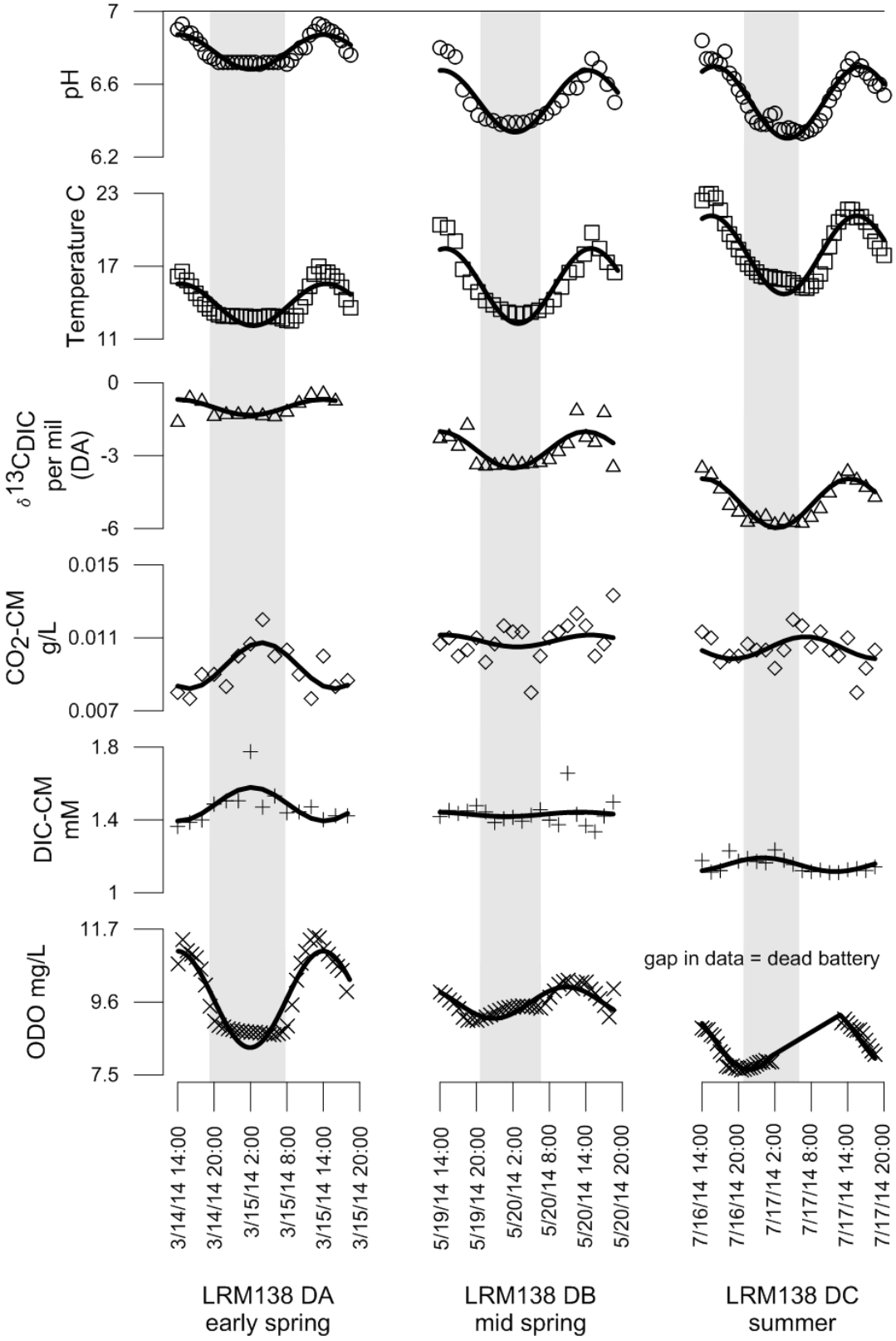

Figure 29. LRM138. Cyclical behavior of parameters that showed diel behavior during at least one diel sampling period. Note the different scales for some parameters, these are used to better show the magnitude change of the parameter.

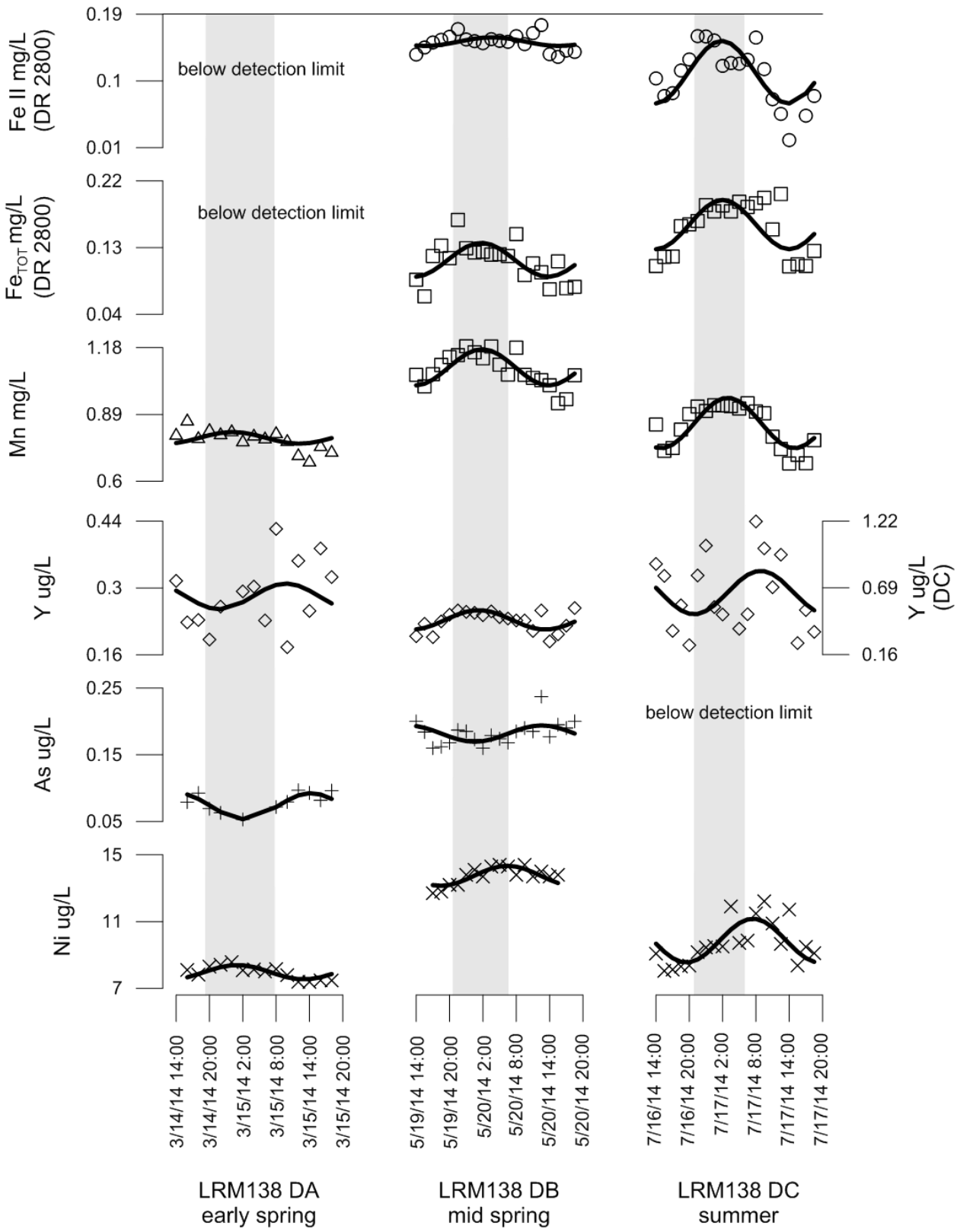

Figure 30. LRM138. Cyclical behavior of parameters that showed diel behavior during at least one diel sampling period.

magnitude in average concentration (Table 15) from March through July as well as p-value thereby resulting in significant cosine model diel patterns in March but not in May or July. However, Mn also increased in average concentration by almost an entire order of magnitude from March to May, but decreased in p-value thus showing more significant cosine model diel patterns. Yet, during July, Mn had an average concentration closer in magnitude to March but had significant cosine model diel patterns. Here, the amplitude (cosine model) change in Mn during July was greater than during March by two orders of magnitude. Ni had an increase in amplitude from March to July with a decrease in p-value but no clear trend in average concentration. These examples indicate a possible relationship between amplitude, concentration, and significant diel patterns.

5.8 Comparison of parameters between LRM050 and LRM138 from March through July

5.8.1 Temperature, pH, DIC, and related parameters

Temperature, pH, and ODO were the only parameters that had significant cosine model diel patterns at both locations and during each season. LRM050 averaged lower pH and temperature values than LRM138. LRM050 is closer to the portal and has less influence from the environment than LMR138 on temperature, pH, and biological reactions. Average ODO values were more similar between sites but LRM138 had a larger amplitude change in ODO (Tables 14 and 15). DIC did not have significant cosine model diel patterns during any season at LRM050 but it did at LRM138 during March and July. Average DIC concentrations at LRM050 were consistently higher than at LRM138. If diel cycles of DIC are generated by photosynthesis, then the higher DIC concentrations at LRM050 could be sufficient to "hide" such a cycle. CO_2 had a significant diel cycle at both locations during March and CO_2 concentrations were higher at LRM050. However in May and July, the largest and smallest CO_2 concentrations occurred at LRM138; CO_2 concentrations at LRM050 fell between the largest and smallest concentrations at LRM138. Values (permil) of $\delta^{13}C_{DIC}$ were more enriched at LRM138 in May and July than at LRM050 (but more enriched at LMR050 during March). If photosynthesis is a controlling factor of DIC cycling at LRM138, then generally more enriched values would be expected at LRM138 as algae and other organisms uptake lighter ^{12}C.

Table 15. LRM138. Cosine model results of statistically significant parameters

Parameter	DA			DB			DC		
	Mean	**Amp.**	**p-value**	**Mean**	**Amp.**	**p-value**	**Mean**	**Amp.**	**p-value**
pH	6.78	9.52E-2	**<0.01**	6.51	1.70E-1	**<0.01**	6.50	1.97E-1	**<0.01**
Temperature (C)	13.8	1.72	**<0.01**	15.4	3.09	**<0.01**	17.9	3.22	**<0.01**
ODO (mg/L)	9.68	1.39	**<0.01**	9.58	4.54E-1	**<0.01**	8.57	9.20E-1	**<0.01**
CO_2-CM (g/L)	9.47E-3	1.26E-3	**<0.01**	2.08E-2	3.27E-4	6.28E-1	1.05E-2	6.07E-4	8.48E-2
DIC-CM (mM)	1.49	9.24E-2	**<0.01**	1.43	1.21E-2	8.49E-1	1.15	3.79E-2	**<0.01**
$\delta^{13}C_{DIC}$ (permil)	-1.01	3.24E-1	2.52E-2	-2.76	7.55E-1	**<0.01**	-4.96	1.01	**<0.01**
Fe(II) (mg/L)	BDL			1.53E-1	5.75E-3	2.30E-1	1.12E-1	4.22E-2	**<0.01**
Fe_{TOT} (mg/L)	BDL			1.14E-1	2.29E-2	**<0.01**	1.91E-1	3.32E-2	**<0.01**
Mn (mg/L)	7.89E-1	2.53E-2	3.17E-1	1.09	7.85E-2	**<0.01**	8.53E-1	1.10E-1	**<0.01**
Y (ug/L)	2.82E-1	2.70E-2	6.60E-1	2.33E-1	2.03E-2	**<0.01**	6.53E-1	1.72E-1	1.88E-1
As (ug/L)	7.29E-2	1.96E-2	**<0.01**	1.82E-1	1.22E-2	8.05E-2	BDL		
Ni (mg/L)	7.96	4.32E-1	**<0.01**	13.7	5.99E-1	**<0.01**	9.86	1.31	**<0.01**

*BDL = below detection limit. See Appendix II for detection limit values.

5.8.2 Fe, Mn, and other elements

Fe(II) and Fe_{TOT} concentrations were higher by an order of magnitude during all three sampling rounds at LRM050 but did not have a significant cosine model diel pattern until July; whereas at LRM138 Fe(II) showed a significant cosine model diel cycle in May and July. Concentrations of Fe(II) and Fe_{TOT} at LRM050 were almost the same, indicating that almost all Fe present is in the reduced form. Mn and Ni were present in higher concentrations at LRM050 and had consistent diel cycles (cycling at one location only for two or more sampling rounds) at LRM138 but not LRM050. Y, Zn, and As all had generally higher concentrations at LRM050 but less consistent diel cycles. Al had consistent diel cycles at LRM050 but was higher in concentration at LRM138 during May and July. With the exception of Al, higher concentrations of metals coming from the portal could be the reason higher concentrations are also seen at LRM050, these higher concentrations could potentially 'hide' cycling of elements that are observed further downstream (LRM138). However the cycling of Zn during May at LRM050, Y during March at LRM138 and during May at LRM050, and As during March at LRM138 is not explained by this. These cycles could have an underlying relationship with pH, temperature, or other metals/elements.

5.9 Summary of results

Generally, LRM138 had lower concentrations of almost all analytes, higher pH and temperature, and greater fluctuation in cycle magnitude for all parameters. As the seasons progressed, more parameters had significant diel patterns at LRM138. Seasonal progression seemed to have little effect on diel patterns at LRM050. A summary of what parameters cycled during which season is shown in Table 16.

Table 16. Summary of parameters with statistically significant cosine model fit

	March (DA)		May (DB)		July (DC)	
LRM050	pH	K	pH	Al	pH	Al
	temp	Al	temp	Zn	temp	Fe(II)
	ODO	CO_2	ODO		ODO	Fe_{TOT}
LRM138	pH	DIC	pH	Fe_{TOT}	pH	Fe(II)
	temp	As	temp	Mn	temp	Fe_{TOT}
	ODO	Ni	ODO	Ni	ODO	Mn
	CO_2		$\delta^{13}C_{DIC}$	Y	DIC	Ni
					$\delta^{13}C_{DIC}$	

6.0 Discussion

6.1 DIC, DO, and $\delta^{13}C_{DIC}$

Four different studies that focused on diel behavior of DIC and related parameters were chosen for comparison to July data from LRM138. The settings of the studies are a karst river in two different years, a mountain headwater during an algal bloom, and a river contaminated with metals. Each of these studies included some form of DIC, pH, DO and/or $\delta^{13}C_{DIC}$ data over the course of at least 24 hours. These studies were chosen for comparison due to their different settings. The cosine model fit method was applied to all the parameters from each study to ensure that parameters being compared to LRM were measured under the similar circumstances. The data from those papers was obtained and subjected to the same analyses as the new data from this study. Description of the sites follows:

- **Spring fed karst river (Kurz et al. 2013) -** The Ichetucknee River in central Florida is fed by numerous spring sources from the Floridan Aquifer- a carbonate karst aquifer. The aquifer exhibits conduit-matrix exchange with the river. In some locations, the river flows over the limestone unit which hosts the aquifer. The springs themselves have a constant chemical composition individually but chemistry with the soruce. The river is abundant in vegetation (Kurz etal. 2013) due to the clarity of the water which allows for primary productivity of benthic flora. Two separate rounds of data from this river were chosen for comparison- one collected in March of 2009 and one in May of 2010- pH, DIC, DO, and $\delta^{13}C_{DIC}$ were collected during both sampling rounds.
- **Nutrient rich mountain headwater (Poulson and Sullivan 2010) -** The upper Klamath River in southern Oregon is a mountain headwater characterized by poor water quality and frequent algal blooms in the summer months attributed to cyanobacterial algae. Diel data for pH, DIC, DO, $\delta^{13}C_{DIC}$ was collected in June and August 2007 and 2008 (Poulson etal. 2010). The August 2008 data set was chosen for comparison to the data of this study.
- **Mine drainage affected river (Parker et al. 2010) -** The Clark Fork River shed in north western Montana was the location of several diel studies at various creeks and tributaries to the Clark Fork River and along it. This area is home to the largest (by area) EPA Superfund site in the United States (Parker et al. 2010). Mining and smelting centers

located in the nearby towns of Butte and Anaconda contributed to higher than normal dissolved heavy metals in the river shed. The site chosen for comparison is in the upper Clark Fork River shed along a major tributary; data for pH, DIC, and $\delta^{13}C_{DIC}$ were collected in July-August of 2003.

6.1.1 Comparing magnitude, concentration, and phasing of cycles

For DIC, the largest magnitude of cycles were observed in LRM138 and the mine drainage affected river; the largest concentrations of DIC (~14.0 mM) occurred in the mountain headwater during an algal bloom. Concentrations of DIC at all other locations were lower by approximately one order of magnitude (Table 17). The highest pH values (~8.0) occurred in the mine drainage affected river and the lowest at the LRM locations. The highest concentrations of DO occurred at LRM locations (~7.5-9.2) and the karst river, where a maximum DO concentration of 10.0 mg/L occurred (Table 17). DO concentrations at the mountain headwater were an order of magnitude lower. $\delta^{13}C_{DIC}$ was depleted at each location but most depleted at the mountain headwater and most enriched at LRM050. The change in magnitude of $\delta^{13}C_{DIC}$ was comparable at all sites (Table 17).

Generally, pH and DO had consistent phasing at all sites, peaking during the day and decreasing in the late evening and nighttime hours (Fig. 31). DIC had inverse phasing to pH at all locations except for the karst river in 2010, while $\delta^{13}C_{DIC}$ was less consistent. At the karst river in 2009, both LRM sites, and the mine drainage river, $\delta^{13}C_{DIC}$ had the same phasing as DO and pH, increasing during the day and decreasing the late evening and nighttime hours, which is also, inverse to DIC (Fig. 31). At the karst river in 2010, $\delta^{13}C_{DIC}$ was also inverse to DIC but also showed opposite phasing than the other sites, as did DIC. $\delta^{13}C_{DIC}$ showed no general trend at the mountain headwater, likely due to the increased amount of biological activity masking any true cycle.

The LRM138 DIC-cycles had the same general trends as reported in other studies, whether another mine drainage site or a freshwater site (karst). Since the comparison sites had cycles of DIC and related parameters that were attributed to biological processes such as photosynthesis and cellular respiration, it is likely that the same processes are also the responsible mechanisms at LRM138. This is supported by the isotope data at LRM138 and comparison locations being more depleted during hours of darkness and more enriched during

Table 17. Comparison of DIC and related parameters between selected studies and LRM050 and LRM138

	Karst river 2009 (Kurz et al. 2013)		Karst river 2010 (Kurz et al. 2013)		Mountain headwater (Poulson and Sullivan 2010)		Mine drainage river shed (Parker et al. 2010)		LRM138 (July)		LRM050 (July)	
parameter	**Conc.**	**Amp.**	**Conc.**	**Amp.**	**Conc.**	**Amp.**	**Conc.**	**Amp.**	**Conc.**	**Amp.**	**Conc.**	**Amp.**
pH	7.82-8.07	2.58 E-1	7.65-8.39	3.00 E-1	7.72-8.02	3.74 E-2	8.01-8.63	2.80 E-1	5.97-6.15	3.96 E-2	6.32-6.84	1.97 E-1
DIC mM	2.85-3.03	7.54 E-2	2.98-3.11	4.46 E-2	14.0-14.3	6.36 E-2	3.38-3.65	1.29 E-1	2.58-3.35	1.56 E-1	1.11-1.24	3.80 E-2
DO mg/L	3.87-8.20	2.05	3.34-10.0	3.19	1.02 E-1 – 4.73 E-1	1.25 E-1	no data	no data	7.66-8.89	2.35 E-2	7.62-9.11	9.20 E-1
$\delta^{13}C_{DIC}$ permil	-11.5 – -10.3	5.52 E-1	-14.0 – -11.4	1.00	-16.3 – -15.1	1.18 E-1	-12.3 – -11.4	2.44 E-1	-7.79 – -6.51	9.83 E-2	-5.75 – -3.42	1.01

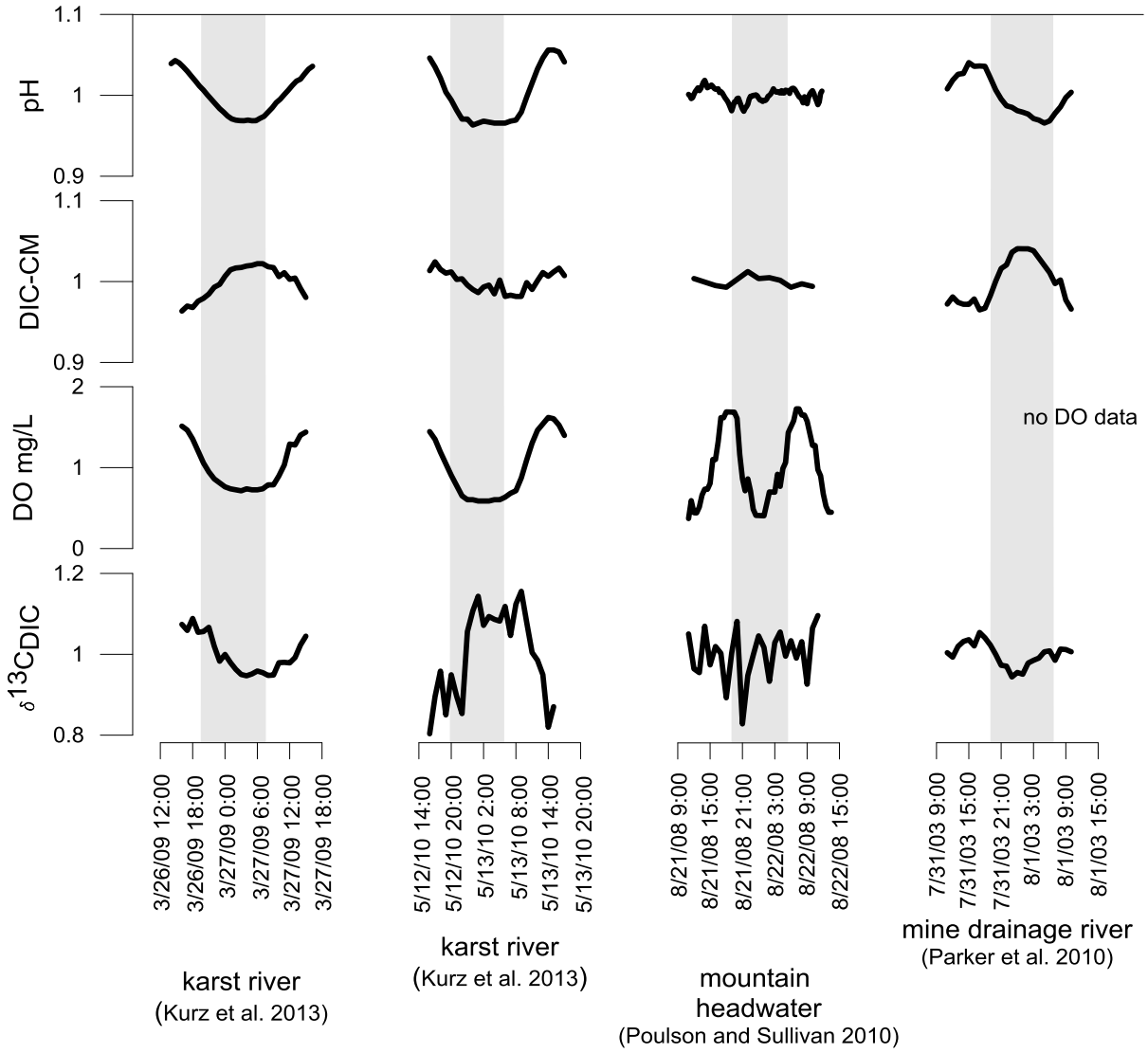

Figure 31. Mean normalized comparison of phasing of selected parameters from different studies.

hours of light. LRM050 has less defined cycles of these parameters (with the exception of pH and ODO) but shows the same general trends.

6.2 Fe, Mn, and trace elements; previous LRM study

Five different studies that focused on the diel patterns of metals were chosen for statistical analysis and comparison to this study. The settings for these studies are: a coal mine drainage stream in central Montana; a rocky mountain headwater; a rocky mountain headwater affected by acid mine drainage; and a spring fed karst river, sampled in two different seasons. These studies were chosen due to their different water types and scope of parameters analyzed. A description of sites follows:

- **Coal mine drainage stream- Montana (Gammons et al. 2010)-** This study took place in the Great Falls Lewiston Coalfield in central Montana. This coalfield is different from other coalfield sites in the western USA because it is a high-S bearing coal mine and has poorer water quality than other coalfields in the area. The area consists of several mine drainage discharge points in an approximately ~90 square kilometer area (Gammons et al. 2010). Gammons sampled several different points along the different CMD affected streams for diel patterns. For comparison to LRM, two sampling sites along the discharge stream from Giffen Spring 500 m downstream and 1200 m downstream of head of the stream of the source.
- **Rocky Mountain headwater (Rocky MHW) (Nimick et al. 2005) -** Prickly Pear Creek in Colorado has been sampled extensively for diel patterns (Nimick et al. 2005) in metal concentrations. A granitic batholith that underlies most of the basin has been historically mined for Cu, Pb, Zn, Au, and Ag and the stream water in the area has had higher concentrations of Cd, Cu, and relative to other freshwaters in the area. Data chosen for comparison with LRM were collected during summer, low flow conditions and include Mn, Zn, and As.
- **Rocky Mountain headwater AMD (Sullivan et al. 1998) -** Peru Creek in central Colorado is a Rocky Mountain headwater stream that has also been contaminated by dissolved metal discharge from nearby abandoned silver mines (Sullivan etal 1998). The contamination here has been attributed to increased acidity in the creek. The data chosen for comparison was Fe and Zn data that were collected in low flow, summer conditions.

- **Karst river (Kurz et al. 2013) -** This setting is the same as previously described. Fe and Mn data collected in March 2009 and Fe data collected in May 2010 were chosen for comparison with LRM.

6.2.1 Comparing magnitude, concentration, and phasing of cycles

The metals chosen for comparison are Fe, Mn, Ni, Zn, and As with LRM050 and LRM138 data from July with the exception of LRM138 March data for As, as this was the only time As showed a significant diel cycle during this LRM study. The cosine model fit and statistical f-test was applied to the data from the other studies to make sure that cycles with similar significance were being compared and to estimate amplitude of the data. Results are shown in Table 18.

The highest concentrations of Fe occurred at LRM050 in July and the CMD location in Montana 500 m downstream from the spring, both reaching maximum concentrations of ~4.0 mg/L (Table 18) but with the greater magnitude occurring at the CMD location in Montana. The highest concentration of Mn occurred at LRM050. The CMD stream at 500 m had the highest concentrations of Ni (Table 18). The Rocky mountain headwater AMD (Sullivan et al. 1998) had the highest concentrations of Zn (likely due to the metal mine contamination) while the other sites had more comparable Zn concentrations to LRM050 and LRM138. Values of pH were in the same range at all sites except for the karst river (~7.8) and the Rocky MHW (~8.6) (Table 18). The only other study to have As data was the Rocky MHW (Table 18), which had higher concentrations of As compared to LRM138 in March (the only time As had a significant diel cycle).

At LRM050 and LRM 138, Fe, Ni, and Zn generally increased during the nighttime and reach peak values in the late night/early morning hours (Fig. 32) when the cosine model fit of the data was statistically significant at α=0.01. The Rocky MHW and the CMD study sites showed similar phasing as LRM, but the Rocky mountain headwater AMD and karst river had peak concentrations of metals in the afternoon to early evening hours. Arsenic at LRM138 had inverse phasing to that of the Rocky MHW study.

Generally, LRM050 has higher concentrations of Fe than seen in the comparison studies, while concentrations of Fe at LRM138 fell within the reported range of Fe concentrations. This

Table 18. Comparison of metal data between selected studies and LRM050 and LRM138

	CMD- Montana (Gammons etal. 2010)		Rocky MHW (Nimick etal. 2005)		Rocky MHW AMD (Sullivan 1998)		karst river (Kurz etal. 2010)		LRM050 (July)		LRM138 (July)	
Metal	**Conc.**	**Amp.**	**Conc.**	**Amp.**	**Conc.**	**Amp.**	**Conc.**	**Amp.**	**Conc.**	**Amp.**	**Conc.**	**Amp.**
Fe	0.30-4.2	1.6	1.8E-2 – 4.9E-2		0.39-0.50	3.6E-2	3.5E-3 – 8.5E-3 3.6E-3 – 5.8E-3	2.0E-3 6.1E-4	3.4-3.7	6.5E-2	0.10-0.20	3.3E-2
Mn	0.85-0.91 5.6E-3 – 8.6E-3	3.0E-2 1.7E-3	1.8E-2 – 4.9E-2	1.5E-2			2.8E-3 – 3.8E-3	6.6E-4	2.5-2.6	1.3E-2	0.68-0.94	0.11
Ni	0.13-0.14 4.1E-2 – 5.1E-2	3.6E-3 4.3E-3							1.9-2.1E-2	4.9E-5	8.0E-3 – 1.2E-2	1.3E-3
Zn	0.21-0.31 8.4E-2 – 0.14	3.8E-2 3.0E-2	1.2E-2 – 7.1E-2	2.7E-2	1.8-1.9	9.9E-3			1.8E-2 - 2.0E-2	2.8E-4	2.5E-3 – 6.8E-3	1.0E-3
As			4.5E-3 – 7.3-2	1.1E-3					1.0E-4 – 3.0E-4	4.5E-6	5.3E-5 - 9.7E-5	1.96E-5
mean pH	6.4 6.8		8.6		N/A		7.7 7.9		6.1		6.5	

Table showing concentration and amplitude from the cosine model of selected metals as well as mean pH. Red values represent the 1200 m location downstream; green values represent the May 2010 data from the karst river. July data from LRM was chosen except for LMR138 As data, which is from March as this was the only time As showed a significant diel cycle.

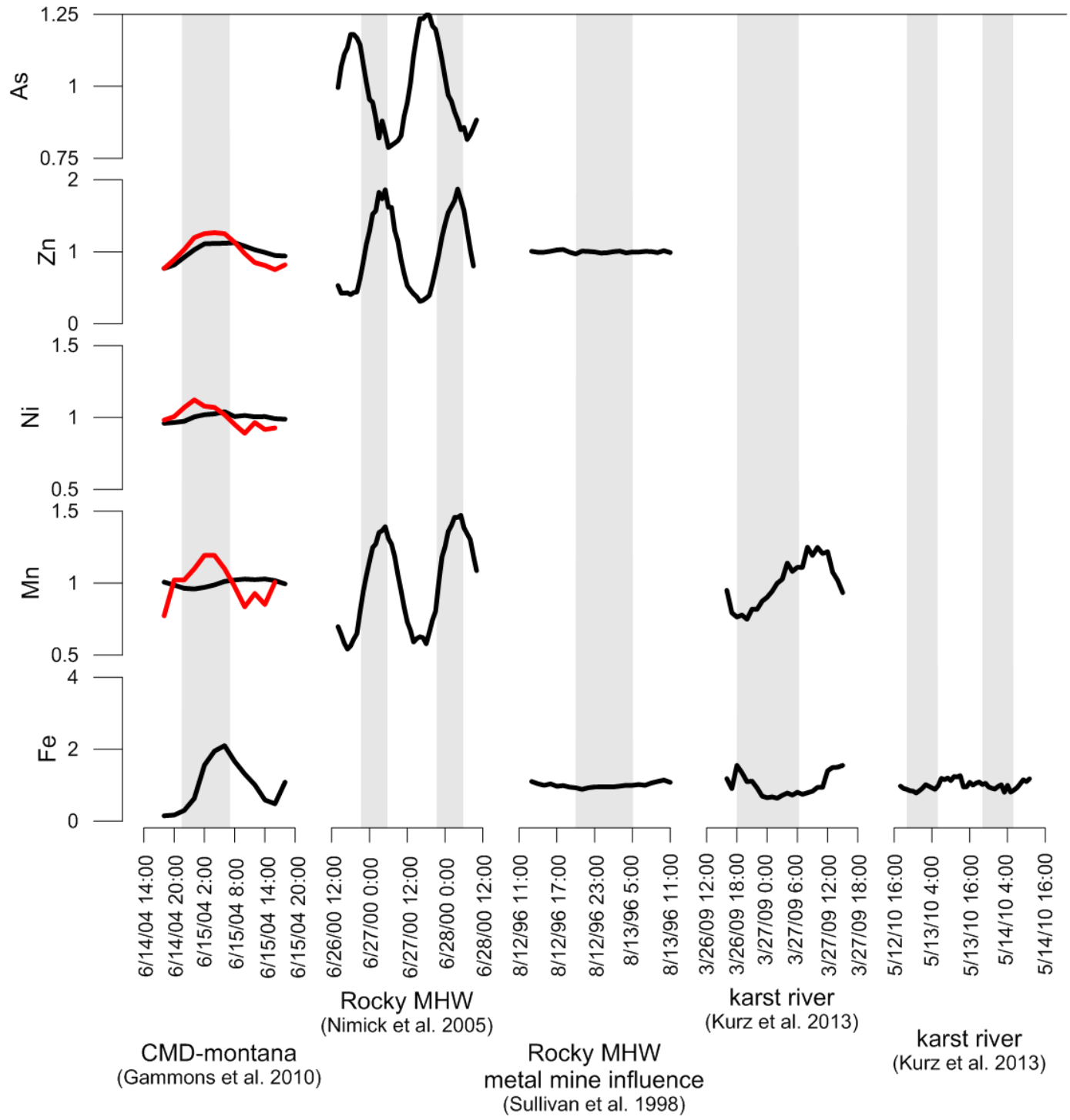

Figure 32. Mean normalized comparison of phasing of selected metals from different studies. For the CMD study, black represents the location 500 m downstream while red represents the location 1200 m downstream.

could be due to LRM050 being closer to the mine drainage portal than other locations. Mn follows a similar pattern but Zn and Ni are generally lower at both LRM locations. Phasing of metals at LRM also follows the patterns of phasing from other studies.

6.3 Comparison to LRM study 2007

In a 2007 study at LRM, Smilley collected diel data for metals, pH, and temperature at various locations along the discharge stream on May 22-23 2007 (Smilley 2007; "LRM2007" data). At this time, the passive treatment of the metal load had just begun and the wetland had just been structured less than one year previous to the data collection. These data were chosen to compare to LRM138 in May because both sets were collected at approximately the same location (Smilley location 3N) and during the same season.

The cosine model fit and statistical analysis of the model was conducted on the LRM2007 data and all parameters had a statistically significant model fit at $\alpha=0.01$ except pH, which had $p=0.299$ (Table 19). The data were graphed on a polar plot with the LRM138 data from May in this study. All of the LRM2007 data (selected metals and pH, Table 19) had peak concentration in the early morning hours just before sunrise except pH and temperature. Fewer metals cycled in the current study at LRM138 than during LRM 2007 and the phasing of metals at LRM138 was also less consistent during 2007 (Fig. 33). Temperature and pH had virtually the same phasing during both sampling periods.

The two sampling periods were then compared for differences in average concentrations to look for evidence of the wetland decreasing metal loads in the discharge stream by calculating the percent change from LRM138 to LRM 2007. All metals except As and Al had over an 100% decrease in concentration from 2007 to 2014; As decreased by ~35% and Al increased by over 1000% (Table 20), the reasons for this increase are unclear.

The decrease in metal concentration, the differences in phasing, and the differences in p-values of the parameters between the LRM 2007 study and this study suggest several possibilities about the effect of the wetland on the metal load. The increase in vegetation in the wetland from 2007 to present (this is a qualitative observation of vegetation amount) could be a cause for the decreased metal load. As more plants grow bigger and larger, uptake of metals used as plant nutrients as well as more developed root systems could lead to a decrease in metal load

Table 19. LRM-2007 wetland Data cosine model results

Parameter	Mean (cosine model)	Mean (raw data)	Amplitude	p-value
pH	6.96	6.96	1.60E-2	0.299
temperature	19.9	20.5	7.31	<0.01
Fe ug/L	439	418	364	<0.01
Mn ug/L	3.08E+3	3.06E+3	226	<0.01
Y ug/L	7.13E-1	6.77E-1	5.37E-1	<0.01
Ce ug/L	4.30E-1	4.10E-1	3.39E-1	<0.01
Al ug/L	15.4	16.3	6.89	<0.01
Ni ug/L	32.3	32.2	2.15	<0.01
As ug/L	2.46E-1	2.43E-1	2.32E-2	<0.01
Zn ug/L	38.8	38.2	6.85	<0.01
Si ug/L	8.48E+3	8.46E+3	455	<0.01
K ug/L	3.70E+3	3.69E+3	100	<0.01

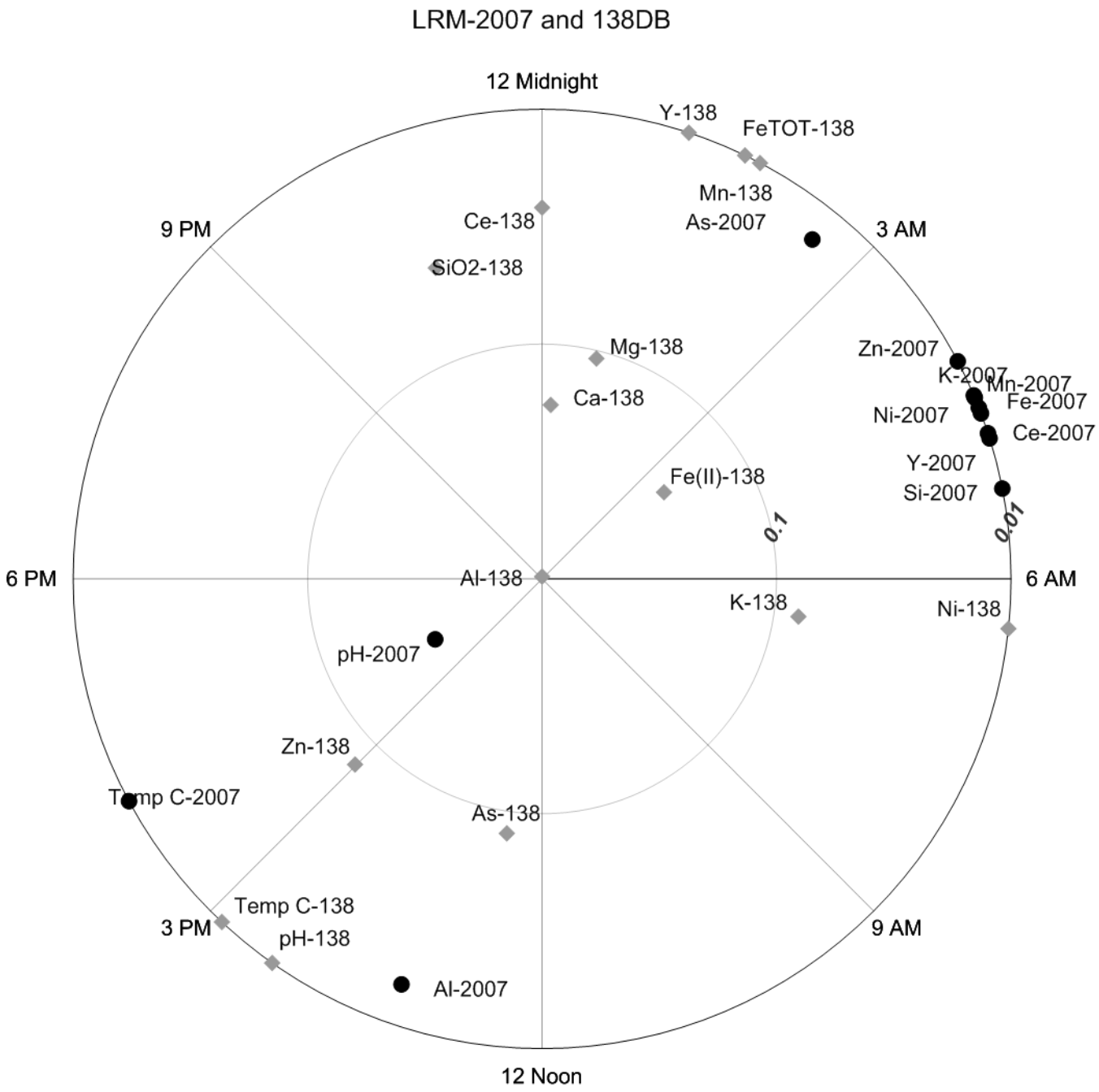

Figure 33. Polar plot showing diel behavior based on the cosine model for LRM2007 (black dots) data and LRM138 in May (gray diamonds).

Table 20. LRM-2007 wetland and LRM138 average parameter concentrations from cosine model

Parameter	Mean (2007)	Mean DB	% change
pH	6.96	6.51	-1.84
temperature	19.9	15.4	-29.2
Fe mg/L	0.439	0.153(FeTOT) 0.114 (Fe(II))	-184 -285
Mn mg/L	3.08	1.08	-185
Y ug/L	0.713	0.233	-206
Ce ug/L	0.430	4.99E-2	-761
Al ug/L	15.4	264	+1.61E3
Ni ug/L	32.3	13.7	-135
As ug/L	0.246	0.182	-35.2
Zn ug/L	38.8	16.2	-139
K ug/L	3.70	3.99	+7.27

downstream. Finally, while few data exist about groundwater and the hyporheic zone at LRM, there is the potential for hyporheic exchange in the area which could lead, not only to decreases in metal load as surface water possibly becomes more concentrated, but also to cycling of metals as groundwater and surface water are exchanged.

6.4 Seasonality and possible mechanisms contributing to cycles

6.4.1 Seasonality

None of the cited studies explicitly addressed seasonality, however the mountain headwater study did include data during two separate months in the same summer and the karst river studies were collected in early and late spring, though in different years. DIC increased in concentration during the summer in the mountain headwater study and pH decreased while $\delta^{13}C_{DIC}$ became more depleted. The seasonal differences in the karst river study are less pronounced except for the differences in DIC which are described in section 6.1.2. During the study of the nutrient rich Rocky Mountain headwater, data were collected in June and August of 2007 and 2008. For June of both years, pH was higher by~1.5-3.5 units. DIC was lower in June by anywhere from 3.0-9.0 mg/L and also showed a larger magnitude change while $\delta^{13}C_{DIC}$ also showed a larger magnitude change in June and was generally more enriched. The diel study at Prickly Pear creek also contained data from different seasons for metal data. The authors of that study noted that phasing was not affected by changes in season. Seasonal differences in diel patterns between the Florida site and Montana/Colorado/Idaho sites could be due the presence of more extreme seasons in the northwest versus Florida.

Generally, at LRM050, there was not a seasonal increase in the number of parameters having diel patterns but rather a few parameters having consistent diel patterns throughout the seasons (pH, temp, ODO, and Al), with other parameters having sporadic diel patterns (CO_2, Zn, K, Fe). At LRM138, there is an increase in parameters with diel patterns as the seasons progressed, with DIC being one of those parameters. This could possibly indicate that seasonality and warming temperatures influence diel patterns in the wetland as a function of increased biological activity and of increased rates of reactions.

6.4.2 Mechanisms

All studies that focused on diel data of DIC and related parameters attributed photosynthesis and cellular respiration with DIC, DO, pH and $\delta^{13}C_{DIC}$ cycles. Generally, as plant material uptakes CO_2 during the day, DIC decreases, pH increases, ODO increases, and the water becomes more enriched in ^{13}C. These studies were undertaken in spring and summer months when biological processes are most active. The karst river study from 2010 also found that these biological processes indirectly affected other chemical processes such as redox reactions and metal sorption. Biological processes are likely the controlling mechanisms at LRM138 but likely have more complicated relationships with metal chemistry due to the higher metal concentrations and lower pH compared to other studies. The studies that focused on metal cycling contributed a variety of factors to cycling: sorption (Nimick et al. 2005 and Gammons et al. 2010), daily streamflow changes, photochemical processes, and biological processes (Sullivan etal 1998), pH-temperature dependent kinetic reactions (Gammons etal 2010).

At LRM, a combination of processes working in concert is likely driving diel patterns. Diel patterns are more pronounced in the wetland than in the channel, as is evidenced by the larger number of parameters having a significant ($p \leq 0.01$) cosine model fit to the data at LRM138 than at LRM050. Photosynthesis and cellular respiration as well nutrient uptake could be driving cycles in pH, DIC, DO, and $\delta^{13}C_{DIC}$, similar to other cited studies, at LRM138. The phasing of pH, DIC, $\delta^{13}C_{DIC,}$ and ODO during May at LRM138 are in agreement with the general diel patterns attributed to these mechanisms. However, as temperature increases during the day, the kinetics of the oxidation reaction of Fe^{2+} could lead to the formation of $Fe(OH)_{3(s)}$ or other hydrous ferric oxides. Metal cations have the potential to sorb on to these oxides, which could contribute to a decrease in dissolved metal cations during the early evening hours (if there is a lag in temperature increase and reaction activation) which was observed at LRM138. However, adsorption and desorption reaction rates are not the same so there is hysteresis between the two processes. The formation of $Fe(OH)_{3(s)}$ could potentially lead to a decrease in pH during the day however this is not observed at LRM138.

Molar ratios of CO_2/O_2 (Fig. 34-35) are less than 1 at LRM138 and greater than 1 at LRM050. If both CO_2 and O_2 are controlled primarily by the photosynthesis-respiration cycle, they should be linearly related with a slope of -1, as observed by de Montety etal (2010). The

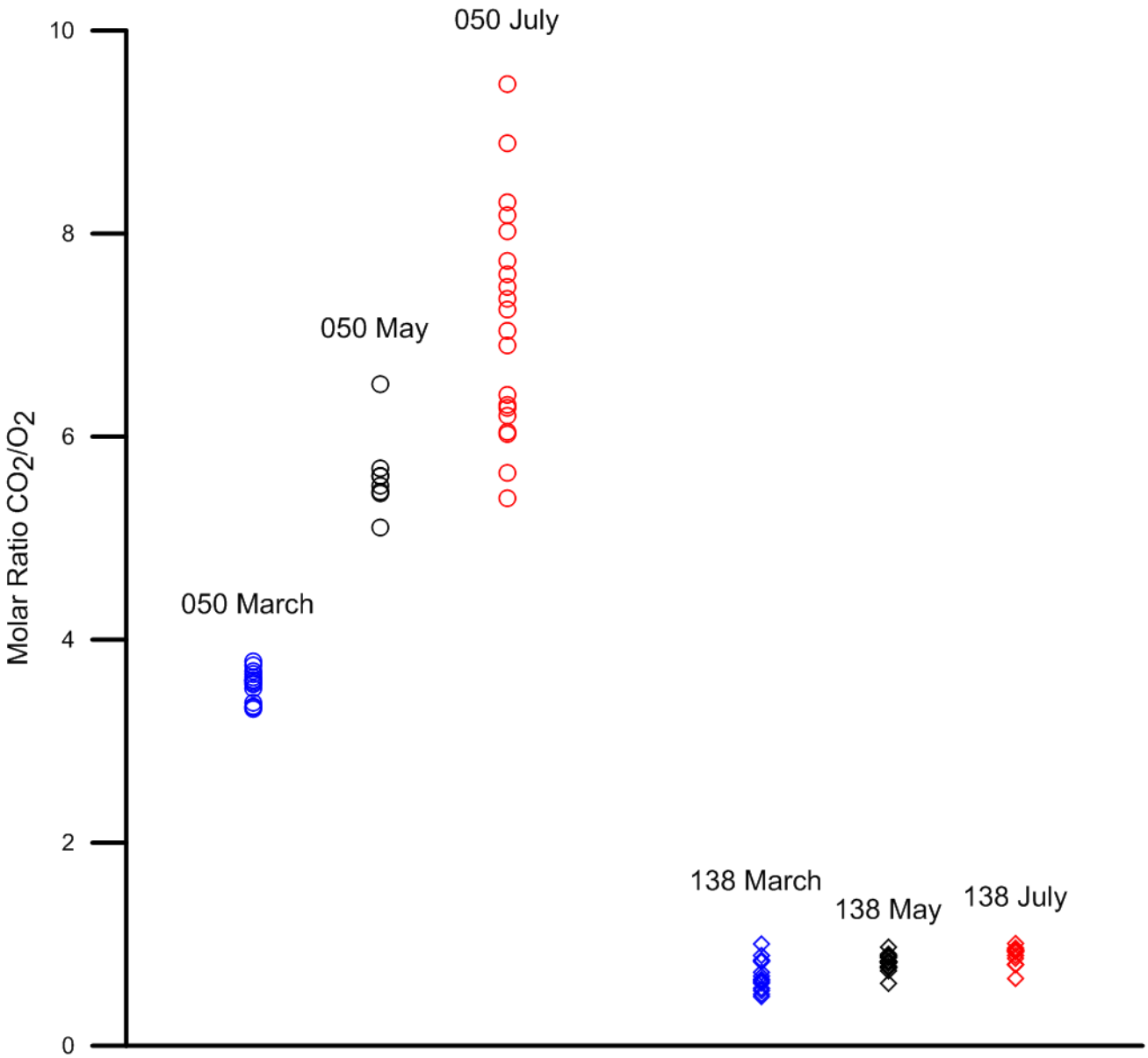

Figure 34. Plot of CO2/O2 molar ratio. LRM138 has a much lower ratio, indicating higher dissolved O2 concentrations there, than at LRM050.

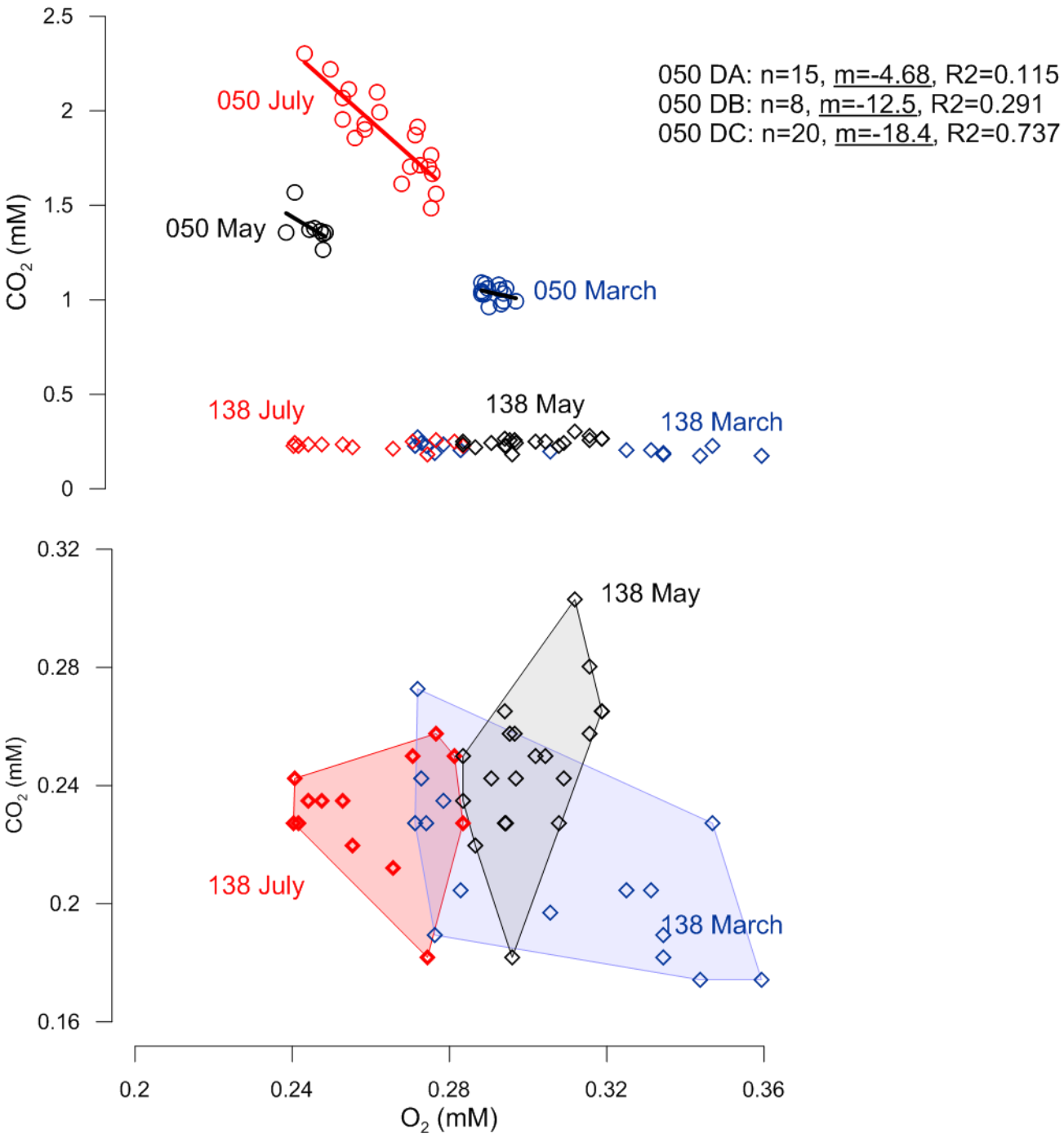

Figure 35. Plot of O2 vs. CO2. The top figure shows both locations on the same scale while the bottom figure shows CO2 concentrations at LRM138 on a smaller scale in order to show the relationship more clearly.

lack of a well-defined molar relationship at LRM138 may be attributed to the presence of a significant chemical and biological oxygen demand from the oxidation of reduced metals and precipitation of hydrolysable metals and biological processes; all of these reactions consume dissolved oxygen. At LRM050, the ratio is much higher due to the high concentrations of CO_2 being discharged from the mine portal. These CO_2-O_2 relationships support the idea that multiple mechanisms drive diel behavior at both locations.

In comparison with LRM138, location LRM050 has less vegetation present and less sunlight available due to tree cover, thus photosynthesis and related biological processes are likely to be less important. This is supported by the lack of defined DIC or $\delta^{13}C_{DIC}$ cycles at LRM050. The metal cycles observed at LRM050 could be due to kinetic oxidation of Fe^{2+} as pH values are not low enough for photoreduction. However, more investigation is needed. Smilley (2007) attributed cycles of metals to pH and temperature sorption reactions.

A previous study at LRM (Vesper and Smilley, 2010) reported that the CO_2-pH relationship downstream from the portal plotted nearly on a degassing line for 20C.However, in the current study, only the furthest downstream locations plot on a CO_2 degassing line and the remaining sites have a greater CO_2 concentration given the pH value of the sample (Fig. 36). This indicates that while degassing does occur at the site, other factors such as metal sorption or photosynthesis/cellular respiration contribute to pH and CO_2 behavior at the site. This is further evidence that a complex relationship of many mechanisms is driving the diel behavior and downstream changes in chemistry at LRM.

Two other possible mechanisms at this site are the roles of organic matter and sediments and the importance of residence time of water. Organic matter and sediments are important as they can be a source of CO_2 (from decay or respiration) or sink for metals as metals sorb onto negatively charged organic particles. Further, there is undoubtedly abundant organic carbon present which would result in high biological oxygen demand which could drive diel behavior of metals and O_2.While the role of organic matter and sediments is likely influencing the diel behavior of several parameters at LRM, further evidence is needed to quantify these mechanisms. Figure 37 provides a conceptual schematic at how organic matter or sediments affect diel behavior at LRM. In daytime hours, increasing water temperature (due to solar radiation) increases the rates of sorption reactions for cationic metals on to the organisms or

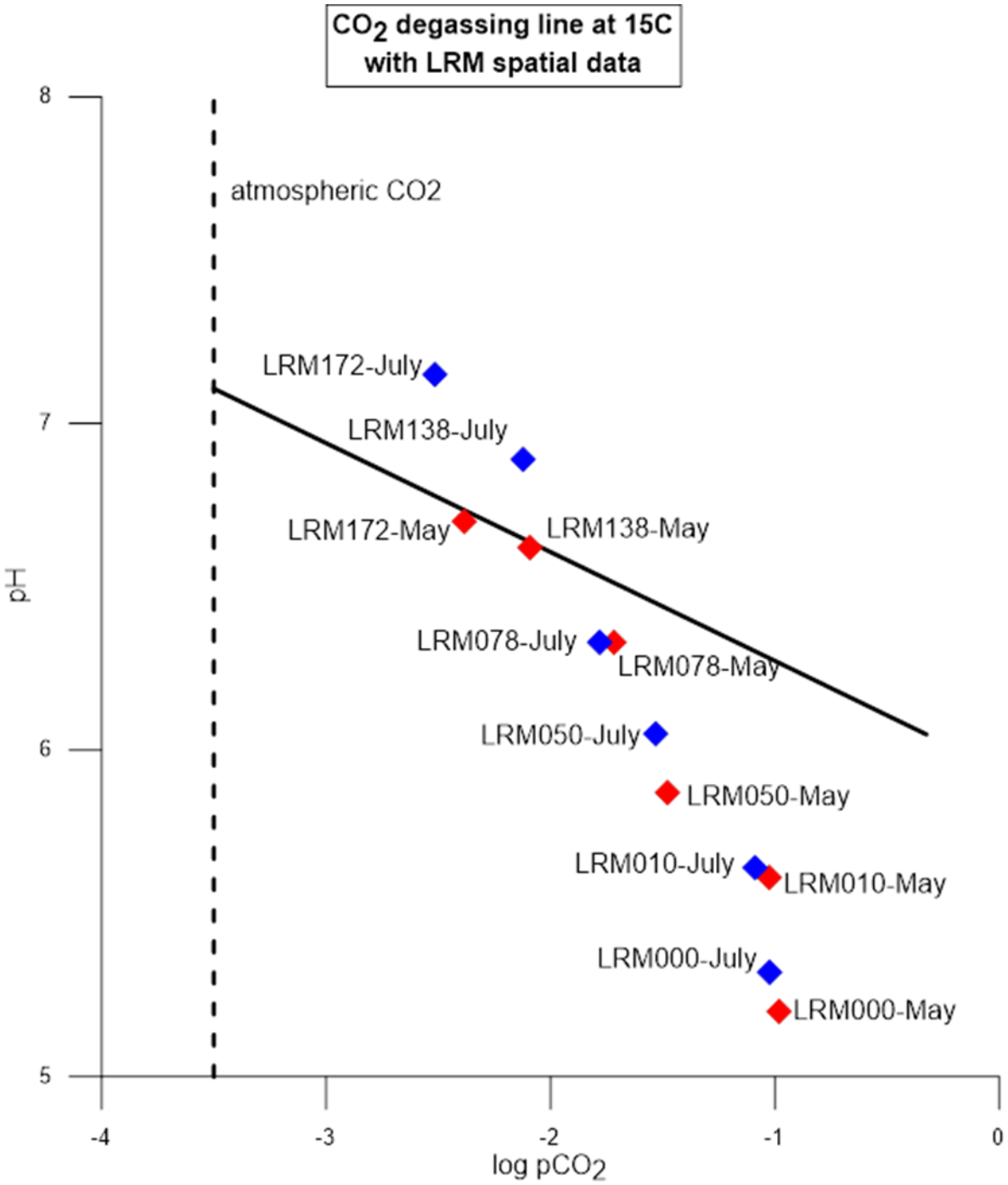

Figure 36. Degassing line of CO2 concentration vs. pH at 15C (the average temperature of the LRM sites) with longitudinal data overlain. The dashed line is atmospheric CO2 concentration. Note the y-axis is on a log scale.

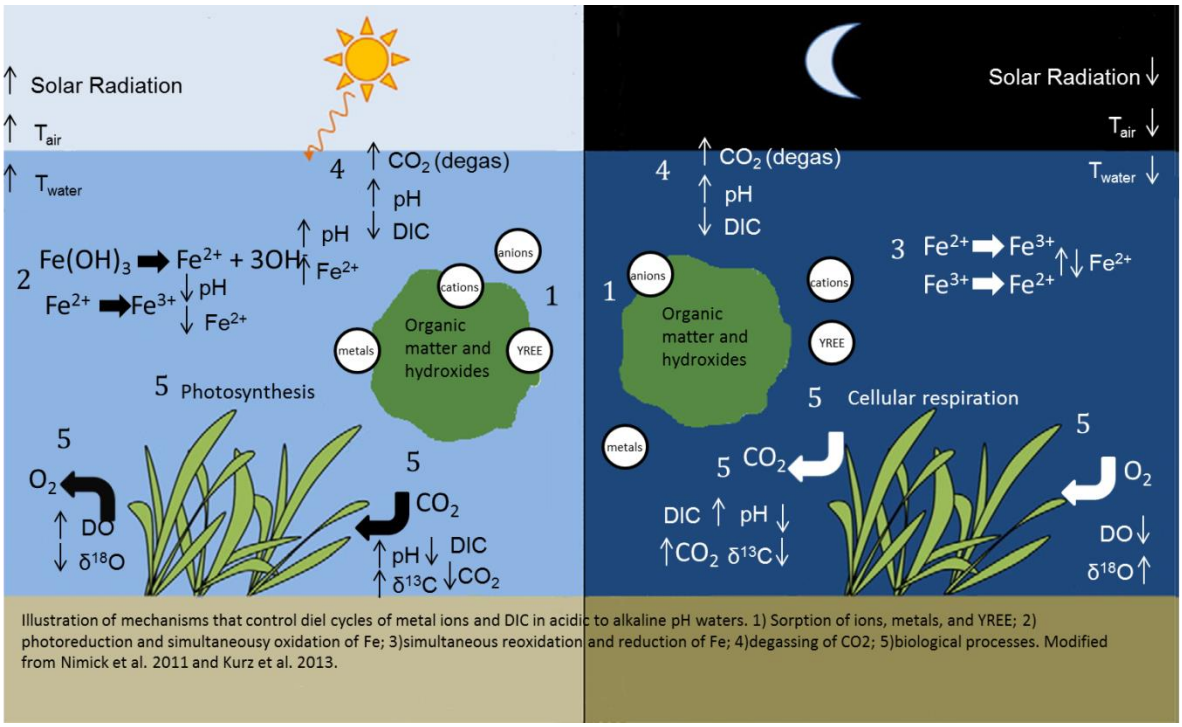

Illustration of mechanisms that control diel cycles of metal ions and DIC in acidic to alkaline pH waters. 1) Sorption of ions, metals, and YREE; 2) photoreduction and simultaneousy oxidation of Fe; 3)simultaneous reoxidation and reduction of Fe; 4)degassing of CO2; 5)biological processes. Modified from Nimick et al. 2011 and Kurz et al. 2013.

Figure 37. Illustration showing diel cycle mechanisms and their effects on different parameters. Adapted from Nimick et al. 2011 and Kurz et al. 2013.

sediments. At nighttime, when the water cools, these metals could possibly be released although the forward and backward reactions are not equal and opposite each other but are simplified as such in Figure 37. The water at LRM138 has been exposed to sunlight by for approximately 2.5 more hours (Vesper and Smilley 2010) than the water at LRM050 as it travels from the portal to the sampling location. The increased amount of solar radiation a sample at LRM138 has been exposed to could allow more time for the reactions to occur, like sorption, thus play a role in the diel behavior that was observed at LRM138.

7.0 Summary and conclusions

This study suggests that diel patterns of DIC and related parameters as well as metals can be influenced by season if the water contains biologically productive organisms. Further, this study suggests that controlling mechanisms for diel patterns in a coal mine drainage setting are not the same throughout the drainage, but are dependent on the changes in chemistry and vegetation. Data collected during this study also supports the hypothesis that heavy metal loads could possibly mask the existence of diel patterns in the presence of a mechanism that is known to contribute to diel patterns, i.e. temperature change or photosynthesis. The statistical analysis used on the model fit to the data indicates that even though cycling can be present at one or more locations in the same drainage and in the same season, those parameters do not necessarily fit a cosine model with the same statistical significance. Further, it shows that similar parameters, for example Y and Ce, do not exhibit the same diel patterns even though they are both part of the YREE group and can behave similarly chemically.

The wetland first installed at the LRM was intended to decrease total daily metal loads into the West Fork River. Evidence collected here in 2007 and during this study (2014) indicate that dissolved metals are decreasing in the drainage over time. However, while the wetland has grown and more vegetation was present in 2014 than in 2007, further study is needed to confirm the effectiveness of the wetland versus other possible causes for metal load reduction, such as hyporheic exchange.

Finally, the change in magnitude of parameters at each individual site and between sites suggests that sufficient water quality data cannot be collected at a single location or at a single time within the same drainage stream. If the effectiveness of a treatment plan, such as a wetland, for CMD streams is to be studied, then sampling should take place at various times of the day, in different locations, and in different seasons.

8.0 References

Barnes, I. (1965). "Geochemistry of Birch Creek, Inyo county, California: a travertine deposting creek in an arid climate." Geochimica et Cosmochimica Acta **29**(2): 28.

Benjamin, M. M. and J. O. Leckie (1981). "Multiple-site adsorption of Cd, Cu, Zn, and Pb on amorphous iron oxyhydroxide." Journal of Colloid Interface Science **79**: 12.

Dandurand, J. L., R. Gour, J. Hoefs, G. Menschel, J. Schot and E. Usdowski (1982). "Kinetically controlled variations of major components and carbon adn oxygen isotopesin a calcite-precipitating spring." Chemical Geology **36**: 17.

de Montety, V., J. B. Martin, M. J. Cohen, C. Foster and M. J. Kurz (2011). "Influence of diel biogeochemical cycles on carbonate equilibrium in a karst river." Chemical Geology **283**(1-2): 14.

Drysdale, R., S. Lucas and K. Carthew (2003). "The influence of diurnal temperatures on the hydrochemistry of a tufa-depositing stream." Hydrological Processes **17**(17): 23.

Dzombak, D. A. and F. M. M. Morel (1990). Surface Complexation and Modeling. Hoboken, N.J., John Wiley.

Finlay, J. C. (2003). "Controls of streamwater dissolved inorganic carbon dynamics in a forested watershed." Biogeochemistry(62): 22.

Gammons, C., D. Nimick, S. Parker, D. Snyder, R. McCleskey, R. Amils and S. Poulson (2008). "Photoreduction fuels biogeochemical cycling of iron in Spain's acid rivers." Chemical Geology **252**(3-4): 12.

Gammons, C. H., T. E. Duaime, S. R. Parker, S. R. Poulson and P. Kennelly (2010). "Geochemistry and stable isotope investigation of acid mine drainage associated with abandoned coal mines in central Montana, USA." Chemical Geology **269**(1-2): 13.

Gammons, C. H., D. A. Nimick, S. R. Parker, T. E. Cleasby and R. B. McCleskey (2005). "Diel behavior of iron and other heavy metals in a mountain stream with acidic to neutral pH: Fisher Creek, Montana, USA." Geochimica et Cosmochimica Acta **69**(10): 12.

Hennen, R. V. (1912). Doddridge and Harrison counties, Wheeling news Litho. Co.

Kurz, M. J., V. de Montety, J. B. Martin, M. J. Cohen and C. R. Foster (2013). "Controls on diel metal cycles in a biologically productive carbonate-dominated river." Chemical Geology **358**: 14.

Kurz, M. J., V. de Montety, J. B. Martin, M. J. Cohen and C. R. Foster (2013). "Controls on diel metal cycles in a biologically productive carbonate-dominated river." Chemical Geology **358**: 61-74.

Liu, Z., Q. L, Sun , L. H., L. C., W. H. and W. J. (2006). "Diurnal variations of hydrochemistry in a travertien deposting stream in Baishuitai, Yunnan, SW China." Aquatic Geochemistry **12**: 19.

Lorah, M. and J. Herman (1988). "The chemical evolution of a travertine-deposting stream: geochemical processes and mass transfer reactions." Water Resources Research **24**(9): 12.

Nimick, D. A., T. E. Cleasby and R. B. McCleskey (2005). "Seasonality of diel cycles of dissolved trace-metal concentrations in a Rocky Mountain stream." Environmental Geology **47**(5): 12.

Nimick, D. A., T. E. Cleasby and R. B. McCleskey (2005). "Seasonality of diel cycles of dissolved trace-metal concentrations in a Rocky Mountain stream." Environmental Geology **47**(5): 603-614.

Nimick, D. A., C. H. Gammons, T. E. Cleasby, J. P. Madison, D. Skaar and C. M. Brick (2003). "Diel cycles in dissolved metal concentrations in streams: Occurrence and possible causes." Water Resources Research **39**(9): 17.

Nimick, D. A., C. H. Gammons and S. R. Parker (2011). "Diel biogeochemical processes and their effect on the aqueous chemistry of streams: A review." Chemical Geology **283**(1-2): 15.

Parker, S. R., C. H. Gammons, S. R. Poulson, M. D. DeGrandpre, C. L. Weyer, M. G. Smith, J. N. Babcock and Y. Oba (2010). "Diel behavior of stable isotopes of dissolved oxygen and dissolved inorganic carbon in rivers over a range of trophic conditions, and in a mesocosm experiment." Chemical Geology **269**(1-2): 11.

Parker, S. R., C. H. Gammons, S. R. Poulson, M. D. DeGrandpre, C. L. Weyer, M. G. Smith, J. N. Babcock and Y. Oba (2010). "Diel behavior of stable isotopes of dissolved oxygen and dissolved inorganic carbon in rivers over a range of trophic conditions, and in a mesocosm experiment." Chemical Geology **269**(1–2): 22-32.

Plummer, L. N., Busenberg, E. (1982). "The solubilities of calcite, argagonite, and vaterite in CO_2-H_2O solutions between 0-90C, and an evaluation of the aqueosu model for teh system $CaCO_3$-CO_2-H_2O." Geochimica et Cosmochimicia Acta **46**(6): 40.

Poulson, S. R. and A. B. Sullivan (2010). "Assessment of diel chemical and isotopic techniques to investigate biogeochemical cycles in the upper Klamath River, Oregon, USA." Chemical Geology **269**(1-2): 9.

Poulson, S. R. and A. B. Sullivan (2010). "Assessment of diel chemical and isotopic techniques to investigate biogeochemical cycles in the upper Klamath River, Oregon, USA." Chemical Geology **269**(1–2): 3-11.

Smilley, M. J. (2007). Determination of diel chemical cycle presence within abandoned coal mine drainage streams in Harrison County, WV. Geology and Geography. West Virginia University Libraries, West Virginia University. **M.S. Geology:** 119.

Spiro, B. and A. Pentecost (1991). "One day in the life of stream- a diurnal inorganic carbon mass balance for a travertien-deposting stream " Geomicrobiology **9**: 11.

Stookey, L. L. (1970). "Ferrozine---a new spectrophotometric reagent for iron." Analytical chemistry **42**(7): 3.

Sullivan, A. B., J. I. Drever and D. M. McKnight (1998). "Diel variation in element concentrations, Peru Creek, Summit County, Colorado." Journal of Geochemical Exploration **64**(1): 5.

Sullivan, A. B., J. I. Drever and D. M. McKnight (1998). "Diel variation in element concentrations, Peru Creek, Summit County, Colorado." Journal of Geochemical Exploration **64**(1): 141-145.

Vesper, D. J. and H. M. Edenborn (2012). "Determination of free CO2 in emergent groundwaters using a commercial beverage carbonation meter." Journal of Hydrology **438-439**: 7.

Vesper, D. J., H. M. Edenborn, A. A. Billings and J. E. Moore (2015). " A field-based method for determination of dissolved inorganic carbon in water based on CO_2 and carbonate equilibria." Water, Air, and Soil Pollution **226**(28): 12.

Weather Underground, http://www.wunderground.com/history/airport/KCKB/2014/3/14/DailyHistory.html, accessed Feb. 2, 2015.

Weather Underground, http://www.wunderground.com/history/airport/KCKB/2014/5/19/DailyHistory.html?req_city=NA&req_state=NA&req_statename=NA, accessed Feb. 2, 2015.

Weather Underground, http://www.wunderground.com/history/airport/KCKB/2014/7/16/DailyHistory.html?req_city=NA&req_state=NA&req_statename=NA, accessed Feb. 2, 2015.

APPENDICES

Appendix I. Methods and derivations

Tutorial: Cosine model fit and statistical analysis

Diel data can be fit using a cosine model because the concentrations of various parameters are expected to increase and decrease according to a similar pattern over time.

The basic cosine equation is:

$$y = \cos(\theta) \quad \text{Eq. 1}$$

To manipulate this equation for real data, more terms are added: mean (M), amplitude (A) phase (H), period (B), and elapsed time (t). This gives the cosine model equation:

$$y = M + A\cos(Bt - H) \quad \text{Eq. 2}$$

- M is the estimated mean of the parameter value in question. It adjusts the cosine curve to center around that value instead of 0 and is in the unit of the given parameter, i.e. mg/L if dealing with a dissolved metal concentration.
- A is amplitude of the curve that covers the range of values for the parameter in question. It also in the units of the parameter in question. It adjusts the curve along the y axis.
- B is the period chosen to represent the cycle. For diel experiments B=0-360°=0-24 hours.
- t is a fraction of elapsed time over period and is unit-less.
- H is the phase of the cosine model fit and adjust the model fit in degrees. It adjusts the model to have maximum and minimum values at approximately the same elapsed as the real data do. It can be used to predict the time of the maximum concentration/value of the parameter. It adjusts the curve along the X axis

The cosine model fit essentially calculates an estimated concentration at time t using the parameters outlined above, the goal is to have the estimated concentrations match the real data while staying within the bounds of the model. The equation can be rewritten thusly:

$$C_t = M + A\cos(Bt - H) \quad \text{Eq. 3}$$

When equations 1 and 3 are compared, it is clear that
$\theta = Bt - H$.

Theta (θ) represents angular measurements in degrees and the parameters B and H are also input into the equation as degrees. However, when using Excel to calculate the cosine model fit (which is the simplest option), degrees must be converted to radians due to the default settings of the program so a degree to radian conversion must be built into the model equation.

Converting the model equation parameters to radians
Phase

The conversion of degrees to radians is:

$360° = 2\,\pi$ rad Eq. 4.

So, the input for phase (H) becomes

$$H° * \left(\frac{2\,\pi\,rad}{360°}\right) = H°\,\pi\,180°^{-1} \quad \text{Eq. 5}$$

and the model equation becomes

$$C_t = M + Acos(Bt - (H°\,\pi\,180°^{-1})) \quad \text{Eq. 6.}$$

Period

The period, B = 360°, represents 24 hours because instead of graphing concentrations as a function of degrees, they are graphed as a function of time. B must also be converted to radians. So,

$$B = 360°\,\pi\,180°^{-1} \quad \text{Eq. 7}$$

and the value of 360° is left in the equation because it is fixed. The final model equation is finally achieved and is

$$C_t = M + Acos((t * 360°\,\pi\,180°^{-1}) - (H\,\pi\,180°^{-1})) \quad \text{Eq. 8.}$$

Calculating model fit and creating a polar plot

The simplest way to calculate the cosine model fit and conduct the subsequent statistical analysis on the model is to use Excel.

Steps to calculate model fit:

1. Calculate the mean of the parameter in question.
2. Calculate the mean error.

$$Mean\ Error = (parameter\ value - mean)^2 \quad \text{Eq. 9.}$$

3. Calculate the model fit. Initially, values for M, A, and H are estimated. In a "good" model fit, M is usually near the calculated mean, A is a value indicating the range or magnitude between the highest and lowest concentration, and H is some value 0-360.
4. Calculate the model error.

$$Model\ Error = (model\ fit - paramter\ value)^2 \qquad \text{Eq. 10.}$$

5. Calculate residual sum squares of the data (or null hypothesis, RSSn) and the residual sum squares of the cosine model fit (RSSc) by simply summing the mean error values for RSSn and the model error values for RSSc.
6. Using the Solver package in Excel, minimize the value of RSSc using the objective references of M, A, and H to obtain the best model fit. It is important to constrain the value of H to be $0 > H < 360°$ and A to be $A \geq 0$. Solver will converge to a solution that minimizes RSSc by changing the values of M, A, and H. If cell references for M, A, and H were wet up in the initial model fit calculation, then the values will automatically be recalculated.
7. Graph elapsed time on the x axis, and model fit and raw data on the y to observe how well the model fits the data.

<u>Steps for statistical analysis and graphing:</u>

8. Calculate the F statistic. The F – test is the statistical technique that most commonly used to when comparing models that have been fit to data.

$$F = \frac{(RSSn - RSSc) \times {df_1}^{-1}}{RSSc \times {df_2}^{-2}} \qquad \text{Eq. 11.}$$

The degrees of freedom are df1 = 2 degrees freedom since 2 'models' are being compared (the raw data and the cosine model fit) and df_2 = # of observations (n) – 3. Thus:

$$F = \frac{\frac{RSSn - RSSc}{2}}{\frac{RSSc}{n-3}} \qquad \text{Eq. 11.}$$

9. Allow excel to calculate the p-value of the f-statistic. Choose an alpha to use as a comparison for the model fit values.
10. Using a polar plot, plot H as the angular plot and p-values as the radial plot. This will plot each parameter a point according to the predicted time of maximum concentration or value and statistical significance of the model fit.

DIC method calculation

After collecting DIC data in the field, as described in section 4.2.2, DIC is then calculated by manipulating the carbonate equilibrium equation and correcting the equilibrium constants for temperature. The most basic DIC equation is

$$DIC = [H_2CO_3^*] + [HCO_3^-] + [CO_3^{2-}] \quad \text{Eq. 12}$$

however, it is more common to work in activities instead of concentrations, so the equation becomes

$$DIC = \frac{[aH_2CO_3^*]}{\gamma_{H_2CO_3}} + \frac{[aHCO_3^-]}{\gamma_{HCO_3^-}} + \frac{[aCO_3^{2-}]}{\gamma_{CO_3^{2-}}} \quad \text{Eq. 13.}$$

The equilibrium equations for these terms are:

$$K_1 \qquad \frac{[aH_2CO_3^*]}{\gamma_{H_2CO_3}} = \frac{a[H^+]}{\gamma_{H^+}} + \frac{[aHCO_3^-]}{\gamma_{HCO_3^-}} \quad \text{Eq. 14}$$

$$K_1 = \frac{\left(\frac{a[H^+]}{\gamma_{H^+}}\right) + \frac{[aHCO_3^-]}{\gamma_{HCO_3^-}}}{\frac{[aH_2CO_3^*]}{\gamma_{H_2CO_3}}} \quad \text{Eq. 15}$$

$$K_2 \qquad \frac{[aHCO_3^-]}{\gamma_{HCO_3^-}} = \frac{a[H^+]}{\gamma_{H^+}} + \frac{[aCO_3^{2-}]}{\gamma_{CO_3^{2-}}} \quad \text{Eq. 16}$$

$$K_2 = \frac{\left(\frac{a[H^+]}{\gamma_{H^+}}\right) + \frac{[aCO_3^{2-}]}{\gamma_{CO_3^{2-}}}}{\frac{[aHCO_3^-]}{\gamma_{HCO_3^-}}} \quad \text{Eq. 17.}$$

The carbonation meter reports an activity of CO_2. Since H_2CO3^* is a combined term for carbonic acid and CO_2 gas and where CO_2 gas is present higher concentrations of up to three orders of magnitude, the CO_2 activity from the carbonation can be used for the activity of $H_2CO_3^*$. With this known term, equations 15 and 17 can be rearranged in terms of aCO_2 and substituted into equation 13 to arrive at the ultimate DIC equation (Eq. 20) used in this study.

$$aHCO_3^- = \frac{K_1}{a_{H^+}\gamma HCO_3^-}\, aCO_2 \quad \text{Eq. 18}$$

$$aCO_3^{2-} = \frac{K_1K_2}{a_{H^+}^2\gamma CO_3^{2-}} \quad \text{Eq. 19}$$

$$DIC = \left[\frac{aCO_2}{\gamma_{CO_2}} + \left(\frac{K_1}{a_H\gamma_{HCO_3^-}}\right)aCO_2 + \left(\frac{K_1K_2}{a_H^2\gamma_{CO_3^{2-}}}\right)\right] x\ 1.1 \quad \text{Eq. 20.}$$

The γH^+ terms are eliminated because they equal 1 and 1.1 is a correction factor for the volume dilution from the buffer addition. The gamma values are constant are as follows and were determined by speciation calculations using Minteq and the Davies Equation for estimating activity coefficients (Vesper et al. 2015).

γCO_2	1.09
γHCO_3^-	0.72
γCO_3^{2-}	0.27

The equilibrium constants are corrected for temperature using the equations from Plummer and Busenberg 1982 (Plummer 1982).

Appendix II. Tabulated data

Table 21. Tabulated data LRM138 DA March 14-15 2014

Parameter		pH	T (C)	ODO mg/L	CO_2 g/L	DIC mM	Fe II	Fe_{TOT}	Mn mg/L	Ca mg/L	Mg mg/L	K mg/L	SiO_2 mg/L	$SO4^{2-}$ mg/L	$\delta^{13}C_{D\ IC}$	Y ug/L	Ce ug/L	Ni ug/L	Zn ug/L	As ug/L	Al ug/L
Date/ time	**3/14 1400**	6.90	16.2	10.7	8.00 E-3	1.36	BDL	BDL	8.07 E-1	151	61.7	3.95	12.4	509	-15.4	3.15 E-1	2.33 E-1	12.2	72.1	2.44 E-1	384
	3/14 1600	6.88	15.5	11.0	7.67 E-3	1.39	BDL	BDL	8.69 E-1	143	59.5	4.43	13.1	508	-0.54	2.28 E-1	5.54 E-2	8.10	17.5	7.90 E-2	BDL
	3/14 1800	6.81	14.2	10.4	9.00E -3	1.40	BDL	BDL	7.92 E-1	145	59.7	4.04	12.0	508	-0.67	2.33 E-1	6.54 E-2	7.82	12.9	9.26 E-2	BDL
	3/14 2000	6.74	13.1	9.05	9.00 E-3	1.49	BDL	BDL	8.27 E-1	158	61.5	3.97	12.3	509	-1.30	1.92 E-1	4.95 E-2	8.30	14.0	6.92 E-2	BDL
	3/14 2200	6.74	12.9	8.84	8.33 E-3	1.50	BDL	BDL	8.09 E-1	145	60.3	3.96	12.1	509	-1.22	2.61 E-1	5.38 E-2	8.41	9.66	6.29 E-2	BDL
	3/15 0000	6.72	12.8	8.77	1.00 E-2	1.50	BDL	BDL	8.22 E-1	154	59.7	3.89	12.2	509	-1.22	7.98 E-1	3.88 E-1	8.57	12.00	1.45 E-1	178
	3/15 0200	6.72	12.8	8.73	1.07 E-2	1.77	BDL	BDL	7.78 E-1	153	60.0	3.86	12.0	509	-1.20	2.93 E-1	9.69 E-2	8.08	9.55	5.29 E-2	BDL
	3/15 0400	6.72	12.8	8.70	1.20 E-2	1.47	BDL	BDL	8.02 E-1	154	58.8	3.87	11.9	509	-1.27	3.03 E-1	1.29 E-1	8.13	11.3	1.14 E-1	46.5
	3/15 0600	6.73	12.9	8.68	1.00 E-2	1.23	BDL	BDL	7.91 E-1	142	59.7	3.88	11.8	502	-1.21	2.32 E-1	4.36 E-2	8.01	18.9	1.23 E-1	BDL
	3/15 0800	6.71	12.5	8.91	1.03 E-2	1.44	BDL	BDL	8.14 E-1	146	61.1	3.89	12.1	510	-1.12	4.24 E-1	1.95 E-2	8.15	20.4	7.17 E-2	143
	3/15 1000	6.80	13.4	10.6	9.00 E-3	1.44	BDL	BDL	7.80 E-1	152	59.2	3.89	11.7	511	-0.76	1.76 E-1	3.10 E-2	7.79	46.2	7.92 E-2	BDL
	3/15 1200	6.87	15.6	11.5	7.67 E-3	1.47	BDL	BDL	7.18 E-1	145	60.4	3.77	11.9	512	-0.40	3.57 E-1	1.88 E-1	7.39	9.81	9.68 E-2	93.5
	3/15 1400	6.92	16.5	11.1	1.00 E-2	1.40	BDL	BDL	6.91 E-1	148	58.3	3.87	11.5	512	-0.36	2.52 E-1	6.76 E-2	7.38	9.00	9.28 E-2	33.2
	3/15 1600	6.88	15.9	10.7	8.33 E-3	1.42	BDL	BDL	7.58 E-1	139	27.6	3.90	11.3	512	-0.66	3.83 E-1	1.77 E-1	7.48	11.9	8.17 E-2	141
	3/15 1800	6.77	13.9	9.78	8.67 E-3	1.42	BDL	BDL	7.34 E-1	143	60.0	3.82	11.7	518	-0.85	3.23 E-1	1.53 E-1	7.78	35.3	9.62 E-2	78.1

Table 22. Cosine model fit data LRM138 DA March 14-15 2014

Parameter	pH	T (C)	ODO mg/L	CO_2 g/L	DIC mM	Fe II	Fe_{TOT}	Mn mg/L	Ca mg/L	Mg mg/L	K mg/L	SiO_2 mg/L	$SO4^{2-}$ mg/L	$\delta^{13}C_{DIC}$	Y ug/L	Ce ug/L	Ni ug/L	Zn ug/L	As ug/L	Al ug/L
Cosine model parameters																				
M	6.77	13.8	9.68	9.47 E-3	1.49	BDL	BDL	7.89 E-1	148	59.8	3.91	12.0	509	-1.01	2.82 E-1	1.30 E-1	7.96	13.3	7.29 E-2	74.4
A	9.52 E-2	1.72	1.39	1.26 E-3	9.24 E-2	BDL	BDL	2.53 E-2	3.21	1.56 E-1	5.60 E-2	1.34 E-1	2.26	3.24 E-1	2.70 E-2	1.370 E-2	4.32 E-1	2.14	1.96 E-2	40.1
H	211	216	209	57.4	33.0	BDL	BDL	2.33	26.4	0.00	283	317	243	209	147	360	14.9	130	214	189
f-stat	234	154	415	9.07	6.53	BDL	BDL	1.07	1.35	5.75 E-2	1.57	3.07 E-1	1.90	4.16	3.64 E-1	5.95 E-2	8.85	7.38 E-1	11.7	5.13 E-2
p-value	1.93 E-41	1.68 E-3	3.41 E-3	1.59 E-3	3.44 E-3	BDL	BDL	3.17 E-1	2.41 E-1	9.35 E-1	1.94 E-1	7.05 E-1	1.46 E-1	2.51 E-2	6.60 E-1	9.33 E-1	1.96 E-3	4.34 E-1	1.08 E-3	5.63 E-2
RSD	1.12	10.3	10.8	13.1	6.64	BDL	BDL	5.82	3.72	1.88	2.26	3.46	0.67	38.9	25.4	75.5	4.90	29.6	18.1	129

Table 23. Tabulated data LRM050 DA March 14-15 2014

Parameter		pH	T (C)	ODO mg/L	CO_2 g/L	DIC mM	Fe II mg/L	Fe_{TOT} mg/L	Mn mg/L	Ca mg/L	Mg mg/L	K mg/L	SiO_2 mg/L	$SO4^{2-}$ mg/L	$\delta^{13}C_{DIC}$	Y ug/L	Ce ug/L	Ni ug/L	Zn ug/L	As ug/L	Al ug/L
Date/ time	**3/14 1500**	no data	no data	9.50	4.37 E-2	2.32	7.99 E-1	7.84 E-1	2.23	143	60.0	3.77	12.2	516	5.28 E-1	2.52	1.52	13.8	20.5	1.15 E-1	108
	3/14 1700	no data	no data	9.28	4.23 E-2	2.24	7.93 E-1	7.86 E-1	2.20	139	58.3	3.92	12.0	517	4.12 E-1	2.45	1.49	13.9	32.4	1.49 E-1	124
	3/14 1900	no data	no data	9.24	4.53 E-2	2.38	8.01 E-1	7.86 E-1	2.22	139	25.5	3.84	12.0	517	1.57 E-1	2.52	1.55	13.6	17.8	1.43 E-1	131
	3/14 2100	no data	no data	9.22	4.60 E-2	2.37	8.07 E-1	7.77 E-1	2.29	143	61.1	3.82	12.6	517	4.83 E-1	2.62	1.59	14.0	17.1	1.57 E-1	145
	3/14 2300	no data	no data	9.23	4.57 E-2	2.38	8.11 E-1	8.01 E-1	2.23	141	60.4	3.88	12.2	518	4.18 E-1	2.63	1.62	14.1	19.5	1.42 E-1	124
	3/15 0100	no data	no data	9.22	4.53 E-2	2.40	8.16 E-1	8.08 E-1	2.18	135	58.9	3.67	12.1	518	4.90 E-1	2.52	1.54	13.7	17.2	1.49 E-1	142
	3/15 0300	no data	no data	9.22	4.80 E-2	2.44	8.21 E-1	8.03 E-1	2.20	146	60.6	3.66	12.3	517	5.67 E-1	2.54	1.55	13.7	18.1	1.57 E-1	129
	3/15 0500	6.23	12.1	9.25	4.77 E-2	2.42	1.16	7.36 E-1	2.14	142	59.0	3.59	12.1	517	3.92 E-1	2.52	1.54	13.4	27.7	1.54 E-1	95.1
	3/15 0700	6.27	12.0	9.27	4.67 E-2	2.36	8.21 E-1	8.32 E-2	2.12	140	59.4	3.54	11.8	518	4.51 E-1	2.50	1.53	13.6	19.3	1.44 E-1	112
	3/15 0900	6.26	12.1	9.36	4.75 E-2	2.36	8.02 E-1	7.59 E-2	2.14	136	60.0	3.50	12.0	518	5.37 E-1	2.40	1.48	14.3	63.0	1.63 E-1	96.7
	3/15 1100	6.28	12.3	9.40	4.55 E-2	2.09	6.98 E-1	7.86 E-1	2.21	146	59.7	3.66	12.2	519	8.75 E-1	2.49	1.54	13.8	19.9	1.54 E-1	96.8
	3/15 1300	6.28	12.4	9.40	4.37 E-2	2.38	7.27 E-1	8.21 E-1	2.13	132	58.2	3.58	11.8	520	-2.26	2.36	1.46	13.8	58.2	1.90 E-1	87.1
	3/15 1500	6.3	12.5	9.42	4.67 E-2	2.45	8.34 E-1	7.71 E-1	2.15	135	59.1	3.74	11.7	519	5.92 E-1	2.51	1.56	13.9	22.8	1.49 E-1	86.9
	3/15 1700	6.31	12.1	9.38	4.30 E-2	2.33	7.84 E-1	8.43E-1	2.11	132	58.1	3.72	11.9	520	3.98 E-1	2.64	1.68	14.1	20.4	1.86 E-1	131
	3/15 1900	6.32	12.2	9.37	4.63 E-2	2.29	7.98 E-1	8.10 E-2	2.16	134	59.1	3.60	12.0	236	4.46 E-1	no data	no data	no data	no data	no data	no data

Table 24. Cosine model fit data LRM050 DA March 14-15 2014

Parameter	pH	T (C)	ODO mg/L	CO_2 g/L	DIC mM	Fe II mg/L	Fe_{TOT} mg/L	Mn mg/L	Ca mg/L	Mg mg/L	K mg/L	SiO_2 mg/L	$SO4^{2-}$ mg/L	$\delta^{13}C_{DIC}$	Y ug/L	Ce ug/L	Ni ug/L	Zn ug/L	As ug/L	Al ug/L
Cosine model parameters																				
M	6.29	12.1	9.30	4.58 E-2	2.35	7.95 E-1	7.92 E-1	2.18	139	59.4	3.68	12.1	517	4.95 E-1	2.52	1.55	13.8	26.5	1.54 E-1	115
A	2.21 E-2	2.84 E-1	9.35 E-2	1.62 E-3	5.98 E-2	2.67 E-2	7.95 E-3	3.69 E-2	2.45	5.46 E-1	1.35 E-1	1.59 E-1	7.02 E-1	1.26 E-1	8.11 E-2	4.58 E-2	1.08 E-1	12.3	4.78 E-3	24.6
H	285	206	190	66.2	18.8	358	285	323	58.8	39.5	299	6.78	187	148	335	325	247	158	168	337
f-stat	85.9	41.3	174	6.01	1.60	1.98	2.49 E-1	2.04	1.11	1.38	8.05	1.82	1.30	2.43	5.22	2.48	8.20 E-1	2.58	1.86 E-1	13.9
p-value	5.51 E-18	6.03 E-12	6.33 E-36	7.74 E-3	1.91 E-1	1.36 E-1	7.27 E-1	1.29 E-1	3.04 E-1	2.35 E-1	2.59 E-3	1.57 E-1	2.52 E-1	9.25 E-2	1.25 E-2	8.88 E-2	4.09 E-1	8.18 E-1	8.05 E-1	2.74 E-4
RSD	0.30	1.44	7.90	3.79	3.92	4.64	3.50	2.32	3.35	1.593	3.47	1.90	0.22	32.1	3.18	3.65	1.72	56.2	11.9	17.4

Table 25. Tabulated data LRM138 DB May 19-20 2014

Parameter		pH	T (C)	ODO mg/L	CO_2 g/L	DIC mM	Fe II mg/L	Fe_{TOT} mg/L	Mn mg/L	Ca mg/L	Mg mg/L	K mg/L	SiO_2 mg/L	$SO4^{2-}$ mg/L	$\delta^{13}C_{DIC}$	Y ug/L	Ce ug/L	Ni ug/L	Zn ug/L	As ug/L	Al ug/L
Date/ time	**5/19 1400**	6.80	20.4	9.89	1.07 E-2	1.42	1.36 E-1	8.66 E-2	1.06	159	61.4	3.73	13.2	615	-2.21	1.99 E-1	5.22 E-2	15.2	23.2	2.00 E-1	187
	5/19 1530	6.78	20.0	9.66	1.10 E-2	1.42	1.45 E-1	6.42 E-2	1.01	152	57.9	3.67	2.5	620	-2.13	2.25 E-1	6.51 E-2	14.0	14.7	1.84 E-1	126
	5/19 1700	6.72	18.4	9.41	1.00 E-2	1.44	1.52 E-1	1.19 E-1	1.07	152	59.9	3.60	12.7	619	-2.52	1.97 E-1	3.87 E-2	12.7	11.4	1.60 E-1	408
	5/19 1830	6.50	16.0	9.07	1.03 E-2	1.45	1.55 E-1	1.33 E-1	1.11	151	59.1	3.76	12.6	619	-1.66	2.30 E-1	5.04 E-2	12.8	21.2	1.62 E-1	568
	5/19 2000	6.44	15.1	9.07	1.10 E-2	1.48	1.60 E-1	1.16 E-1	1.14	150	59.3	3.75	13.0	620	-3.29	2.44 E-1	5.12 E-2	13.2	13.5	1.68 E-1	136
	5/19 2130	6.41	14.2	9.17	9.67 E-3	1.44	1.70 E-1	1.67 E-1	1.15	151	59.9	3.89	12.8	618	-3.34	2.53 E-1	5.39 E-2	13.2	17.3	1.87 E-1	618
	5/19 2300	6.40	13.7	9.3	1.07 E-2	1.39	1.56 E-1	1.29 E-1	1.19	161	62.4	3.72	13.5	BDL	-3.31	2.50 E-1	5.30 E-2	13.8	14.9	1.85 E-1	130
	5/20 0030	6.39	13.3	9.41	1.17 E-2	1.41	1.54 E-1	1.23 E-1	1.16	158	62.0	3.78	13.2	609	-3.29	2.48 E-1	5.20 E-2	14.1	12.2	1.73 E-1	319
	5/20 0200	6.39	13.2	9.45	1.13 E-2	1.41	1.51 E-1	1.24 E-1	1.13	152	60.7	4.08	13.0	622	-3.18	2.43 E-1	4.97 E-2	13.7	13.4	1.60 E-1	200
	5/20 0330	6.39	13.1	9.49	1.13 E-2	1.39	1.56 E-1	1.21 E-1	1.19	153	61.4	4.21	12.8	619	-3.27	2.51 E-1	5.27 E-2	14.3	15.4	1.79 E-1	150
	5/20 0500	6.40	13.2	9.47	8.00 E-3	1.43	1.54 E-1	1.21 E-1	1.11	150	59.0	4.48	12.4	620	-3.24	2.39 E-1	5.13 E-2	14.4	13.2	1.74 E-1	153
	5/20 0630	6.43	13.4	9.42	1.00 E-2	1.46	1.53 E-11	1.19 E-1	1.06	142	56.3	3.85	12.1	623	-3.19	2.36 E-1	4.66 E-2	14.3	14.8	1.68 E-1	264
	5/20 0800	6.45	13.8	9.74	1.10 E-2	1.40	1.60 E-1	1.48 E-1	1.18	154	62.2	4.16	13.0	623	-3.08	2.32 E-1	4.90 E-2	13.8	14.0	1.85 E-1	587
	5/20 0930	6.5	14.9	10.1	1.13 E-2	1.37	1.50 E-1	9.29 E-2	1.06	143	56.6	3.98	12.1	624	-2.74	2.32 E-1	5.18 E-2	14.4	32.4	1.90 E-1	105
	5/20 1100	6.57	16.3	10.2	1.17 E-2	1.66	1.64 E-4	1.09 E-1	1.05	150	59.3	3.94	12.3	633	-2.41	2.10 E-1	4.42 E-2	13.7	18.1	1.85 E-1	374
	5/20 1230	6.58	16.7	10.1	1.23 E-2	1.43	1.75 E-1	9.67 E-2	1.04	146	58.1	4.03	12.46	630	-1.06	2.53 E-1	7.37 E-2	14.0	56.1	2.37 E-1	288
	5/20 1400	6.67	16.6	10.2	1.17 E-2	1.37	1.36 E-1	7.37 E-2	1.02	151	60.0	4.21	12.6	621	-2.15	1.88 E-1	4.24 E-2	13.7	37.7	1.77 E-1	205
	5/20 1530	6.73	19.5	9.85	1.00 E-2	1.34	1.32 E-1	1.11 E-1	9.39 E-1	146	57.0	4.17	12.5	616	-2.37	2.03 E-1	4.45 E-2	13.8	16.4	1.95 E-1	146
	5/20 1700	6.66	17.7	9.50	1.07 E-2	1.42	1.41 E-1	7.52 E-2	9.56 E-1	145	56.4	4.19	12.2	624	-1.14	2.21 E-1	5.15 E-2	14.7	26.6	1.90 E-1	162
	5/20 1830	6.52	16.5	9.98	1.33 E-2	1.50	1.39 E-1	7.71 E-2	1.06	148	58.7	3.96	13.1	614	-3.39	2.58 E-1	5.34 E-2	15.2	19.5	2.00 E-1	130

Appendix II. Table 6. Cosine model fit data LRM138 DB May 19-20 2014

Parameter	pH	T (C)	ODO mg/L	CO_2 g/L	DIC mM	Fe II mg/L	Fe_{TOT} mg/L	Mn mg/L	Ca mg/L	Mg mg/L	K mg/L	SiO_2 mg/L	$SO4^{2-}$ mg/L	$\delta^{13}C_{DIC}$	Y ug/L	Ce ug/L	Ni ug/L	Zn ug/L	As ug/L	Al ug/L
Cosine model parameters																				
M	6.51	13.4	9.58	1.08 E-2	1.43	1.53 E-1	1.14 E-1	1.09	151	59.5	3.99	12.7	620	-2.76	2.33 E-1	4.99 E-2	13.7	16.2	1.82 E-1	264
A	1.70 E-1	3.09	4.50 E-1	3.27 E-4	1.21 E-2	5.75 E-3	2.28 E-2	7.85 E-2	2.78	1.25	1.51 E-4	2.97 E-1	5.02	7.55 E-1	2.03 E-2	3.03 E-3	5.99 E-1	2.83	1.22 E-2	11.7
H	215	223	162	221	196	54.6	25.6	27.7	0	13.9	98.4	341	152	209	18.2	0	96.1	225	188	0
f-stat	240	384	129	4.26 E-1	1.48 E-1	1.42	5.48	14.0	1.67	2.24	2.61	3.43	4.85	10.4	7.44	4.03	13.1	2.67	2.58	2.04 E-2
p-value	1.64 E-41	1.68 E-52	2.45 E-30	6.28 E-1	8.49 E-1	2.30 E-1	8.87 E-3	9.74 E-5	1.81 E-1	1.08 E-1	7.85 E-2	3.99 E-2	1.41 E-2	5.17 E-4	2.54 E-3	2.63 E-2	2.27 E-1	7.53 E-2	8.05 E-2	9.78 E-1
RSD	2.06	15.1	3.77	10.1	4.57	7.46	23.9	6.66	3.25	3.26	5.71	2.96	0.86	27.9	9.19	6.98	2.16	25.0	48.1	62.8

Table 26. Tabulated data LRM050 DB May 19-20 2014

Parameter		pH	T (C)	ODO mg/L	CO_2 g/L	DIC mM	Fe II mg/L	Fe_{TOT} mg/L	Mn mg/L	Ca mg/L	Mg mg/L	K mg/L	SiO_2 mg/L	$SO4^{2-}$ mg/L	$\delta^{13}C_{DIC}$	Y ug/L	Ce ug/L	Ni ug/L	Zn ug/L	As ug/L	Al ug/L
Date/ time	5/19 1445	6.24	13.0	7.63	5.97 E-2	2.56	1.94	1.33	2.60	159	62.4	4.09	14.7	634	-5.57	2.72	1.59	21.1	32.4	3.22 E-1	134
	5/19 1615	6.22	13.0	7.93	5.93 E-2	2.64	1.96	2.01	2.56	155	61.0	4.38	13.8	637	3.64 E-1	2.80	1.60	20.7	30.9	2.92 E-1	145
	5/19 1745	6.22	12.7	7.91	6.00 E-2	2.37	1.89	1.96	2.54	154	60.5	4.29	13.7	638	-5.71	2.84	1.60	21.0	25.9	2.94 E-1	156
	5/19 1915	6.16	12.6	7.70	6.90 E-2	2.84	1.96	2.02	2.43	146	57.8	4.24	13.3	640	-1.68 E-1	2.95	1.67	20.4	50.2	3.39 E-1	160
	5/19 2045	6.20	12.5	7.82	6.03 E-2	2.72	1.95	2.03	2.65	164	63.4	4.23	14.5	641	-5.84	2.89	1.62	21.7	51.8	3.29 E-1	213
	5/19 2215	6.21	12.4	7.86	6.07 E-2	2.61	1.96	2.04	2.53	156	60.4	4.34	13.6	630	-5.84	2.84	1.61	21.2	23.6	3.03 E-1	170
	5/19 2345	6.22	12.4	7.93	5.57 E-2	2.60	1.96	2.04	2.43	151	58.3	4.05	13.4	617	-5.70	2.85	1.58	21.6	24.8	3.05 E-1	169
	5/20 0115	6.23	12.3	7.95	5.97 E-2	2.58	1.96	2.02	2.58	159	61.5	4.28	14.2	632	-5.66	2.85	1.57	20.7	24.5	2.99 E-1	200
	5/20 0245	6.23	12.3	no data	5.77 E-2	2.54	1.94	2.05	2.44	149	58.1	4.53	13.3	511	-5.69	2.87	1.59	21.7	25.1	2.95 E-1	166
	5/20 0415	6.23	12.3	no data	5.87 E-2	2.54	1.95	2.02	2.53	154	60.1	4.70	13.5	639	-5.65	2.84	1.60	21.3	26.7	3.24 E-1	144
	5/20 0545	6.23	12.4	no data	5.77 E-2	2.49	1.98	2.06	2.54	154	60.9	4.70	13.7	636	-5.76	2.81	1.60	21.6	67.4	3.25 E-1	150
	5/20 0715	6.22	12.5	no data	6.63 E-2	2.58	2.02	1.88	2.56	154	60.6	4.35	13.9	640	-5.82	2.90	1.63	21.9	31.8	3.15 E-1	144
	5/20 0845	6.21	12.6	no data	6.23 E-2	2.68	2.00	2.06	2.59	158	61.5	4.58	13.8	622	-5.96	2.82	1.55	22.0	113.0	2.90 E-1	158
	5/20 1015	6.21	12.8	no data	6.33 E-2	2.60	1.96	2.02	2.58	157	61.3	4.38	14.1	639	-5.78	2.76	1.52	21.6	163.0	3.23 E-1	78.1
	5/20 1145	6.20	12.8	no data	6.43 E-2	2.79	2.00	2.05	2.59	159	61.5	4.54	14.1	640	-6.16	2.93	1.63	21.8	80.2	3.31 E-1	138
	5/20 1315	6.2	13.0	no data	6.57 E-2	2.64	1.99	2.04	2.51	150	59.1	4.42	13.5	640	-5.89	2.85	1.61	21.4	98.9	3.55 E-	104
	5/20 1445	6.22	13.1	no data	6.83 E-2	2.60	1.96	2.05	2.68	161	63.1	4.45	14.4	619	-5.85	2.83	1.59	21.5	66.5	3.15 E-1	110
	5/20 1615	6.21	13.0	no data	6.20 E-2	2.49	2.02	2.09	2.46	144	57.9	4.55	13.1	638	-5.88	2.99	1.64	22.0	65.3	3.21 E-1	133
	5/20 1745	6.14	12.9	no data	7.23 E-2	2.97	1.99	2.05	2.51	152	60.2	4.34	13.7	633	-6.63	3.07	1.71	22.4	51.1	3.49 E-1	185
	5/20 1915	6.07	12.8	no data	9.43 E-2	3.12	2.09	2.09	2.66	161	63.1	4.66	14.04	645	-6.75	3.06	1.68	23.2	42.3	3.08 E-1	269

Table 27. Cosine model fit data LRM050 DB May 19-20 2014

Parameter	pH	T (C)	ODO mg/L	CO_2 g/L	DIC mM	Fe II mg/L	Fe_{TOT} mg/L	Mn mg/L	Ca mg/L	Mg mg/L	K mg/L	SiO_2 mg/L	$SO4^{2-}$ mg/L	$\delta^{13}C_{DIC}$	Y ug/L	Ce ug/L	Ni ug/L	Zn ug/L	As ug/L	Al ug/L
Cosine model parameters																				
M	6.21	12.6	8.01	6.34 E-2	2.65	1.87	2.00	2.55	155	60.6	4.42	13.8	634	-5.88	2.87	1.60	21.5	53.6	3.16 E-1	156
A	2.46 E-2	3.50 E-1	1.95 E-1	4.80 E-3	1.13 E-1	1.02 E-1	5.95 E-2	3.35 E-2	6.61 E-1	5.57 E-1	1.12 E-1	1.57 e-1	1.98	1.78 E-2	5.33 E-1	3.24 E-2	1.04 E-1	40.7	8.94 E-3	43.0
H	88.0	216	125	360	231	162	15.1	188	162	195	120	199	222	76.8	300	287	160	161	205	340
f-stat	17.3	804	29.3	1.80	2.30	2.35 E-1	5.53 E-1	9.29 E-1	6.52 E-2	4.50 E-1	2033	6.07 E-1	2.55 E-1	1.57	1.87	3.55	1.06 E-1	9.85	1.11	9.02
p-value	2.14 E-7	2.47 E-68	2.49 E-9	1.62 E-1	7.92 E-2	7.71 E-1	5.32 E-1	3.73 E-1	9.30 E-1	6.12 E-1	1.35 E-1	5.19 E-1	7.54 E-1	2.00 E-1	1.51 E-1	3.64 E-2	8.89 E-1	6.67 E-4	3.12 E-1	1.03 E-3
RSD	0.60	2.02	1.10	13.1	6.56	2.13	8.19	2.88	3.31	2.85	4.15	3.07	1.23	9.80	3.12	2.71	2.93	70.2	5.89	27.3

Table 28. Tabulated data LRM138 DC July 16-17 2014

Parameter		pH	T (C)	ODO mg/L	CO_2 g/L	DIC mM	Fe II mg/L	Fe_{TOT} mg/L	Mn mg/L	Ca mg/L	Mg mg/L	K mg/L	SiO_2 mg/L	$SO4^{2-}$ mg/L	$\delta^{13}C_{DIC}$	Y ug/L	Ce ug/L	Ni ug/L	Zn ug/L	As ug/L	Al ug/L
Date/ time	7/16 1400	6.84	22.4	8.85	1.13 E-2	1.18	1.03 E-1	1.05 E-1	8.45 E-1	162	58.1	6.04	13.7	549	-3.42	8.81 E-1	5.51 E-1	9.08	5.78	1.32 E-1	266
	7/16 1530	6.74	23.0	8.66	1.10 E-2	1.11	7.97 E-2	1.18 E-1	7.32 E-1	144	51.8	5.62	12.8	551	-3.69	7.86 E-1	4.39 E-1	8.04	4.20	1.61 E-1	240
	7/16 1700	6.71	21.6	8.17	9.67 E-3	1.12	8.36 E-2	1.18 E-1	7.45 E-1	137	49.8	5.46	12.3	554	-4.28	3.49 E-1	1.82 E-1	8.12	2.98	BDL	86.8
	7/16 1830	6.66	19.6	7.73	1.00 E-2	1.23	1.14 E-1	1.60 E-1	8.24 E-1	143	51.7	5.47	12.7	572	-4.96	5.52 E-1	3.25 E-1	8.31	3.30	BDL	147
	7/16 2000	6.57	18.4	7.69	1.00 E-1	1.17	1.29 E-1	1.61 E-1	8.92 E-1	145	53.0	5.51	12.6	559	-5.23	2.35 E-1	1.06 E-1	8.34	3.29	BDL	50.8
	7/16 2130	6.48	17.2	7.70	1.07 E-2	1.19	1.60 E-1	1.66 E-1	9.24 E-1	144	52.8	5.46	12.4	555	-5.65	7.89 E-1	4.68 E-1	9.17	6.46	BDL	191
	7/16 2300	6.39	16.5	7.81	1.03 E-2	1.17	1.60 E-1	1.87 E-1	9.05 E-1	142	52.1	5.44	12.3	557	-5.50	1.03	5.99 E-1	9.45	5.47	1.38 E-1	250
	7/16 0030	6.38	16.1	7.92	1.03 E-2	1.16	1.55 E-1	1.79 E-1	9.30 E-1	143	52.1	5.55	12.5	557	-5.41	5.38 E-1	2.95 E-1	9.43	4.58	BDL	113
	7/17 0200	6.44	16.0	no data	9.33 E-3	1.24	1.20 E-1	1.87 E-1	9.30 E-1	140	51.4	5.40	12.3	556	-5.75	4.79 E-1	2.57 E-1	9.51	4.77	BDL	97.7
	7/17 0330	6.35	15.9	no data	1.03 E-2	1.18	1.24 E-1	1.79 E-1	9.26 E-	143	52.5	5.38	12.2	557	-5.58	2.17	1.31	11.9	11.6	2.84 E-1	426
	7/17 0500	6.35	15.6	no data	1.20 E-2	1.16	1.23 E-1	1.91 E-1	9.16 E-1	141	51.4	5.47	12.3	559	-5.66	3.66 E-1	1.97 E-1	9.72	4.07	BDL	78.3
	7/17 0630	6.33	15.2	no data	1.17 E-2	1.12	1.29 E-1	1.85 E-1	9.39 E-1	141	51.6	5.36	12.0	558	-5.69	4.81 E-1	2.84 E-1	9.86	4.10	BDL	100
	7/17 0800	6.35	15.4	no data	1.05 E-2	1.12	1.59 E-1	1.90 E-1	9.03 E-1	139	50.9	5.33	12.4	558	-5.46	1.22	8.24 E-1	11.5	6.62	BDL	263
	7/17 0930	6.40	16.4	no data	1.13 E-2	1.12	1.16 E-1	1.97 E-1	8.95 E-1	142	51.9	5.41	12.1	558	-5.09	1.00	6.75 E-1	12.2	6.80	BDL	222
	7/17 1100	6.51	15.6	no data	1.03 E-2	1.11	7.53 E-2	1.54 E-1	7.94 E-1	141	51.0	5.40	12.1	595	-4.44	6.96 E-1	4.36 E-1	10.9	4.79	BDL	152
	7/17 1230	6.60	20.7	9.07	1.00 E-2	1.11	5.55 E-2	2.02 E-1	7.40 E-1	141	50.9	5.43	12.1	561	-3.89	9.54 E-1	5.62 E-1	9.66	4.99	BDL	222
	7/17 1400	6.70	21.7	9.00	1.10 E-2	1.13	2.02 E-2	1.05 E-1	6.77 E-1	140	50.3	5.46	12.1	563	-3.56	1.87	1.17	11.7	9.31	1.75 E-2	392
	7/17 1530	6.68	21.0	8.78	8.00 E-3	1.13	BDL	1.08 E-1	7.15 E-1	147	52.9	5.47	12.3	563	-3.91	2.52 E-1	1.26 E-1	8.36	2.53	BDL	50.4
	7/17 1700	6.66	20.6	8.50	9.33 E-3	1.12	5.31 E-2	1.05 E-1	6.89 E-1	140	50.5	5.36	12.0	564	-4.22	5.14 E-1	3.03 E-1	9.48	3.36	BDL	113
	7/17 1830	6.59	19.0	8.09	1.03 E-2	1.14	7.97 E-2	1.26 E-1	7.78 E-1	147	53.3	5.50	12.8	564	-4.62	3.41 E-1	1.92 E-1	9.10	3.28	BDL	71.4

Table 29. Cosine model fit data LRM138 DC July 16-17 2014

Parameter	pH	T (C)	ODO mg/L	CO_2 g/L	DIC mM	Fe II mg/L	Fe_{TOT} mg/L	Mn mg/L	Ca mg/L	Mg mg/L	K mg/L	SiO_2 mg/L	$SO4^{2-}$ mg/L	$\delta^{13}C_{DIC}$	Y ug/L	Ce ug/L	Ni ug/L	Zn ug/L	As ug/L	Al ug/L
Cosine model parameters																				
M	6.50	17.9	8.57	1.05 E-2	1.15	1.12 E-1	1.61 E-1	8.53 E-1	142	51.7	5.44	12.3	558	-4.96	6.53 E-1	3.91 E-1	9.86	4.59	1.21 E-1	180
A	1.97 E-1	3.22	9.20 E-1	6.07 E-4	3.80 E-2	4.22 E-2	3.32 E-2	1.10 E-1	1.52	6.94 E-1	5.25 E-2	1.26 E-1	6.98 E-1	1.01	1.73 E-1	1.35 E-1	1.31	1.02	1.03 E-2	48.5
H	241	232	145	106	0	27.7	30.0	44.0	301	344	290	273	205	215	133	134	112	106	62.9	134
f-stat	408	345	3.81	2.52	7.64	11.3	7.20	26.9	1.66	2.52	3.47	9.81 E-1	1.23 E-1	46.2	1.63	2.23	9.14	4.74	2.58 E-1	8.95 E-1
p-value	1.24 E-54	7.48 E-51	9.04 E-39	8.48 E-2	2.28 E-3	3.67 E-4	2.94 E-3	1.30 E-6	1.82 E-1	8.53 E-2	3.91 E-2	3.53 E-1	8.71 E-1	2.07 E-8	1.88 E-1	1.09 E-1	9.70 E-4	1.56 E-2	7.52 E-1	3.87 E-1
RSD	2.31	13.6	6.08	8.78	3.31	37.1	22.9	11.2	1.85	1.86	1.28	2.12	0.73	16.8	46.1	53.5	13.3	27.4	37.4	61.0

Table 30. Table 11 Tabulated data LRM050 DC July 16-17 2014

Parameter		pH	T (C)	ODO mg/L	CO_2 g/L	DIC mM	Fe II mg/L	Fe_{TOT} mg/L	Mn mg/L	Ca mg/L	Mg mg/L	K mg/L	SiO_2 mg/L	$SO4^{2-}$ mg/L	$\delta^{13}C_{DIC}$	Y ug/L	Ce ug/L	Ni ug/L	Zn ug/L	As ug/L	Al ug/L
Date/ time	**7/16 1445**	6.14	13.1	8.81	6.53 E-2	2.59	3.34	3.47	2.56	141	51.3	5.55	14.4	568	-6.51	4.76	3.49	19.3	18.6	2.99 E-1	86.6
	7/16 1615	6.15	13.3	8.85	6.87 E-2	2.58	3.30	3.46	2.55	140	51.3	5.55	13.9	564	-6.69	3.18	1.95	20.3	19.1	BDL	96.2
	7/16 1745	6.10	13.1	8.64	7.50 E-2	2.74	3.31	3.43	2.54	140	51.2	5.58	14.3	608	-7.11	3.21	1.94	20.0	18.7	BDL	149
	7/16 1915	6.03	13.1	8.19	8.17 E-2	2.93	3.38	3.49	2.58	143	52.0	5.62	14.1	571	-7.35	3.48	2.29	20.3	19.6	2.06 E-1	507
	7/16 2045	5.97	13.0	7.78	1.01 E-2	3.35	3.39	3.52	2.56	142	52.0	5.66	14.1	571	-7.52	3.15	1.88	19.9	19.1	BDL	196
	7/16 2215	6.03	13.0	8.37	9.23 E-2	3.09	3.40	3.53	2.53	140	51.1	5.61	14.3	571	-7.42	3.33	1.95	20.5	19.5	1.31 E-1	155
	7/16 2345	6.06	12.9	8.57	7.1 E-2	2.73	3.43	3.56	2.52	140	51.2	5.51	13.9	572	-6.87	3.22	1.92	20.5	18.5	BDL	157
	7/17 0115	6.10	13.0	8.14	9.30 E-2	3.15	3.37	3.59	2.52	140	51.3	5.58	13.9	573	-7.38	3.35	1.86	20.2	19.8	1.76 E-1	175
	7/17 0245	6.01	12.9	8.09	8.60 E-2	2.94	3.44	3.59	2.50	140	51.1	5.50	13.8	571	-7.43	3.98	2.48	20.4	20.3	2.22 E-1	187
	7/17 0415	6.01	12.9	8.09	9.10 E-2	3.10	3.45	3.61	2.51	139	50.8	5.51	13.8	572	-7.46	3.25	1.88	19.7	19.9	1.27 E-1	204
	7/17 0545	6.13	12.9	8.79	7.50 E-2	2.64	3.50	3.64	2.53	141	51.2	5.59	14.1	573	-6.86	3.35	1.97	19.7	18.7	1.77 E-1	136
	7/17 0715	6.14	12.9	8.82	7.33 E-2	2.70	3.48	3.65	2.46	137	50.3	5.47	13.4	576	-7.07	3.15	1.91	19.8	19.0	BDL	147
	7/17 0845	6.12	13.0	8.81	7.77 E-2	2.66	3.49	3.65	2.48	138	50.4	5.52	13.6	601	-7.20	3.27	1.96	20.6	19.8	1.53 E-1	126
	7/17 1015	6.06	13.1	8.27	8.37 E-2	2.98	3.45	3.64	2.60	145	53.0	5.65	14.1	572	-7.41	3.30	1.96	20.7	19.0	BDL	165
	7/17 1145	6.10	13.2	8.68	8.23 E-2	2.95	3.46	3.64	2.48	138	50.4	5.50	13.5	305	-7.67	3.15	1.97	20.4	18.8	BDL	139
	7/17 1315	6.10	13.2	8.70	8.43 E-2	2.81	3.47	3.64	2.52	140	51.2	5.53	13.6	574	-7.15	3.31	1.98	21.2	19.6	1.24 E-1	116
	7/17 1445	6.06	13.2	8.39	8.77 E-2	3.03	3.37	3.61	2.45	137	49.8	5.42	13.5	573	-7.32	3.07	1.89	19.6	18.9	BDL	148
	7/17 1615	6.12	13.2	8.72	7.53 E-2	2.79	3.41	3.58	2.47	137	50.1	5.46	13.8	582	-7.22	3.16	1.74	19.8	19.0	1.92 E-1	134
	7/17 1745	6.04	13.1	8.27	8.50 E-3	3.01	3.43	3.60	2.49	138	50.3	5.42	13.9	510	-7.44	3.24	1.86	20.5	19.5	1.79 E-1	152
	7/17 1845	6.00	13.1	7.99	9.77 E-3	3.25	3.44	3.63	2.50	138	50.5	5.44	13.8	591	-7.79	3.14	1.86	19.9	18.9	1.25 E-1	177

Table 31. Cosine model fit data LRM050DC July 16-17 2014

Parameter	pH	T (C)	ODO mg/L	CO_2 g/L	DIC mM	Fe II mg/L	Fe_{TOT} mg/L	Mn mg/L	Ca mg/L	Mg mg/L	K mg/L	SiO_2 mg/L	$SO4^{2-}$ mg/L	$\delta^{13}C_{DIC}$	Y ug/L	Ce ug/L	Ni ug/L	Zn ug/L	As ug/L	Al ug/L
Cosine model parameters																				
M	6.07	13.1	8.47	8.26 E-2	2.90	3.42	3.59	2.52	140	51.0	5.53	13.9	574	-7.25	3.36	1.97	20.2	19.3	1.46 E-1	154
A	3.96 E-1	1.74 E-1	2.35	5.93 E-3	1.56 E-1	5.46 E-2	6.45 E-2	1.32 E-2	2.38 E-1	1.86 E-1	2.24 E-2	1.35 E-1	4.57	9.83 E-2	2.35 E-2	6.40 E-2	4.93 E-2	2.77 E-1	4.50 E-3	30.9
H	166	220	161	0	340	103	114	300	19.9	0	0	0	118	174	146	38.8	123	41.5	0	360
f-stat	22.4	302	20.1	1.77	2.50	7.97	4.13	5.13 E-1	5.44 E-2	2.52 E-1	4.00 E-1	1.01	2.48 E-1	3.82 E-1	1.52 E-2	6.14 E-1	4.75 E-2	1.66	2.70 E-2	5.96
p-value	4.91 E-9	3.03 E-46	1.89 E-8	1.66 E-1	8.63 E-1	1.89 E-3	3.07 E-3	5.73 E-1	9.41 E-1	7.58 E-1	6.56 E-1	3.45 E-1	7.59 E-1	6.59 E-2	9.83 E-1	5.14 E-1	9.48 E-1	1.84 E-1	9.70 E-1	6.43 E-3
RSD	0.81	1.04	3.59	11.8	7.65	1.69	1.94	1.56	1.50	1.47	1.30	2.03	3.29	4.44	11.3	8.33	2.32	2.60	37.5	21.5

Table 32. Method detection limits

Parameter	Method	Detection limit
CO_2	CM	0.14 mM
DIC	CM	0.14 mM
Fe(II)	DR2800 spectrometer	2.0 mg/L
Fe_{TOT}	DR2800 spectrometer	2.0 mg/L
Mn	ICP OES	0.025 mg/L
Ca	ICP OES	5 mg/L
Mg	ICP OES	5 mg/L
K	ICP OES	5 mg/L
SiO_2	ICP OES	0.025 mgL
SO_4^{2-}	IC	0.036 mg/L
Y	ICP MS	0.010 ug/L
Ce	ICP MS	0.010 ug/L
Ni	ICP MS	0.100 ug/L
Zn	ICP MS	0.100 ug/L
As	ICP MS	0.100 ug/L
Al	ICP MS	0.100 ug/L

CO_2 and Fe both had values at various points in this study close to the detection limit but were included in analysis and discussion due to the goals of the study.

Appendix III. Summary graphs

DA: March 14-15 2014

LRM050

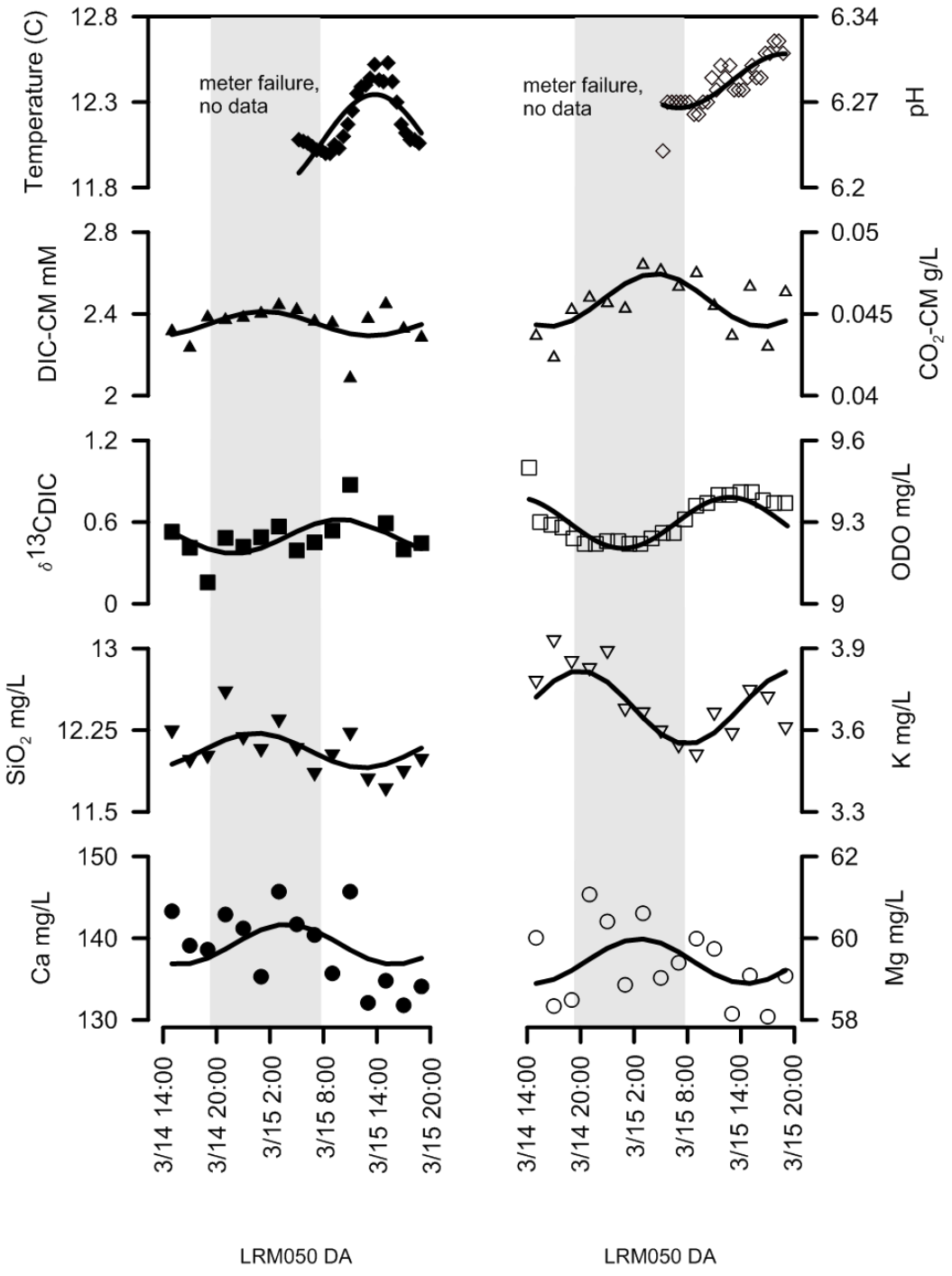

Figure 38. Summary graph of analytes and parameters (symbols) with cosine model fit (curved lines).

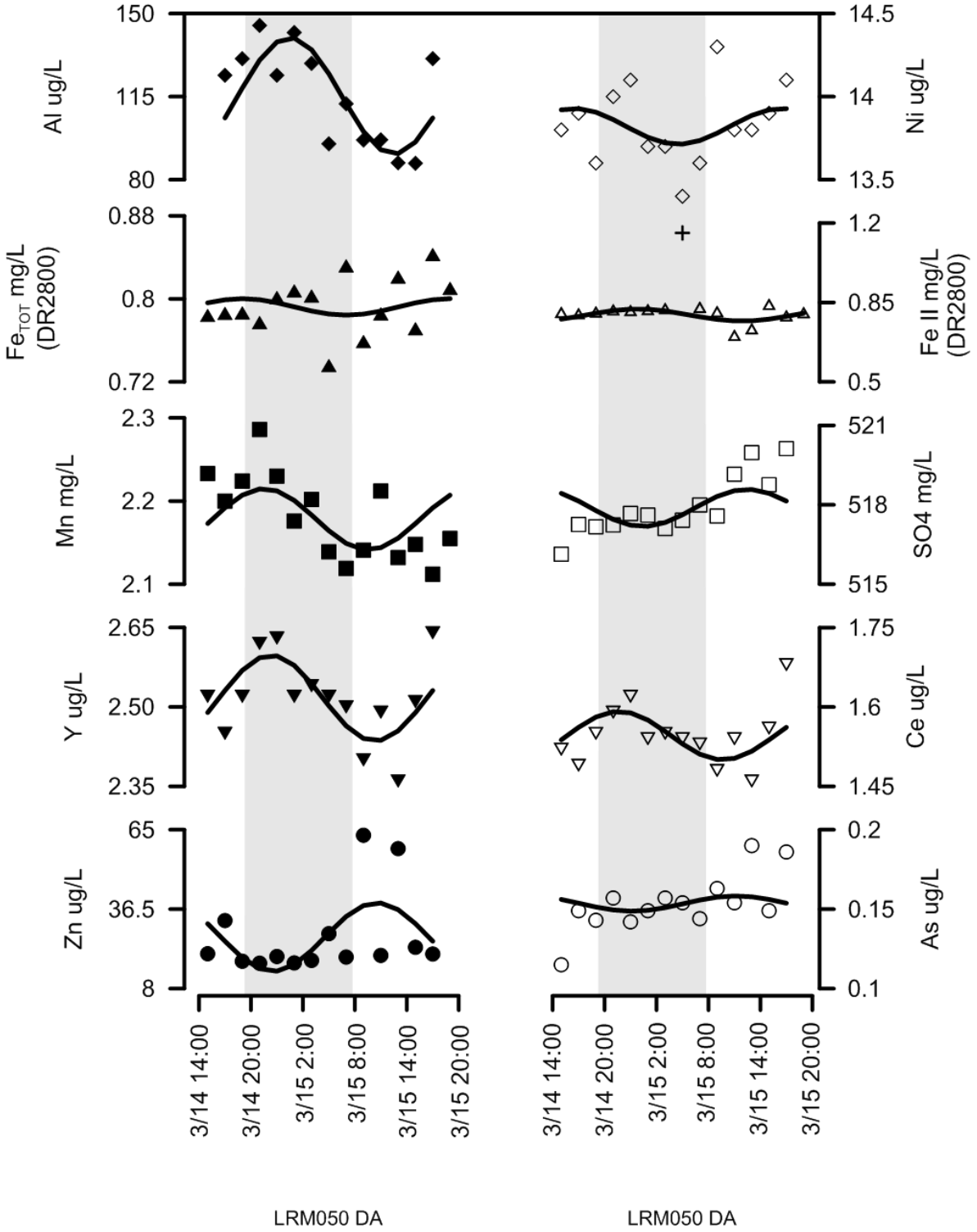

Figure 39. Summary graph of analytes and parameters (symbols) and cosine mode fit (curved lines). Cross symbols represent data points that were excluded from the cosine model fit analysis. Points were excluded if they were believed to be falsely high or low or otherwise unreliable.

LRM138

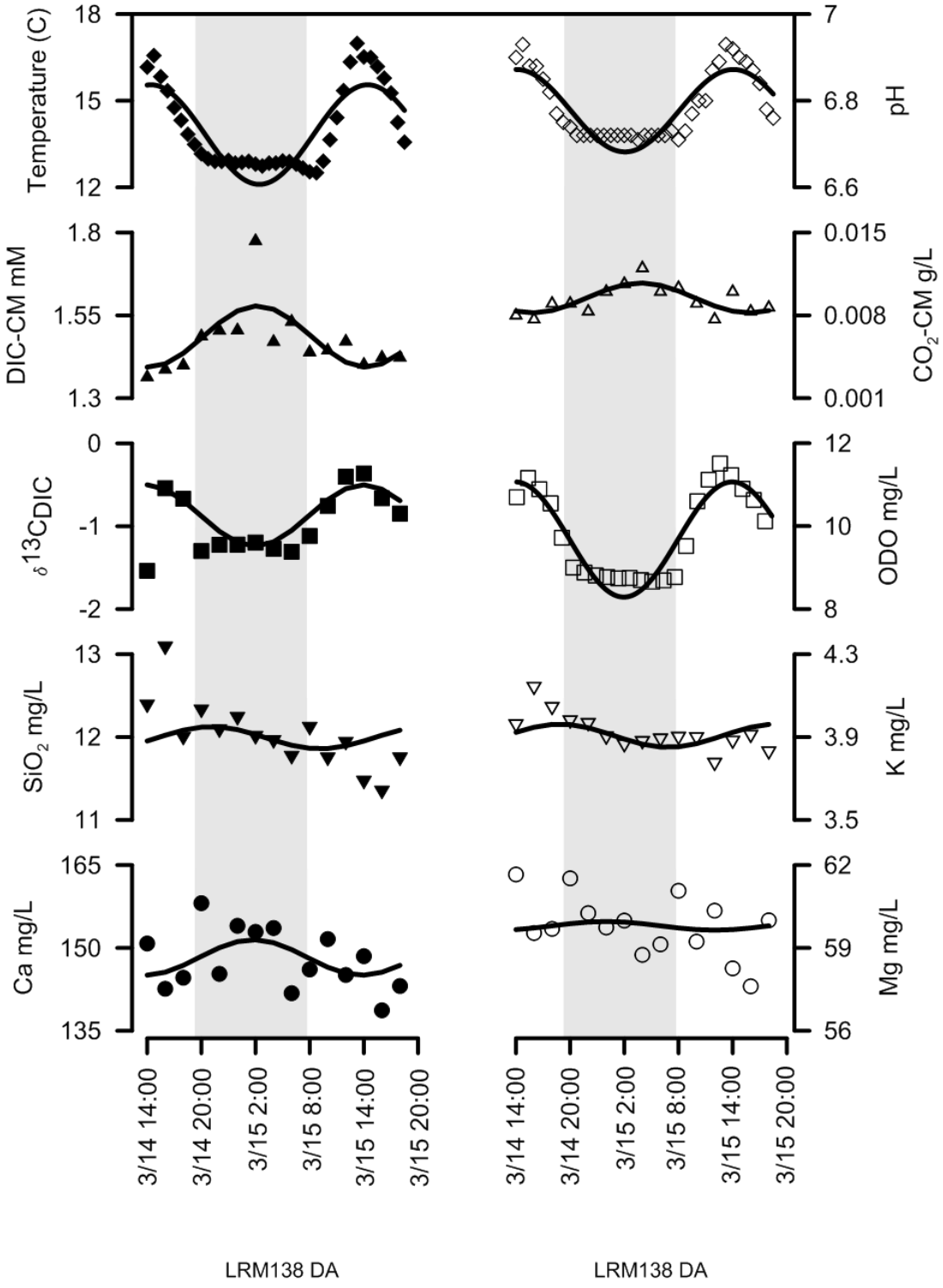

Figure 40. Summary graph of analytes and parameters (symbols) with cosine model fit (curved lines).

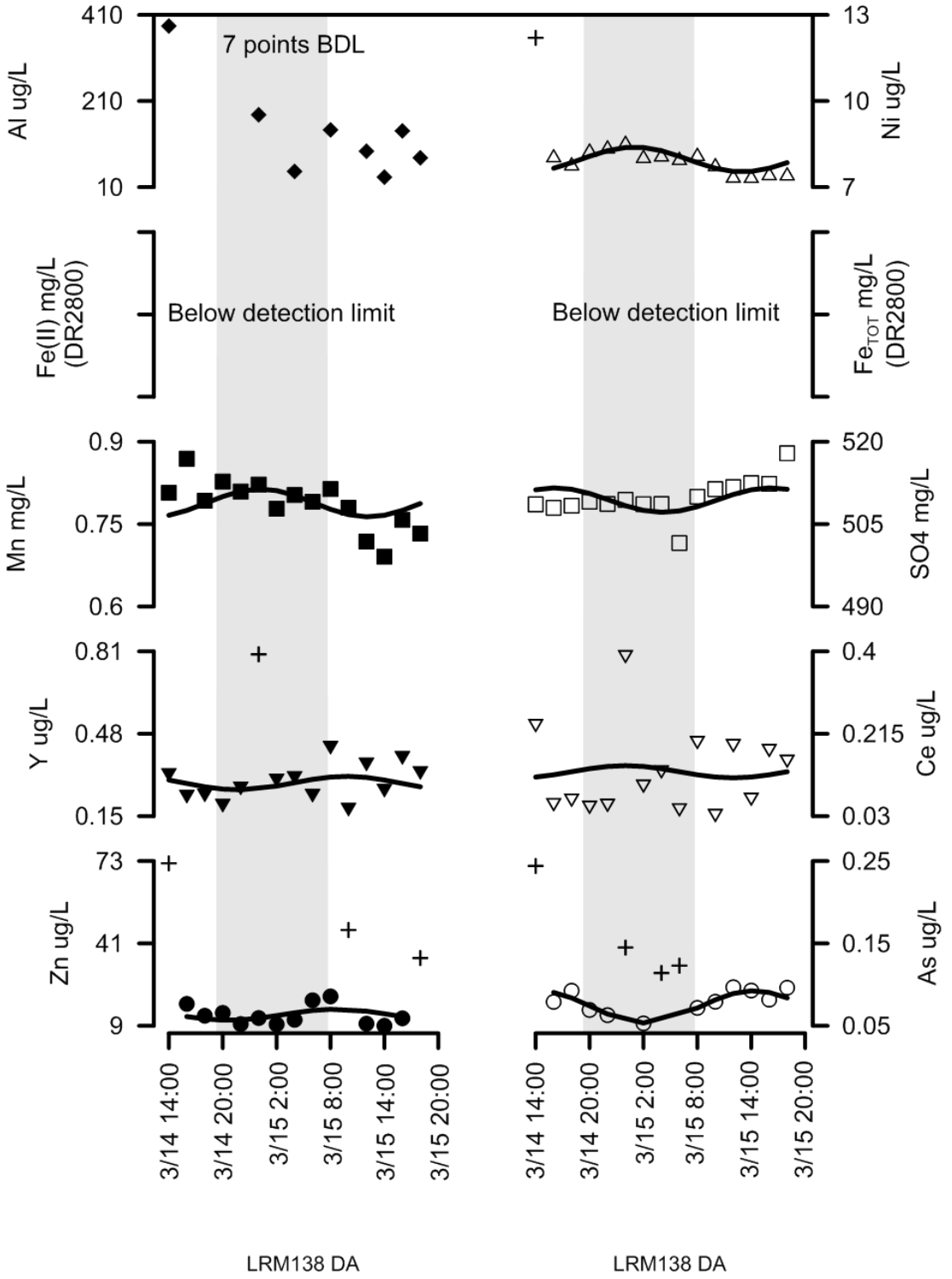

Figure 41. Summary graph of analytes and parameters (symbols) and cosine mode fit (curved lines). Cross symbols represent data points that were excluded from the cosine model fit analysis. Points were excluded if they were believed to be falsely high or low or otherwise unreliable.

DB: May 19-20 2014

LRM050

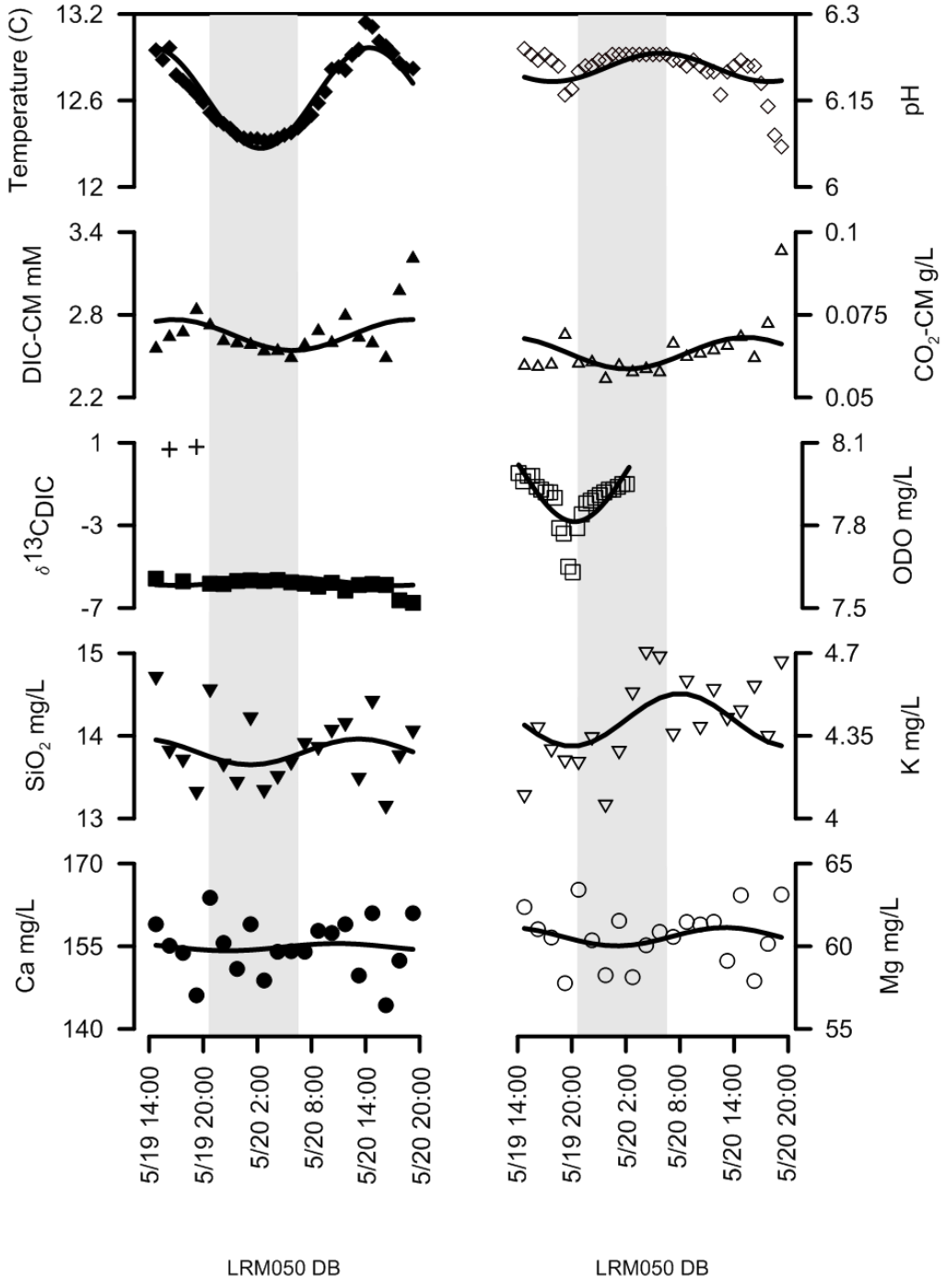

Figure 42. Summary graph of analytes and parameters (symbols) with cosine model fit (curved lines).

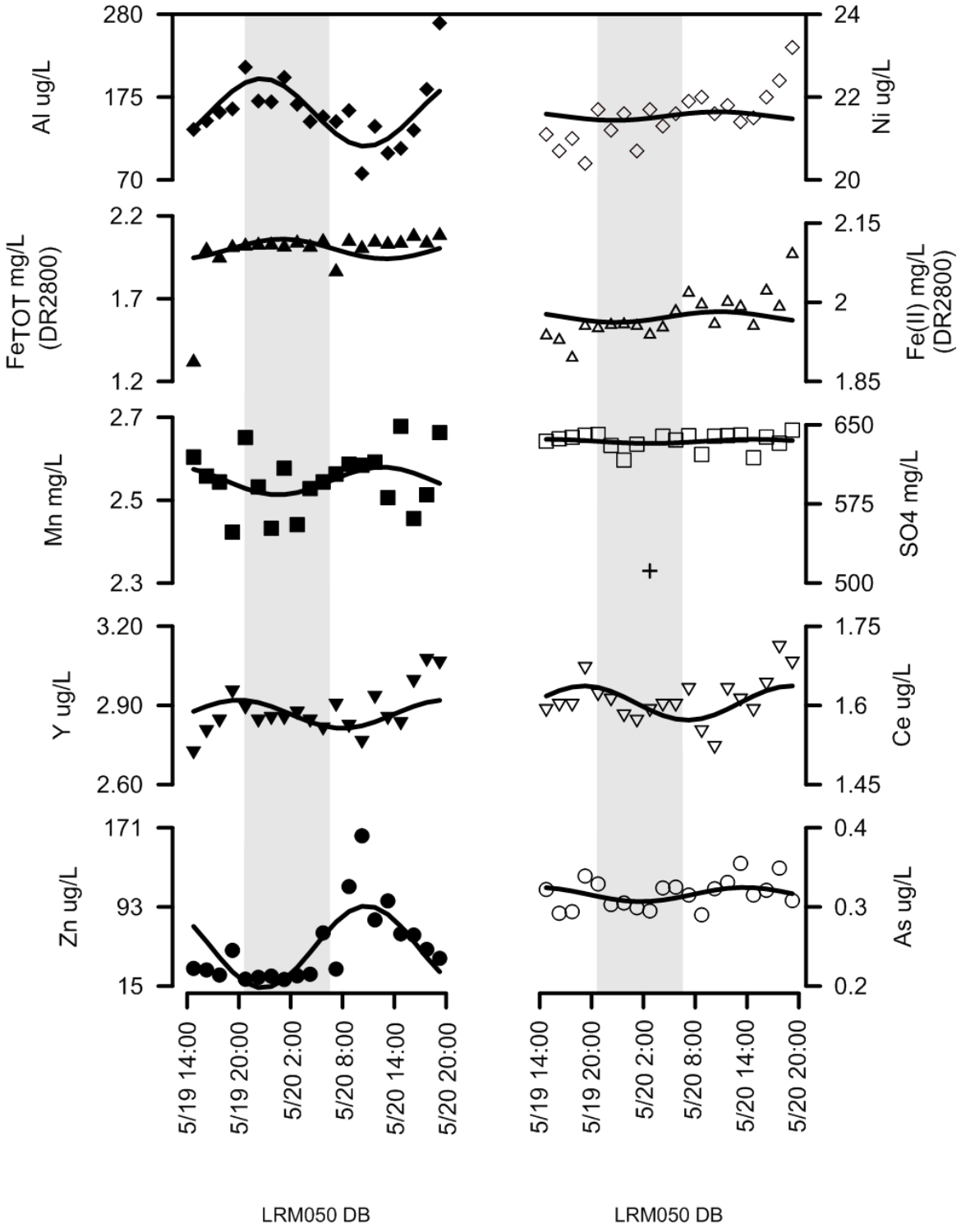

Figure 43. Summary graph of analytes and parameters (symbols) and cosine mode fit (curved lines). Cross symbols represent data points that were excluded from the cosine model fit analysis. Points were excluded if they were believed to be falsely high or low or otherwise unreliable.

.

LRM138

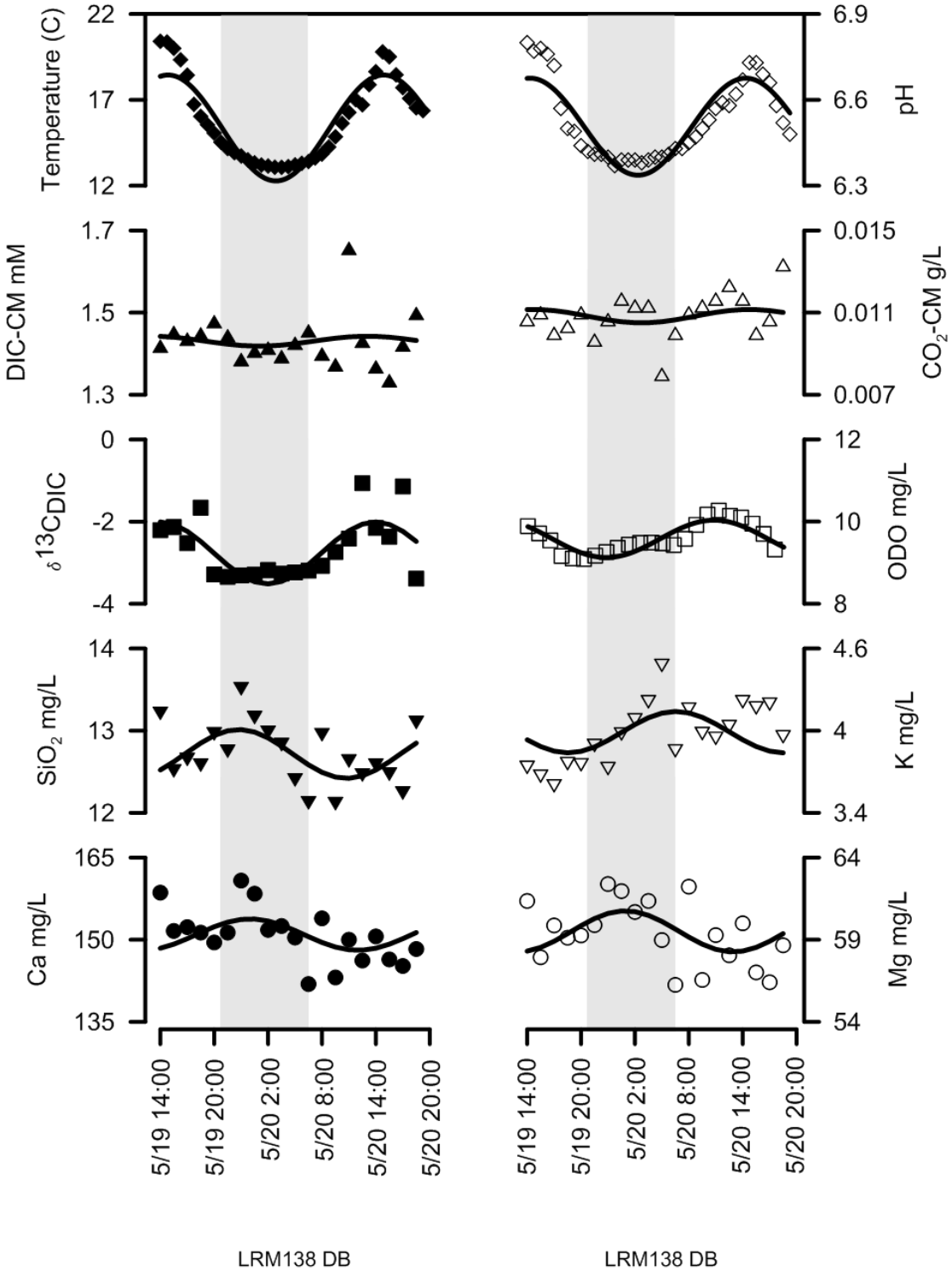

Figure 44. Summary graph of analytes and parameters (symbols) with cosine model fit (curved lines).

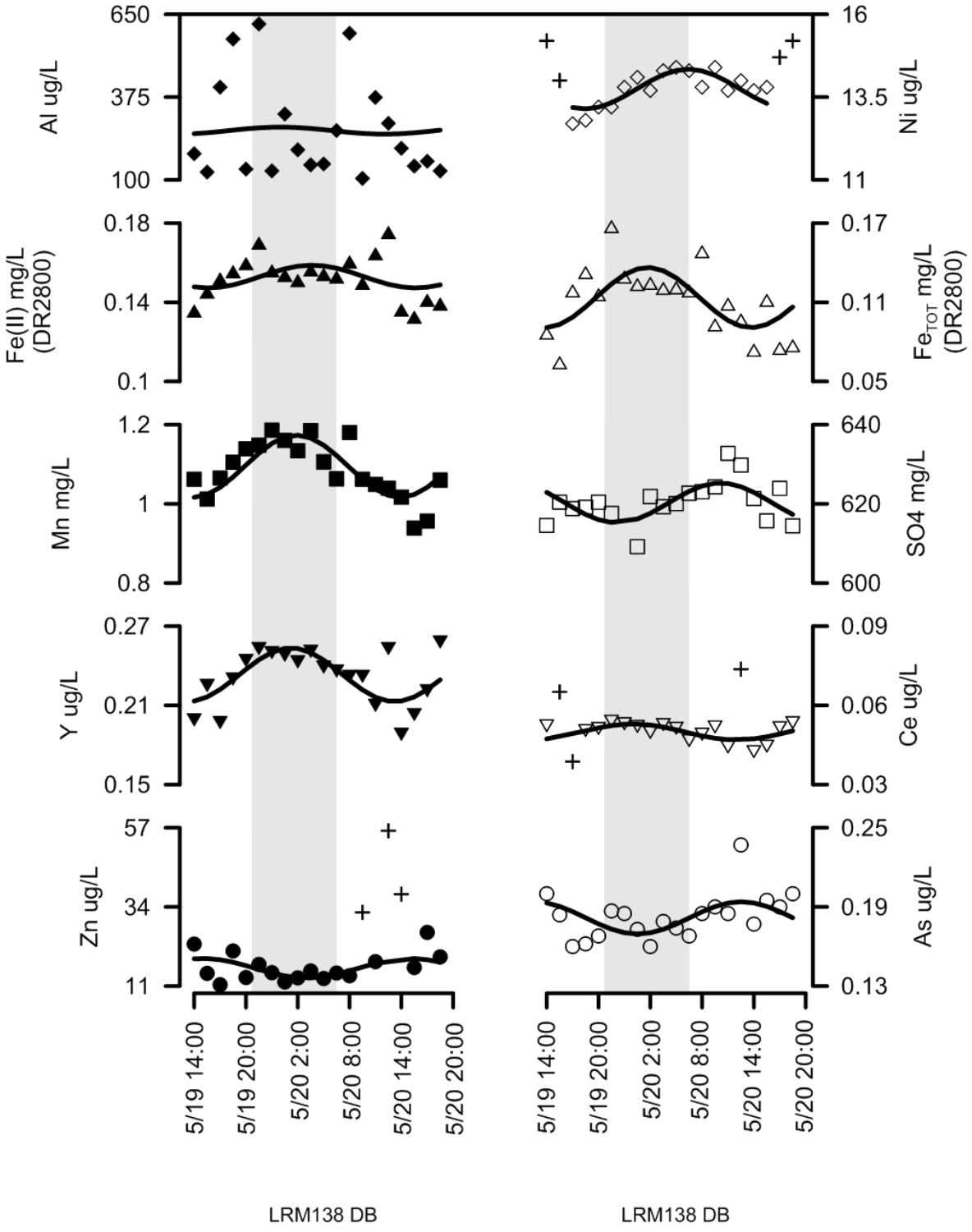

Figure 45. Summary graph of analytes and parameters (symbols) and cosine mode fit (curved lines). Cross symbols represent data points that were excluded from the cosine model fit analysis. Points were excluded if they were believed to be falsely high or low or otherwise unreliable.

DC: July 16-17 2014

LRM050

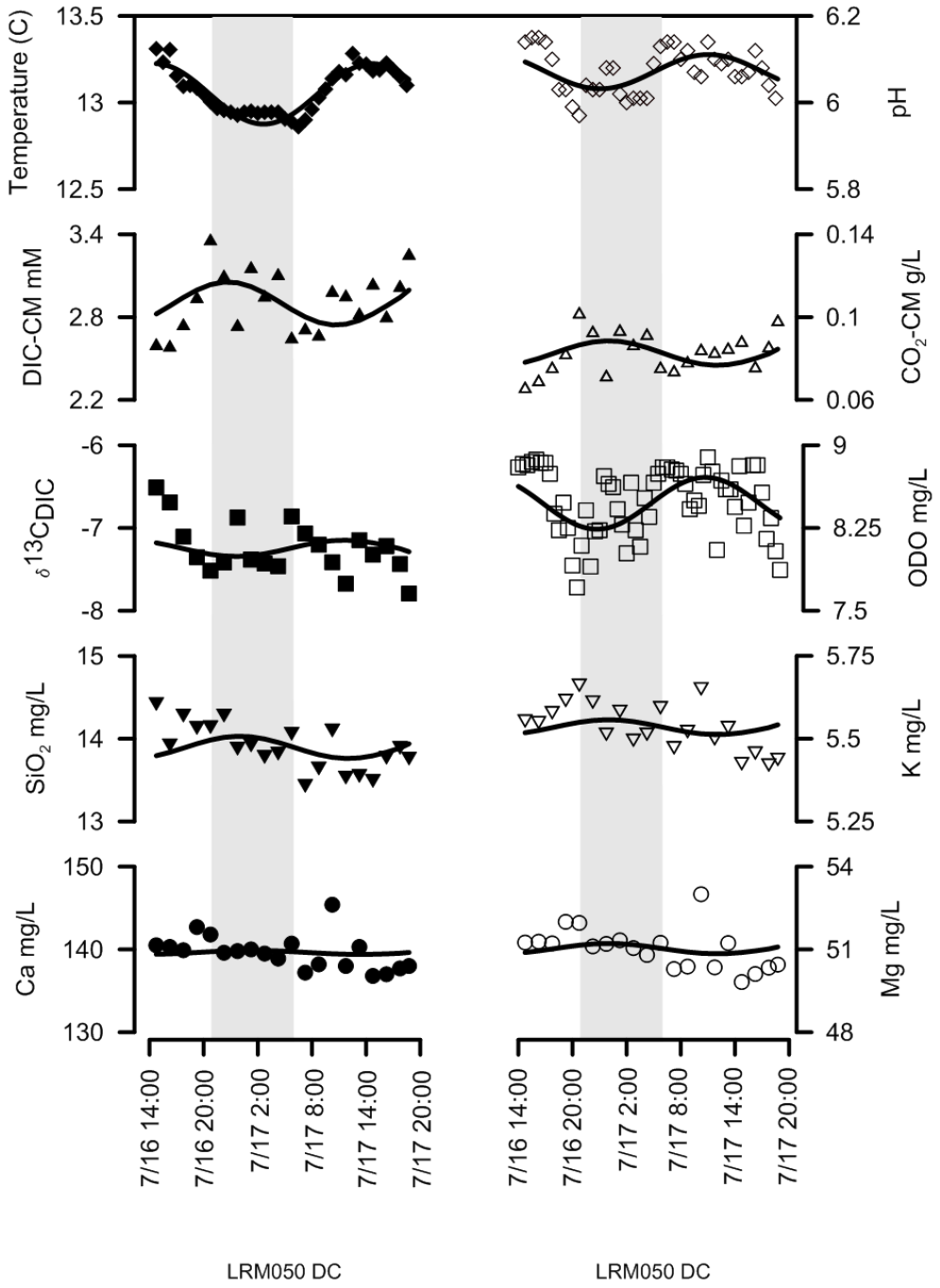

Figure 46. Summary graph of analytes and parameters (symbols) with cosine model fit (curved lines).

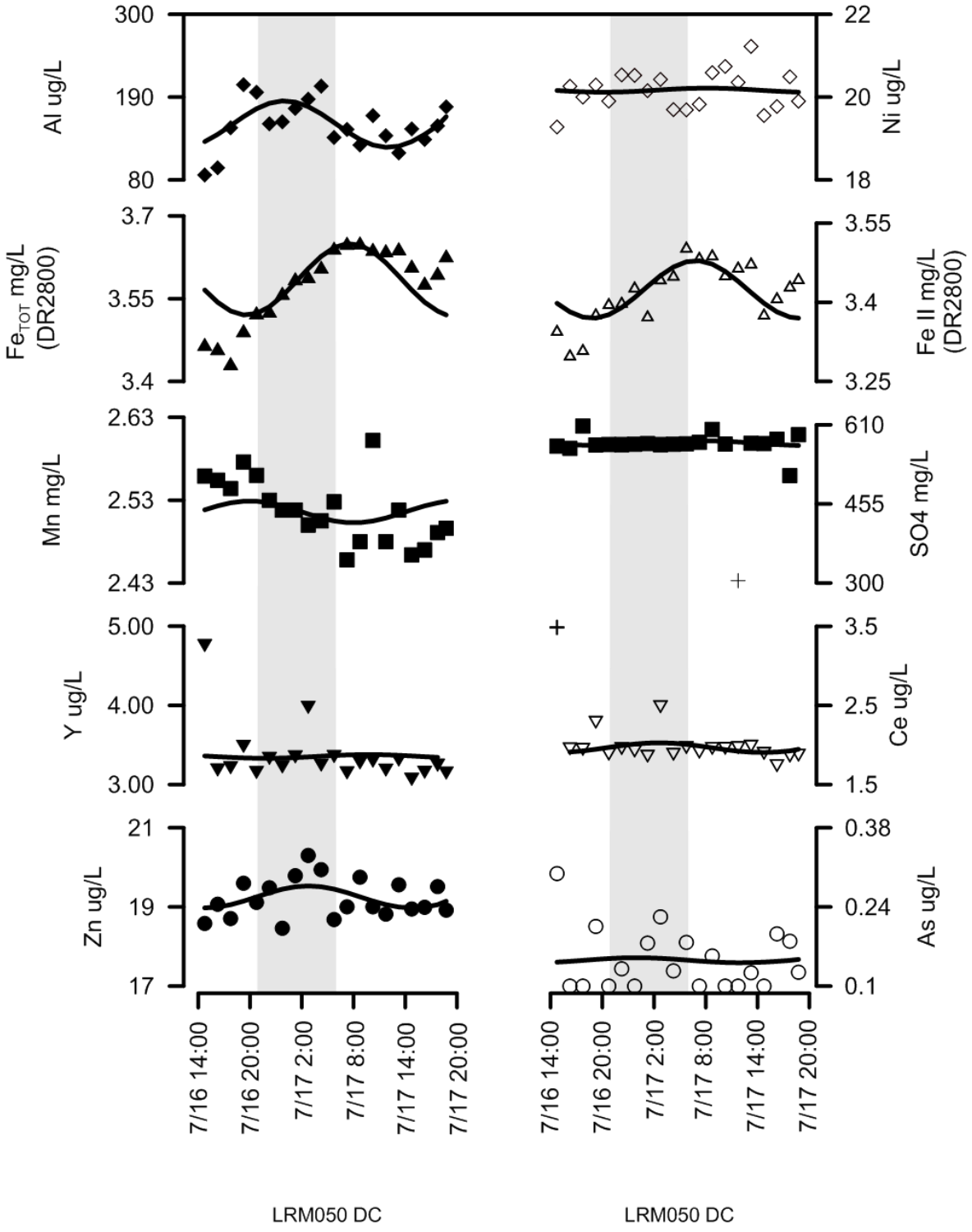

Figure 47. Summary graph of analytes and parameters (symbols) and cosine mode fit (curved lines). Cross symbols represent data points that were excluded from the cosine model fit analysis. Points were excluded if they were believed to be falsely high or low or otherwise unreliable.

LRM138

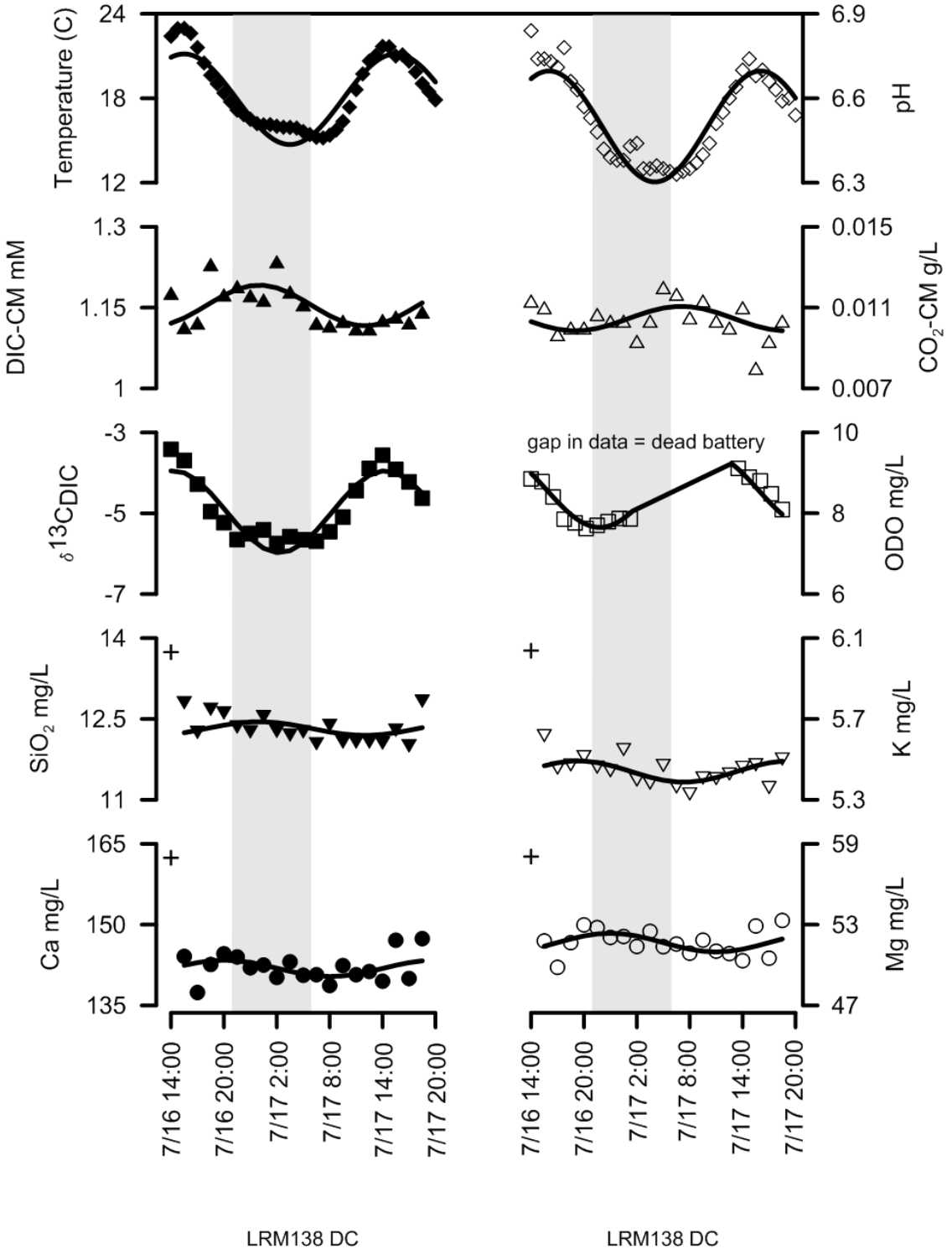

Figure 48. Summary graph of analytes and parameters (symbols) and cosine mode fit (curved lines). Cross symbols represent data points that were excluded from the cosine model fit analysis. Points were excluded if they were believed to be falsely high or low or otherwise unreliable.

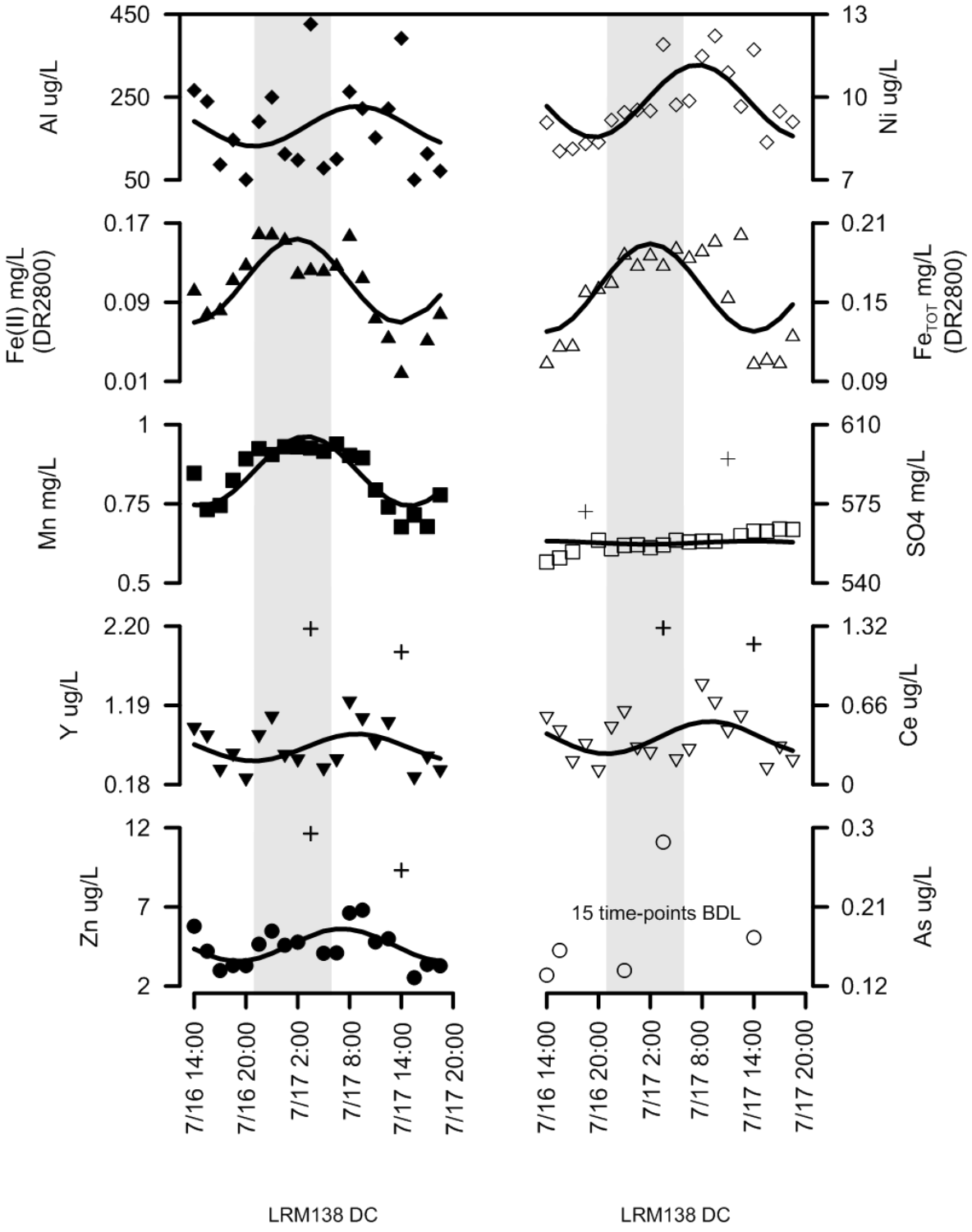

Figure 49. Summary graph of analytes and parameters (symbols) and cosine mode fit (curved lines). Cross symbols represent data points that were excluded from the cosine model fit analysis. Points were excluded if they were believed to be falsely high or low or otherwise unreliable.